Master Thesis

Multi-Horizon Prediction of Power Consumption during Dynamic Positioning Operations: Physical, Data-Driven and Hybrid Model Approaches

Technical University of Delft
Jens de Boer

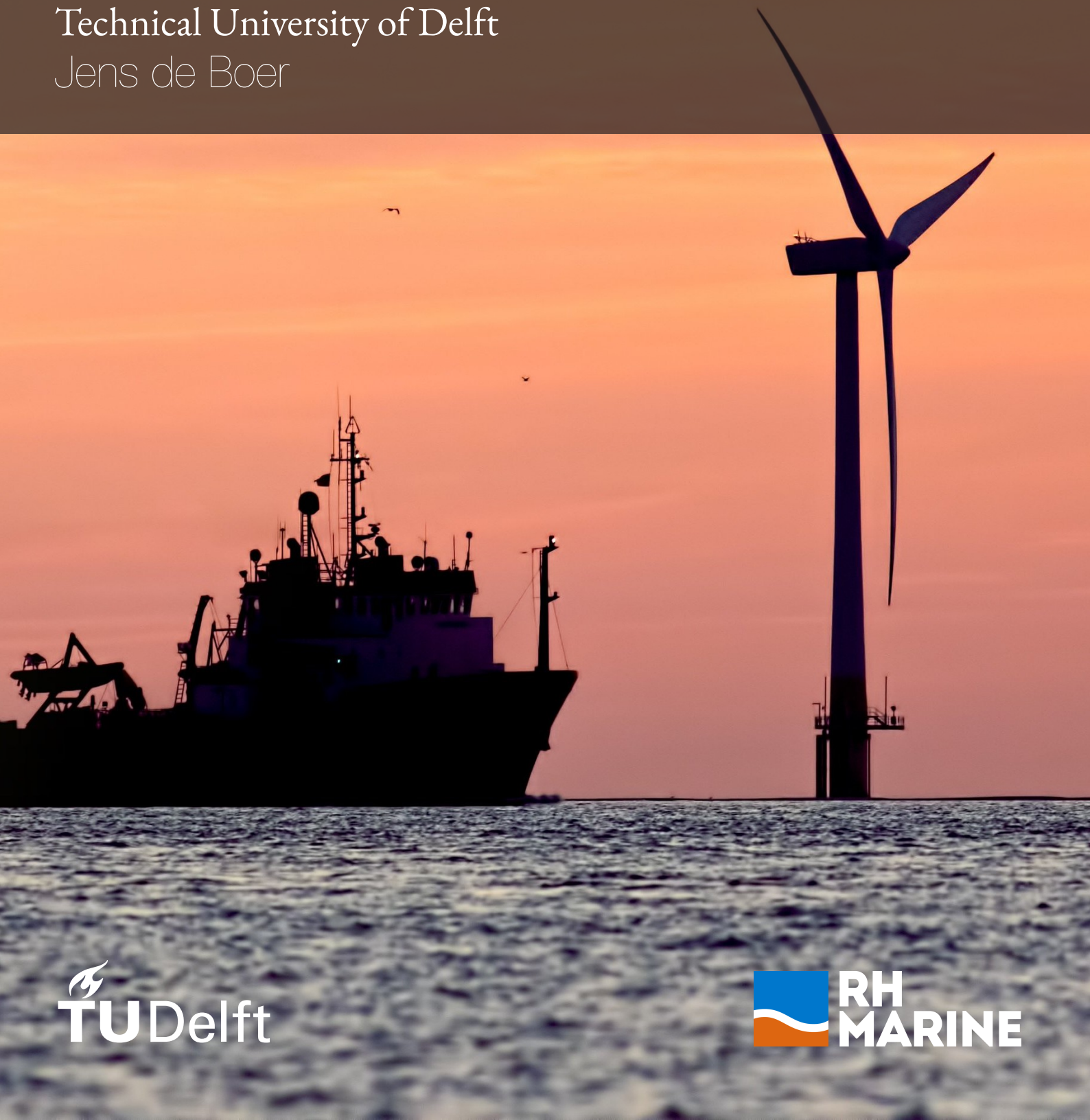

TU Delft

RH MARINE

Thesis for the degree of MSc in Marine Technology in the specialization of *Marine Engineering*

Multi-Horizon Prediction of Power Consumption during Dynamic Positioning Operations: Physical, Data-Driven and Hybrid Model Approaches

By

J.O.B. de Boer

Performed at

RH Marine Netherlands

January 17, 2023

Company supervisors

Responsible supervisor:	D. Mitropoulou, MSc
E-mail:	despoina.mitropoulou@rhmarine.com
Daily supervisor:	M. Wittingen, MSc
E-mail:	martijn.wittingen@rhmarine.com

Thesis exam committee

Chair:	Prof. K. Visser
Staff member:	Dr. A. Coraddu
Staff member:	Dr. R. Ferrari
Company member:	M. Wittingen, MSc

Author details

Student number:	4435087
E-mail:	j.bokmadeboer@gmail.com

Cover Image: Offshore support vessel at offshore wind park [1]

Abstract

A significant decrease in greenhouse gas emissions can be achieved by including a prediction of future power consumption in the control of ships' power plants during transits. Moreover, including a prediction of power consumption in the Energy Management System (EMS) during Dynamic Positioning (DP) operations can also contribute to a reduction in greenhouse gas emissions. However, predictions of future power consumption for DP operations, as well as its implementation in an EMS, have not been investigated widely, since this is a complex task for a relatively specific application. This research aims to investigate how power consumption during DP operations can most accurately be predicted for near-future and far-future, within reduced computational requirements for real-time applications.

In this research, six different approaches for power consumption prediction are investigated. These approaches can be categorized into projection models, which determine the power consumption independent of time based on the environmental conditions, and forecast models, which rely on the recent past behaviour of the system.

The four projection models consist of two Physical Models (PMs), a Data-Driven Model (DDM), and a hybrid model. The first PM is the static model, in which the environmental loads are directly compensated by the thrusters, hence the ship is assumed not to move. The second PM is the dynamic model, in which the motions of the ship are also modelled. Then, the DDM projection is based on Kernel Regularized Least Squares (KRLS) to capture the nonlinear relation between environmental conditions and power consumption based on historical data. Lastly, the hybrid projection model is an integration of the dynamic model in the DDM.

Afterwards, two forecast models are developed, being one DDM and one hybrid model. The DDM forecast is based on a combination between KRLS and Time Series (TS) forecasting. The hybrid forecast is an integration of the dynamic model in the DDM forecast.

Simulations are performed for each model using a data set provided by RH Marine. The DDMs show the most accurate results, taking into account the required computational effort. The results show that the forecast model, using the combination between KRLS and TS, predicts the near-future at 1 s in the future with 2.8 % error, increasing to 6.9 % at 120 s in the future. Afterwards, the projection model, using merely KRLS, predicts the far-future up to the length of the operation horizon with an accuracy of 11.2 %, based on the weather forecast. This multi-horizon prediction of power consumption can enable the EMS to make accurate short-term decisions in the control of the power plant and to define optimal scheduling of the power plant components over the complete horizon of the DP operation.

Preface

This master thesis "Multi-Horizon Prediction of Power Consumption during Dynamic Positioning Operations: Physical, Data-Driven and Hybrid Model Approaches" is written as completion of the Master Maritime Technology at the Technical University of Delft. The knowledge gathered in this research is also highly relevant for the cooperating company, RH Marine, as this can be used to enhance their systems.

My personal affection with ships started at lower school by being put in a little sailing boat by my parents. From that moment on, my enthusiasm for the maritime world and technology in general has only grown, leading to the logical choice of studying maritime technology at the TU Delft. During the masters, the topic of dynamic positioning appealed to me, and this led to the search of a topic that is related to this. Together with Andrea Coraddu and Despoina Mitropoulou, we came to this topic, being interesting to all parties.

At first, I would like to thank my two daily supervisors, Andrea Coraddu from the TU Delft and Martijn Wittingen from RH Marine. Andrea has always offered me the opportunity to discuss points ranging from the bigger picture to rather specific questions. Martijn has given me throughout the project a critical view on my decisions, which helped me raise the level of the research. I highly appreciate their guidance and support throughout the complete research. Furthermore, I would like to express my gratitude to Jake Walker for his help towards a working model and to the team at RH Marine for their support.

Not only during this research, but during the complete studies, my parents have been of amazing support, for which I am extremely grateful. Furthermore, I would like to thank my two brothers, Ties and Skip, the rest of my family, my friends, and my roommates for hearing the stories during this research and the rest of the studies. With this thesis, being a student has come to an end for me, and I have absolutely enjoyed all elements of it, being diverse, challenging, but most of all fun.

Jens de Boer
Delft, January 2023

Contents

List of Figures

List of Tables

Abbreviations

BBM Black Box Model. 8, 9, 23

COG Centre of Gravity. ix, 14

DDM Data-Driven Model. i, 6, 9, 10, 17, 20, 22–24, 28, 34–45
DG Diesel Generator. 2, 3, 27–29, 43, 81
DOF Degrees of Freedom. viii, 11, 12, 14, 15, 77
DP Dynamic Positioning. i, v, 1–5, 9, 10, 14, 16, 17, 23, 26, 28, 30, 43–46, 79, 82

EFCM Equivalent Fuel Consumption Minimization. 2
EMS Energy Management System. i, v, 1–5, 42–46
EOM Equations of Motions. 9, 13, 14, 16, 42, 44, 45

GBM Grey Box Model. 8, 9, 22, 23

KRLS Kernel Regularized Least Squares. i, viii, ix, 9, 10, 17–19, 21–24, 26, 43–46

MAE Mean Absolute Error. 25, 35, 39
MAPE Mean Absolute Error Percentage. 25, 35, 39, 42, 45
MPC Model Predictive Control. 2, 44
MRQ Main Research Question. 1, 4, 5, 45, 46

PID Proportional Integral Derivative. v, ix, 15, 16, 42, 44, 45
PM Physical Model. i, viii, 6, 9, 10, 16, 17, 22, 23, 28, 34–36, 38, 42, 45, 79
PMS Power Management System. 2
PPMC Pearson Product Moment Correlation. vi, viii, 25, 28, 29, 34, 35

REP Relative Error Percentage. 25, 35, 39
RLS Regularized Least Squares. ix, 17–19
RMSE Root Mean Squared Error. 17, 18, 25, 35, 39
RPM Rotations per Minute. 28, 29

SRQ Sub Research Question. 1, 4–6, 45, 46

TS Time Series. i, v, ix, 9, 10, 17, 20–23, 26, 43, 45, 46

WBM White Box Model. 8, 9, 23

Nomenclature

α	Factor for scaling ship dimensions
Δ	Ship displacement
Δ^+	Amount of considered samples in the future
Δ^-	Amount of considered samples in the past
η	Earth fixed ship position in 3 DOF
γ_{curr}	Current angle relative to the ship
γ_{wave}	Mean wave angle relative to the ship
γ_{wind}	Wind angle relative to the ship
$\hat{y}_i$	Estimated value of dependent variable at moment i
$\hat{y}_i^{PM}$	Power consumption estimation of PM at moment i
λ	Regularization parameter
ν	Body fixed ship velocity in 3 DOF
ν_{max}	Maximum velocity in 3 DOF
ρ_{air}	Density of air
ρ_{sw}	Density of sea water
ρ_{x_i,x_j}	PPMC - correlation between feature x_i and x_j
σ	Kernel shape factor
τ_{env}	Net environmental forces and moment on ship
τ_{req}	Required net force and moment
$\tau_{thr,max}$	Maximum net combined thruster force in 3 DOF
τ_{thr}	Net combined thruster force in 3 DOF
A	Added mass matrix
A_L	Lateral projected area of ship above water
A_T	Transverse projected area of ship above water
A_{ij}	Hydrodynamic coefficients for $i \in \{1,2,6\} \wedge j \in \{1,2,6\}$
c	Weight vector of KRLS model
C_A	Added mass centripetal and Coriolis matrix
$c_{1,i}$	Constant for relation between thrust and rotational speed of thruster i
$c_{2,i}$	Constant for relation between power and rotational speed of thruster i
$C_{curr,i}$	Current coefficient for sway and yaw respectively for $i \in \{y, \psi\}$
c_i	Constant for relation between power and thrust of thruster i
C_{RB}	Rigid body centripetal and Coriolis matrix
$C_{wave,i}$	Wave coefficient for surge, sway and yaw respectively for $i \in \{x, y, \psi\}$
$C_{wind,i}$	Wind coefficient for surge, sway and yaw respectively for $i \in \{x, y, \psi\}$
D_L	Linear damping matrix

D_{NL}	Non-linear damping matrix
e_{pos}	Body-fixed position error
e_{vel}	Body-fixed velocity error
$f(x)$	KRLS model
$f_i(x)$	Model for forecast i samples in the future
$h(x, w)$	RLS model
H_s	Significant wave height
I_{zz}	Rotational moment of inertia around the z-axis
$k(x_i, x_j)$	Kernel function
K	Kernel matrix
k	Amount of folds in k-fold cross validation
K_d	Derivative PID gain
K_i	Integral PID gain
K_p	Proportional PID gain
L_{oa}	Overall ship length
M	Number of independent variables indexed by m
M_w	Number of independent variables with forecast availability indexed by m_w
M_{RB}	Rigid body mass matrix
N	Total amount of samples indexed by i
n	Kernel size
n_i	Rotational speed of thruster i
N_t	Number of thrusters
P_i	Power consumption of thruster i
P_{thr}	Total power consumption of all thrusters combined
Rn	Reynolds number
S	Wetted area of the hull
T	Draught of the ship
T_i	Thrust force of thruster i
T_{surge}	Typical time constant for surge motion
T_{sway}	Typical time constant for sway motion
T_{wave}	Mean wave period
T_{yaw}	Typical time constant for yaw motion
V_{curr}	Current speed
V_{wind}	Wind speed
w	Weights of RLS model
$x'(\Delta^-, \Delta^+)$	TS input
X	Set of independent variables
x_i^m	Data point at sample i of independent variable m
x_g	Longitudinal location of COG
Y	Set of dependent variables
y_i	Data point at sample i of dependent variable

1 Introduction

The environmental footprint of the maritime sector needs to be reduced in order to contribute to the limitation of the increase of the earth's temperature. DP ships nowadays emit greenhouse gasses by consuming fossil fuels during their station keeping operations. The energy efficiency of the ship is highly dependent on the system controlling the components in the power plant, the EMS. Previous research on EMS for a transit has shown high performance when optimizing over a certain period in the future. Previous research on EMS for a DP operation, however, has been limited to relatively low complexity strategies that do not take future power consumption into account. Nonetheless, including future power consumption in the EMS can significantly increase the efficiency of the system, enabling a considerable reduction of greenhouse gas emission during DP operations. The main issue, however, is that research on future power consumption during DP operations is limited. Therefore, this research aims to investigate how the power consumption during a DP operation can be predicted, such that this can be implemented in the future in an EMS to further improve energy efficiency during DP operations.

This chapter comprises the introduction and the motivation for the research by elaborating on the paragraph above. This starts with a description of the societal background in Section 1.1. Afterwards, in Section 1.2, the state-of-the-art considering EMSs is elaborated. Following from this, the research gap is described, as shown in Section 1.3. Then, the Main Research Question (MRQ) and three associated Sub Research Questions (SRQs) are formulated in Section 1.4. The research is demarcated afterwards, in Section 1.5. Lastly, the structure of this thesis is briefly described in Section 1.6.

1.1. Background

In the past century, the emission of greenhouse gasses has increased significantly, which is mainly caused by the consumption of fossil fuels [2]. As a consequence of this increase in greenhouse gasses, the temperature of the earth has been rising [2]. The ecosystem of the earth is significantly affected by this, mainly in a negative way. In order to curtail this negative impact, countries all over the world have joined their efforts to limit the increase in temperature to $2°C$ [3]. In order to achieve this, the European Union has set a goal to have a net-zero emission of greenhouse gasses by 2050 [4]. This requires all industries to become significantly more sustainable.

The maritime sector has a significant share in the emission of greenhouse gasses [5]. Therefore, measures need to be taken in order to reduce the environmental footprint of the maritime sector. Nowadays, ships are mainly powered by combustion engines that consume fossil fuels. As shore power recently only consists for 26.5 % of renewable energy [6], ships that receive their energy (partially) from shore power are also likely to be indirectly provided with fossil fuels. Therefore, to reduce the environmental footprint of the maritime sector, the energy consumption needs to be minimized.

A more specific category of the maritime sector is ships that are part of the offshore industry. The ships that operate in this industry often need to maintain position for multiple hours. The conventional method to remain

on position is to use anchors. However, keeping position with anchors requires a considerable amount of time to settle and after this, the ship is not flexible anymore in case the position would have to be changed.

Since the 1960s, DP systems have been increasingly used to maintain position [7]. This system automatically controls the thrusters to ensure the ship maintains a certain set position. Therefore, position can be set within minutes, and the ship becomes highly flexible. The downside of this is that active thrusters are used to counteract the environmental loads. Thrusters are provided with power by the power plant to operate. The power plant mainly uses fossil fuels as energy source, contributing to the emission of greenhouse gasses and thus to the increase of the earth's temperature.

The power plants on board of DP ships become increasingly complex to enable high energy efficiency. Power plants consist for example of multiple different Diesel Generator (DG)s, batteries and fuel cells. These components all have their own characteristics in terms of limitations and operational efficiency. Less advanced ships are equipped with a Power Management System (PMS), which controls the components in the power plant to ensure the grid is stable. More advanced ships are equipped with an EMS, which manages the energy in the ship on a larger scale. This more holistic way of managing the power plant enables achieving a higher energy efficiency with respect to conventional strategies.

Managing the components in the power plant is a complex task due to the large variety in possible settings. As research has shown, the benefits of an advanced power plant can only be harvested when being controlled accurately. Therefore, the importance of having an accurate EMS in a complex ship is high [8].

1.2. State-of-the-art

Maintaining position in a DP operation requires an advanced control strategy of the components in the power plant. The way these components are controlled have a significant influence on their energy efficiency, since each component has specific characteristics in terms of efficiency and operational constraints. The EMS on board of ships is responsible for the control of the power plant components and therefore has a large influence on the total energy efficiency during a DP operation [8].

A considerable number of studies has investigated methods to improve power plant efficiency by improving EMS performance. Rule-based or state-based studies required low computational effort and have shown to reach near-optimal results [9–11]. Equivalent Fuel Consumption Minimization (EFCM) strategies used optimization algorithms and also considered the mechanical impact of the control strategy on the power plant components [12–15]. More advanced strategies for the algorithm of the EMS utilized Model Predictive Control (MPC) to minimize fuel consumption for the transit of a ship [16–21]. The results of the MPC strategies, in which future states of the ship are taken into account, have shown high performance in terms of energy efficiency and other objectives in for example the reduction of wear and tear on the components in the power plant.

In an earlier stage of this research, a literature review on this topic has been performed[1]. During this research, the focus of the research has been changed, leading to the fact that the literature review is not completely applicable to this research anymore. Therefore, the complete literature review is located in Appendix A and not included in the main body of the report.

The actual research deviates at two main points from the literature review. One large focus point of the literature review is the methodology to model the physics of the DP system, while the data analytics part is small. For the actual research, multiple models are developed, being physical, data-driven, and hybrid. The literature review did not contain an extensive investigation on literature considering approaches for the latter two.

The second deviation is the assumption that the research would consist of two stages: the development of a power forecast and its implementation in an EMS. However, the extension of the development of the power forecast with data-driven and hybrid approaches extended the research in such a way that it is considered as one complete research. The implementation of the power forecast in an EMS is therefore not considered as part of this research. Nonetheless, a power forecast is only relevant once integrated in an EMS, hence research on this should be performed in the future.

[1] This thesis is the final part of the master Maritime Technology. The literature review was performed at an earlier stage of this master, as in accordance with the master guidelines. This was graded separately and is therefore not part of this thesis.

1.3. Research gap

Modern ships have a sophisticated power plant in which multiple components are included, such as multiple DGs, batteries and fuel cells. Each component has its own characteristics regarding operational constraints and efficiencies. The control of the power plant components can therefore highly affect the total performance, and thus the total energy efficiency. Controlling the power plant is a complex task, however, as the amount of settings in the power plant is large, and the optimal settings are not always evident. For this reason, EMSs have been developed to control the energy in the power plant.

A certain control setting in a certain situation could be the most efficient for that moment, but over the complete operation horizon, this may not be the most efficient setting. For example, if a wind gust will occur in one hour, then the instantaneous optimization will treat this differently than the optimization over the complete horizon. If the gust will arrive in one hour, the instantaneous optimal setting will now continue as regular, but needs to start an extra DG as soon as the wind gust arrives, which causes all DGs to run in a less efficient region. More advanced EMS strategies nowadays use indirect measures to account for fluctuations, such as reactively allowing a deviation from the reference position or aiming a certain reference state of charge of the battery. The disadvantage of these strategies, however, is the fact that the duration of the change in wind speed is not accounted for, resulting in possibly inaccurate response.

In the same situation, but with an EMS that optimizes over the complete horizon, the system can now start to charge the batteries by slightly increasing the powers of the running DGs. Then, during the wind gust, the battery can be depleted, such that no extra DG needs to be started. If no battery were part of the power plant, the system could still treat the wind gust by now moving slightly upwind and allowing to move slightly downwind during the wind gust, or take other measures within the control of the power plant. The system would treat a longer change in wind speed differently than a temporal change in wind speed. Therefore, including knowledge about the future in the EMS can result in the minimal energy consumption over the complete operating horizon.

To indicate the gap in literature, previous studies can be categorized regarding the type of EMS that has been investigated. A visual representation of this is shown in Figure 1.1. In the figure, each ball refers to a certain research and its location indicates the type of EMS that is considered. The horizontal axis specifies the type of operation that is considered in the research. At the left, a transit considers a trip from one location to another. In the middle, towing considers a tug, which has a varying operational profile. Lastly, at the right, a DP operation is considered in which the ship maintains position. Furthermore, the vertical axis signifies the sophistication of the EMS in the research. At the bottom, a basic EMS regards a system that does not optimize, but determines the configuration on a set of rules. In the middle, instantaneous optimization is performed in the EMS that calculates the optimal set points for the power plant at that particular moment. At the top, an EMS is considered that includes future knowledge to determine the optimal set points for the complete operation horizon.

The research gap follows from the figure when considering the area in which the balls are located. At the top right quadrant, no balls are located. This indicates that previous studies concerning EMSs for DP operation do not include future load in their operating strategy. However, as the EMS has a significant impact on the performance of the power plant, also during DP operations, including future load can improve performance considerably with respect to the state-of-the-art EMS during DP. The main issue for the inclusion of future load, however, is the fact that research on a prediction of power consumption is limited. Therefore, the development of a power forecast during DP operations is highly relevant.

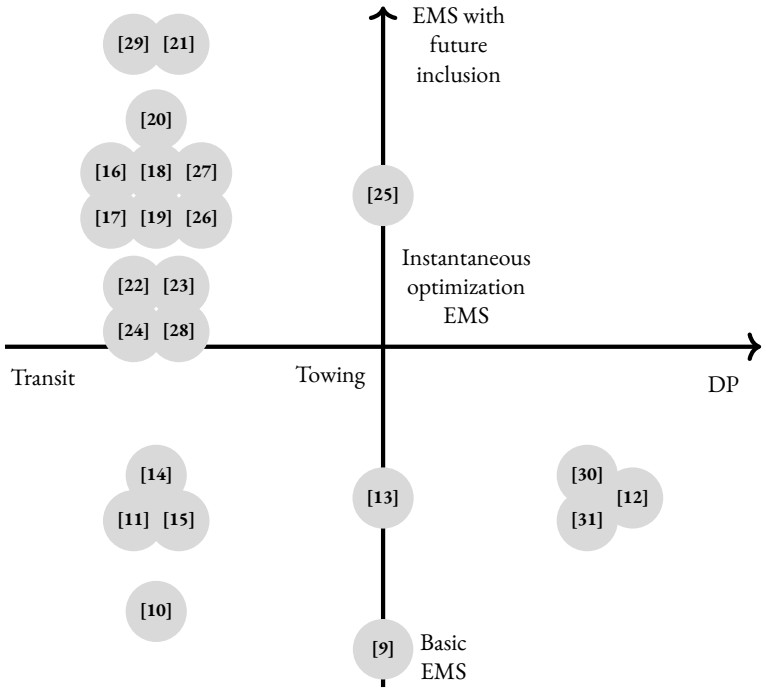

Figure 1.1: Categorization previous research regarding EMS

1.4. Research questions

The MRQ for this research stated below:

MRQ:	How can the power consumption of a dynamic positioning operation of a ship real-time be predicted most accurately?

The MRQ can be decomposed in a number of elements. Firstly, the subject of the question is *the power consumption of a dynamic positioning operation of a ship*, considering the amount of power that is consumed to keep the ship on position during a DP operation. Furthermore, the main verb in the question is *predicted*, meaning that future estimates are to be made of the power. This prediction is to be made *real-time*, meaning that the computational effort needs to be considered, such that it would be able to run live on the ship. Lastly, the performance of the prediction is determined by calculating the error and assessing which methods predict *most accurately*.

The MRQ is supported with three SRQs, which are stated below:

SRQ1:	How can the instantaneous power consumption of a DP operation be predicted?

The first SRQ aims to find a model that predicts the power consumption during a DP operation instantaneously. This means that time is irrelevant, and the power consumption is estimated based on the conditions at that moment.

SRQ2:	How can the near-future power consumption of a DP operation be predicted?

The second SRQ is one step further than the first SRQ. For this, the power consumption in the near-future is to be predicted. The length of the near-future prediction horizon is not defined in advance, but will follow from the methods. Based on the results, considering the prediction length and the accuracy, a specific application can be identified.

SRQ3:	How can the far-future power consumption of a DP operation be predicted?

The last SRQ aims to predict the power consumption for a larger time horizon, being the far-future. Again, dependent on the method, the length of this horizon can be identified. Typically, a prediction will become less accurate when predicting further in the future, and thus the added value can decrease. Therefore, the tradeoff between prediction horizon length and accuracy is taken into account when identifying the application of the far-future prediction.

1.5. Scope

This research is performed within certain boundaries to prevent extending the subject, as the time to perform the research is limited. Furthermore, by demarcating the subject, the research can be focussed on a precise development of this particular topic. The demarcation points are elaborated below.

Firstly, the power consumption prediction will only be applicable to the DP operation of a ship and not to any other operational mode. The applicability of the research is any regular DP ship, but the results are generated using one specific ship as required information and data of this ship is available and provided by RH Marine. The available data contains information about the actual power that is generated. Outside this region, no information about the power consumption is known. Therefore, the choice is made to focus on the region of the data within the range of the data. The models are developed to predict most accurately within this range, not considering their extrapolation performance.

Secondly, the dataset contains values of raw sensor measurements of the environmental conditions, but these are not combined in the data to an unambiguous set of environmental conditions. The wind measurements consist of three sensors that do not yield the same values, and no wave information is included. Therefore, the signals are combined and modified to obtain a practicable dataset for the environmental condition. Although these modifications are performed thoughtfully, the fidelity of these modifications is not questioned in this research.

Another demarcation point is considering the length of the forecast horizon. This will be in the order of magnitude of the length of the DP operation, which is assumed to be 12 hours approximately. The power consumption is highly dependent on the weather conditions. Beyond the magnitude of the length of the DP operation, the stochastic nature of the environmental conditions will increase the uncertainties, making the associated power prediction uncertain too. Furthermore, the length of the operation horizon is a logical length, as the EMS, which will eventually use this future load, should manage the components in the power plant for DP purposes throughout the complete operation horizon regardless.

A ship that is equipped with a DP system is a sophisticated ship. Therefore, the assumption is made that the ship is equipped with a weather forecast system. This weather forecast system is based on advanced meteorological models. As these models are highly sophisticated, the power consumption forecast is based on these and no forecasts of the weather are made within this research. As this research has no influence on the weather forecast, the models are only assessed on their own performance, irrespective of the accuracy of the weather forecast.

The power prediction is made to be implemented in an EMS. EMSs for DP that take future load into account are limited. The aim of this research is only to develop the power consumption prediction. The way the power prediction should be implemented in an EMS or the actual development of such an EMS is not part of this research.

1.6. Thesis structure

After the introduction, the thesis starts with an elaboration of the theoretical framework in Chapter 2. Here, the choice of methods and the development of the models are elaborated. Afterwards, in Chapter 3, the dataset is described to define the input for the models. The results following from this are presented in Chapter 4. These results are then discussed in Chapter 5 to obtain a better understanding of the performance of the models and their application. In this chapter, recommendations are also formulated for future research on this topic. Lastly, in Chapter 6, the thesis is concluded by answering the SRQs and the MRQ.

2

Theoretical Framework

This chapter contains the description of the theoretical framework of the research. Firstly, the choice of methods are described in Section 2.1, which also contains the structure of the models. Afterwards, the models, which can be categorized in three types, are individually elaborated. This starts with a description of the PMs in Section 2.2. Afterwards, in Section 2.3, the DDMs are elaborated. The last type of model is a hybrid form between the latter two, the hybrid models, as described in Section 2.4. This chapter ends with a description of the set-up of the results in Section 2.5.

2.1. Method description

This section contains the description of the methods that are used for this research. Throughout the research, a distinction is made between a forecast and a projection, which is explained in Section 2.1.1. Following from this, a choice can be made for the algorithms, which is elaborated in Section 2.1.2. Lastly, in this research, six models are made, of which the structure is described in Section 2.1.3.

2.1.1. Forecast v/s projection

The SRQs that are introduced in Section 1.4 indicate a distinction between predictions of near-future power consumption and predictions of far-future power consumption. This distinction is maintained throughout the complete research in the terminology of the models. This considers an explicit distinction between a forecast and a projection. The general difference between these terms is described in the book of Saaty and Vargas [32] as:

> "We project when we calculate the numerical value associated with a future event. We forecast [...] by relying on data of past happenings to generate or cast data for future happenings." [2]

A projection is thus the calculation of a future value by considering the conditions at that moment. This means that for the determination of the value, time is irrelevant. A requirement to develop a projection is the fact that the future conditions have to be known. The forecast, on the other hand, is based on information of past events. This is used to predict values for future events. Therefore, time is a relevant factor in a forecast.

Throughout this research, a consistency in terminology is pursued to make a clear distinction between each model. Figure 2.1 contains the general terminology. As the title of this report indicates, a *multi-horizon prediction* is made. The prediction considers the estimation of future values of the power consumption. The multi-horizon part signifies the fact that multiple horizons are considered in this research, which are two in total. The

[2] The second sentence is deviating from the one in the book, being "We forecast [...] on data of past happenings to generate or cast data for future by relying happenings.". This sentence contains a language error in the sequence of the words, thus the sentenced is changed with the minimum amount of required adaptations in order to be correct.

first horizon, the near-future, is in the order of magnitude of a few minutes. For the near-future, forecast models are developed. The second horizon regards the far-future, which is in the range between a few minutes to multiple hours. These models are considered as the projection models and take over after the forecast model horizon.

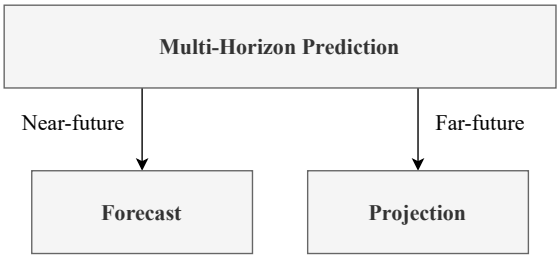

Figure 2.1: Distinction between prediction, forecast, and projection

A more elaborate visualization of the distinction between the forecast models and the projection models is shown in Figure 2.2. The figure shows an example of a graph of the power consumption over time, which is the parameter of which a prediction is to be made. The values of the past power consumption until the current moment, t_0, are known. After this, values need to be predicted, indicated by the empty diamonds. This is done for the near-future, from t_0 to t_f, using the forecast models. The forecast models use past ship states, which capture the past behaviour of the ship, to forecast the values of the power consumption. Afterwards, after t_f, the projection models are used to determine the values of the power consumption. The projection models use the weather forecast to calculate this value. The exact moment for the switch from forecast to projection model, t_f, is dependent on the performance of the models.

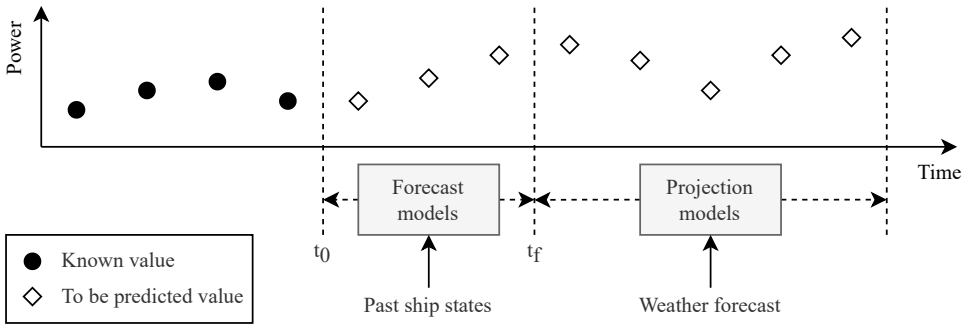

Figure 2.2: Extended distinction between forecast and projection models

In order to be consistent and to offer the same chances to each model, all forecast models are provided with the same input and all projection models are provided with the same input. This is visualized in Figure 2.3 and Figure 2.4. In these figures, each column indicates a parameter, for which the independent variables x_i for $i = \{1, ..., 7\}$ denote the environmental conditions and the dependent variable y denotes the power consumption. Each row is one moment in time, increasing when running lower in the figure. The past data, which is known, is filled black. As a weather forecast is available, these values can also be included in the figure, hence these are filled grey. Lastly, the power consumption in the future needs to be predicted, which are marked with white diamonds. The inputs for each model type is shaded green, while the output of each model is shaded blue.

First, the forecast models are considered, which is shown in Figure 2.3. The input for the forecast models can be classified in three categories. The first category is the recent past data of the environmental conditions. Then, the associated recent past power consumption is the second category. Lastly, the weather forecast at the moment in the future that is to be forecast is the last input. After using this as input for one of the forecast models, one value for the power consumption is estimated.

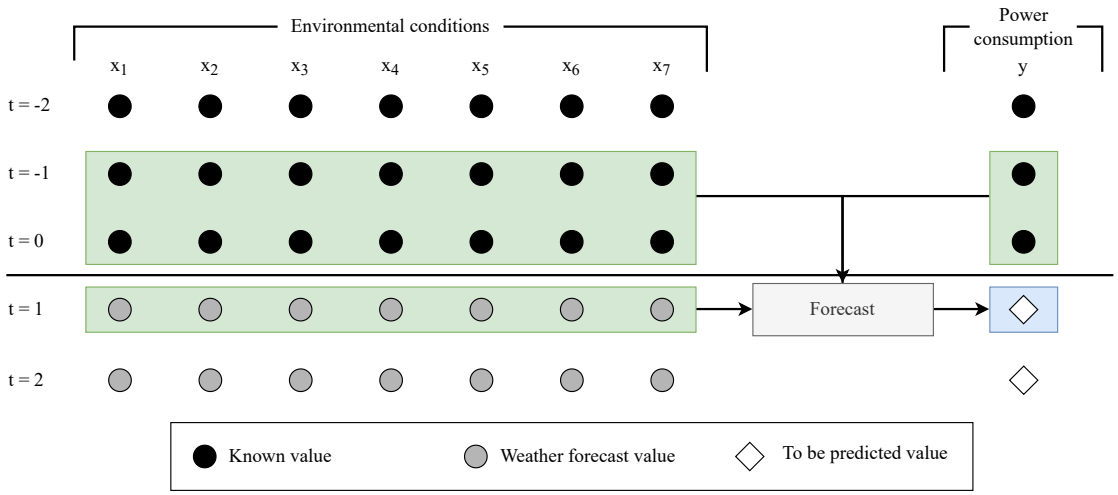

Figure 2.3: Schematic overview of input for near-future forecast models

In Figure 2.4, the schematic overview of the projection models is shown. The input for the projection models is all values for the environmental condition at one certain moment in time. The output for the projection models is the power consumption at that same moment. The models are tuned for past data to capture the instantaneous relation between environmental conditions and power consumption. As this relation is independent of time, it can be used to determine the power consumption in the future by using the weather forecast as input. This way, the power consumption in the future is a projection from the weather forecast.

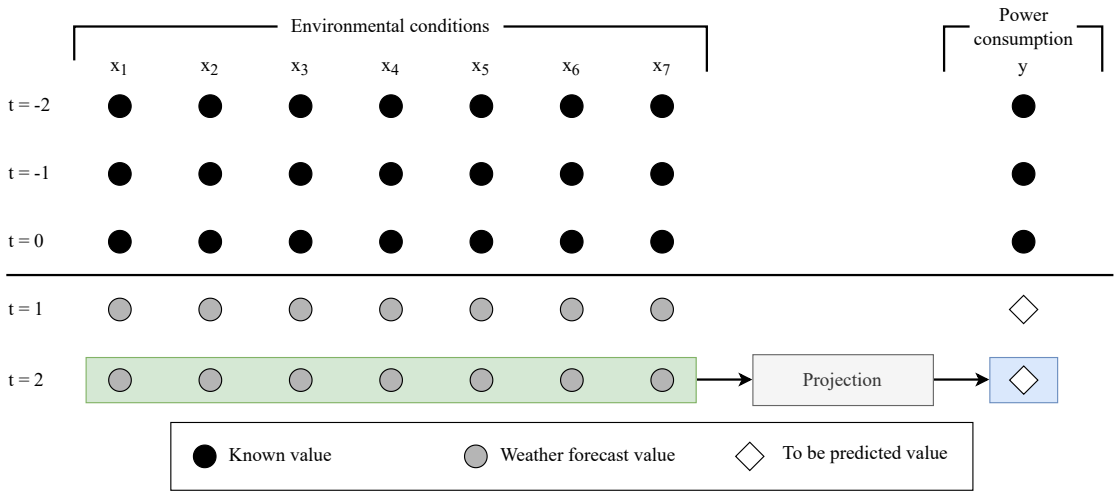

Figure 2.4: Schematic overview of input for far-future projection models

2.1.2. Choice of algorithms

Coraddu et al. [33] made a distinction between a White Box Model (WBM), a Black Box Model (BBM) and a Grey Box Model (GBM). A WBM is a model that is based on the laws of physics to capture the behaviour of the considered system. Such a model does not require a large amount of data to be tuned and is suited for extrapolation, but when operating real-time either requires high computational effort or can result in a low accuracy dependent on the complexity of the model. A BBM utilizes historical data to find the statistical relation between input and output. These models do not require knowledge about the physical system in advance and

can be highly accurate in real time. However, the development of the model requires a large amount of data and computational effort, and the accuracy can decrease significantly when extrapolating. The GBM is a hybrid form of a WBM and a BBM, and it can benefit from the advantages of both, dependent on the objective of the integration between the two. This could be to improve the extrapolation performance of the model, the requirement for a low amount of samples for tuning, increasing the accuracy, or another objective.

The distinction between the three types of models that was used by Coraddu et al. [33] is also used in this research. This is done in order to determine which model shows the highest performance to predict the power consumption during DP operations. Firstly, two PMs are made, which represent the WBMs, that differ in complexity. The first PM is a static model, in which the assumption is made that the ship does not move and that the thrusters directly counteract the environmental loads. The second PM is a dynamic model, in which the ship is moving and the control algorithm responds to the movements of the ship.

Afterwards, a choice is made for the algorithm that is used for the development of a DDM, being the BBM. When considering the choice of algorithm, one cannot expect a certain algorithm to be better than another, as stated by Ho, Pepyne, and Simaan [34]. Only when looking more specifically to the problem, an algorithm choice can be made that may be better than another. Considering the problem of this research, a prediction of the power consumption during DP operations, a certain amount of characteristics can be indicated. Firstly, the parameters that will be used as input are the environmental conditions, which are used to calculate a power. This relation is non-linear. Secondly, the dataset that is available contains approximately 280,000 samples. Therefore, the amount of samples that is to be used can be high. Furthermore, the eventual model should be developed such that it can be implemented real-time. This requires the algorithm to be low in computational complexity. Lastly, for the forecast models, future values of the power consumption are to be estimated based on behaviour in the recent past. This implicates that the sequence of samples should also be included.

Makridakis [35] states: “If we are interested in the over-time behaviour of some phenomenon, we should observe and record its states at equidistant time intervals.”. The dataset contains equidistant recordings of the state of the ship and the associated power consumption. The TS forecasting method pre-processes the data in such a way that the over time behaviour is captured using the recorded states at equidistant time intervals. Moreover, this is done in a way that requires minimal computational effort. Therefore, the choice is made to use TS forecasting to pre-process the data for the forecast models.

The performance of a forecast model at a certain point in future is dependent on the amount of past information that is included. When forecasting multiple points in the future, each will require a certain amount of information of the past to be included. This amount will typically be larger when forecasting further in the future. This results in a varying amount of inputs for each point in the future that is estimated. Therefore, a method should be implemented that is able to handle this varying amount of inputs. Hainmueller and Hazlett [36] describe in their article the KRLS method, which does not significantly increase in complexity when including more inputs. Furthermore, this method is able to include a rather large amount of input samples that are used for tuning, which is beneficial due to the large amount of samples that is available. Lastly, KRLS is based on expressing the similarity between samples and this enables capturing the non-linear relation between input and output.

2.1.3. Model structure

In this research, six models are developed, of which the structure is shown in Figure 2.5. Here, the structure as explained in Section 2.1.1 is again included. At the left, the projection models are located, which take the environmental conditions as input to determine the power consumption at the same moment. At the right, the forecast models are shown, which use past behaviour of the ship as input to calculate the power consumption a certain period ahead in the future. The models can be categorized in another way, using the horizontal shaded bars. Blue signifies the PMs, yellow considers the DDMs, and green is a combination between a PM and a DDM that become the hybrid models. In the figure, the continuous arrows signify an actual value of the estimation of power consumption is transmitted. A dashed line considers an extension of one model to obtain a new model.

As the categorization of the models is now explained, the exact model structure can be indicated. Firstly, the static model is a PM in which the assumption is made that the ship does not move, such that the thrusters directly counteract the environmental loads. The dynamic model is an extension of the static model, in which the ship is allowed to move by implementation of Equations of Motions (EOM) and a controller that determines the

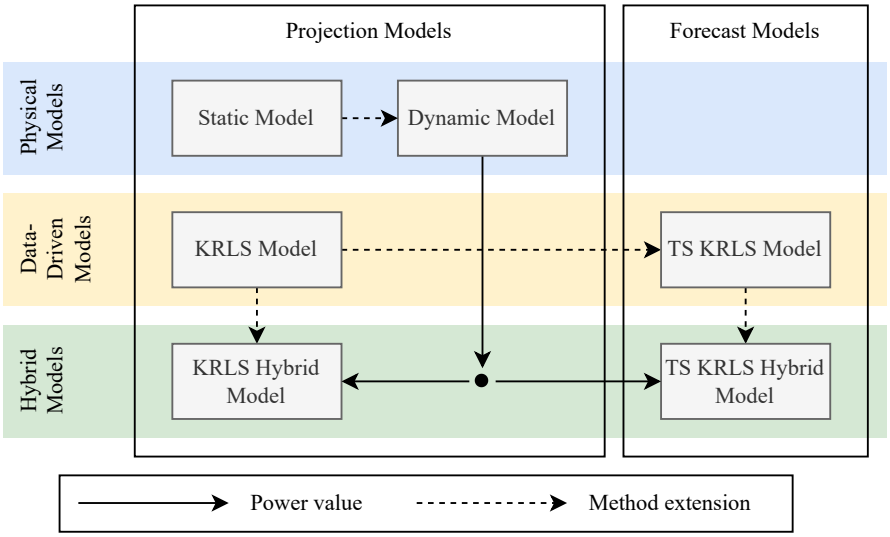

Figure 2.5: Structure of models

required forces and moment. Considering the DDMs, first, a projection model to calculate the power is made using a model based on the KRLS method described by Hainmueller and Hazlett [36]. In the DDM forecast model, the KRLS method is used again, but now integrated with a TS approach, as also used by Walker et al. [37], to obtain the forecast. Lastly, the hybrid projection model and hybrid forecast model use the methods from respectively the DDM projection and the DDM forecast. The difference, however, is found in the fact that the output of the dynamic model is also used as input of the hybrid models.

2.2. Physical models

In this section, the PMs are elaborated in two stages. At first, in Section 2.2.1, the static model is explained. Here, the assumption is made that the ship does not move during its DP operation. In Section 2.2.2 afterwards, the dynamic model is elaborated in which the motions of the ship are included. The dynamic model is an extension of the static model, so only the extensional elements are elaborated in the dynamic model section.

2.2.1. Static model

For the static model, the assumption is made that the ship does not move. This requires the loads that the environment exerts on the ship to be directly compensated by the thrusters. This results in a net force of zero, and thus in a static system. As the motion is zero, time will not affect the power consumption of the ship. Therefore, the static model can be an instantaneous model only dependent on the environmental loads acting on the ship at a certain instant.

The static model is schematically shown in Figure 2.6. The input for the model is the environmental conditions, consisting of wind, waves, and current. This input is converted into net forces that the environment exerts on the ship in the *Environmental Loads* block. Then, the *Thrust Allocation* determines the set points of the thrusters to comply with the net forces. The *Thrust to Power* block converts the thruster force into the power consumption of the thruster and by summing all, the instantaneous power consumption of the thrusters is calculated.

Figure 2.6: Static model overview

Environmental Loads
The environmental loads consist of wind, wave and current loads. Each environmental load exerts a force in surge direction and a force in sway direction, as well as a yawing moment. The environmental loads are denoted by τ_{env}, of which the components are shown in equation 2.1 and further elaborated in the subsequent paragraphs.

$$\tau_{env} = \begin{bmatrix} \tau_{env,x} \\ \tau_{env,y} \\ \tau_{env,\psi} \end{bmatrix} = \begin{bmatrix} F_{wind,x} + F_{wave,x} + F_{curr,x} \\ F_{wind,y} + F_{wave,y} + F_{curr,y} \\ M_{wind,\psi} + M_{wave,\psi} + M_{curr,\psi} \end{bmatrix} \tag{2.1}$$

Wind The wind loads are calculated using the coefficients derived by Blendermann [38], which are included in Appendix B. The wind coefficients are dependent on the angle of the wind with respect to the ship and are different for each DOF. The equations to calculate the forces and moment are shown in equation 2.2. In this, the wind speed is the actual wind speed at that moment in time. This results in the fact that the force and moment exerted by the wind are fluctuating at the same frequency as the wind speed.

$$\begin{aligned} F_{wind,x} &= \frac{1}{2}\rho_{air} C_{wind,x}(\gamma_{wind}) A_T V_{wind}^2 \\ F_{wind,y} &= \frac{1}{2}\rho_{air} C_{wind,y}(\gamma_{wind}) A_L V_{wind}^2 \\ M_{wind,\psi} &= \frac{1}{2}\rho_{air} C_{wind,\psi}(\gamma_{wind}) A_L L_{oa} V_{wind}^2 \end{aligned} \tag{2.2}$$

in which:

ρ_{air}	$[kg/m^3]$	-	Density of air
A_T	$[m^2]$	-	Transverse projected area of ship above water
A_L	$[m^2]$	-	Lateral projected area of ship above water
L_{oa}	$[m]$	-	Overall length of the ship
$C_{wind,i}$	[-]	-	Wind coefficient for surge, sway and yaw respectively for $i \in \{x, y, \psi\}$
γ_{wind}	$[rad]$	-	Wind angle relative to the ship
V_{wind}	$[m/s]$	-	Wind speed

Waves The wave loads acting on the ship are dependent on three parameters. The first parameter is the mean period of the waves that encounter the ship, for which the load will change in a non-linear way. The load will also change non-linearly dependent on the second parameter, which is the mean wave angle. The last parameter is the square of the significant wave height, which is linearly related to the wave load. As described in the book of Fossen [39], the wave loads can be divided into first order and second order wave loads. First order wave loads are in the wave frequency and have a mean value of zero. The second order wave loads are non-zero slowly varying mean wave drift forces. As the first order wave loads have zero mean, the considered wave loads are only the slowly varying loads.

A combination between wave period and wave angle results in a coefficient in each DOF. By multiplication with the square of the significant wave height, the wave load is calculated. The coefficients are scaled from a similar ship. The applicability is only for one specific ship, as the coefficients are dependent on the shape of the hull and other properties of the ship. For each DOF, a plot in 2D and in 3D of the coefficient is shown in Appendix B. The calculation of the wave loads is shown in equation 2.3.

$$\begin{aligned} F_{wave,x} &= C_{wave,x}(\gamma_{wave}, T_{wave}) H_s^2 \\ F_{wave,y} &= C_{wave,y}(\gamma_{wave}, T_{wave}) H_s^2 \\ M_{wave,\psi} &= C_{wave,\psi}(\gamma_{wave}, T_{wave}) H_s^2 \end{aligned} \tag{2.3}$$

in which:

$C_{wave,i}$	[-]	-	Wave coefficient for surge, sway and yaw respectively for $i \in \{x, y, \psi\}$
γ_{wave}	$[rad]$	-	Mean wave angle relative to the ship
T_{wave}	$[s]$	-	Mean wave period
H_s	$[m]$	-	Significant wave height

Current The current loads are calculated according to the method described by Faltinsen [40]. Regarding sway and yaw, graphs are given that indicate the value of the sway force and yaw moment based on the angle of the current with respect to the ship. These values are made non-dimensional to enable scaling. For the surge motion, the ship is a slender body and the current velocities are relatively low. This results to the fact that the frictional component of the resistance is dominant in the surge direction. Therefore, only the frictional component is used to determine the surge force of the current. The result is shown in equation 2.4.

The current loads are directly calculated from the current velocity. Therefore, these loads are fluctuating with the same frequency as the current velocity. However, the current velocity is relatively constant, and thus the current load is too.

$$\begin{aligned} F_{curr,x} &= \frac{0.075}{(log_{10}(Rn)-2)^2}\frac{1}{2}\rho_{sw}SV_{curr}^2 cos(\gamma_{curr})|cos(\gamma_{curr})| \\ F_{curr,y} &= \frac{1}{2}\rho_{sw}C_{curr,y}(\gamma_{curr})L_{oa}TV_{curr}^2 \\ M_{curr,\psi} &= \frac{1}{2}\rho_{sw}C_{curr,\psi}(\gamma_{curr})L_{oa}^2TV_{curr}^2 \end{aligned} \tag{2.4}$$

in which:

Rn	[-]	-	Reynolds number
ρ_{sw}	$[kg/m^3]$	-	Density of seawater
S	$[m^2]$	-	Wetted area of the hull
L_{oa}	$[m]$	-	Overall length of the ship
T	$[m]$	-	Draught of the ship
$C_{curr,i}$	[-]	-	Current coefficient for sway and yaw respectively for $i \in \{y, \psi\}$
γ_{curr}	$[rad]$	-	Current angle relative to the ship
V_{curr}	$[m/s]$	-	Current speed

Thrust Allocation

The thrust allocation algorithm determines the configuration in which the thrusters of the ship should be set. This configuration is based on the required force in surge and sway and the required moment in yaw. In the situation that the amount of DOF in the thruster configuration is larger than three, the system is indefinite and the amount of solutions becomes infinite. An optimization algorithm can then be implemented to determine the thruster configuration.

The optimization algorithm that is used for the thrust allocation is quadratic programming with a linearization for the azimuth thrusters. The objective function in quadratic programming is a quadratic function, enabling a minimization of the absolute value. A linearization is applied to avoid having to use a computationally expensive solver that deals with non-linear constraints. The linearization is applied for the azimuth thrusters, as each has two DOF that are coupled to each other.

The quadratic programming algorithm for this research consists of an objective function, equality constraints and non-equality constraints. A mathematical definition of the settings is shown in equation 2.5 as deduced from [41]. The variables that need to be determined, the force set point of each thruster, are denoted by x. The objective is to minimize the total absolute force provided by all thrusters combined. This is indicated as $\underset{x}{min}\ \left(\frac{1}{2}x^T H x\right)$ where H is a diagonal matrix of weights, which are all appointed equal for this research. The equality constrains, $A_{eq} \cdot x = b_{eq}$, ensure that the net force of the thrusters is equal to the input. For the static model, the input is therefore equal to the environmental loads, thus $b_{eq} = \tau_{env}$. Lastly, the non-equality constraints, represented as $A \cdot x \leq b$, ensure that the thrusters remain within their thrust boundaries and that the azimuths are not set in a configuration in which they would interfere.

Interfering would occur as one azimuth directs its outflow to another thruster, leading to a high velocity and turbulent inflow for the downstream thruster. This is prevented by excluding those regions from the solution space and defining a certain feasible space. The solution space for quadratic programming has to be convex, which is not possible when excluding certain angles from a circle. Therefore, in case of one infeasible space per thruster, two distinct optimization problems per thruster need to be defined, each capturing a different convex solution space. The optimal configuration should be chosen based on the lowest value of the objective function. This is further described by Wei et al. [42].

$$\min_{x} \left(\frac{1}{2} x^T H x \right) \quad \text{such that} \quad \begin{cases} A_{eq} \cdot x & = b_{eq}, \\ A \cdot x & \leq b \end{cases} \tag{2.5}$$

Thrust to Power

The calculation of the power consumption of a thruster is complex, but can be approximated using basic laws of physics. In reality, the power consumption is dependent on the characteristics of the electric motor, the design of the propeller, the inflow of the water, and a number of other aspects. In this research, however, the power is calculated using the basic laws of physics, as limited knowledge about the thrusters is known.

According to the laws of physics, a force is quadratically dependent on the speed. Also, a power is cubicly dependent on the speed. Using these relations, a relation between thrust and power can be determined, which is shown in equation 2.6. In this equation, the coefficient c_i can be determined based on a known operating point, the nominal values for the thrust and the power. The total power consumption of the thrusters is then calculated by taking the sum of all individual thruster powers, which is shown in equation 2.7.

$$\left.\begin{aligned} T_i &= c_{1,i} \cdot n_i^2 \\ P_i &= c_{2,i} \cdot n_i^3 \end{aligned}\right\} \quad \Rightarrow \quad P_i = c_i \cdot T_i^{3/2} \tag{2.6}$$

$$P_{thr} = \sum_{i=1}^{N_t} P_i \tag{2.7}$$

in which:

T_i	$[kN]$	-	Thrust force of thruster i
P_i	$[kW]$	-	Power consumption of thruster i
n_i	$[s^{-1}]$	-	Rotational speed of thruster i
$c_{1,i}$	[-]	-	Constant for relation between thrust and rotational speed of thruster i
$c_{2,i}$	[-]	-	Constant for relation between power and rotational speed of thruster i
c_i	[-]	-	Constant for relation between power and thrust of thruster i
P_{thr}	$[kW]$	-	Total power consumption of all thrusters combined
N_t	[-]	-	Number of thrusters

2.2.2. Dynamic model

The dynamic model is an extension of the static model, in which the motions of the ship are also considered. The schematic overview is shown in Figure 2.7, in which the components from the static moment are coloured blue. These blocks are the same for the dynamic model. The components that are added are the *Equations of Motions* (EOM), the *Controller* and the *Thruster Dynamics*, all shown in purple. In the dynamic model, the environmental loads that are exerted on the ship are not directly compensated by the thrusters. This leads to a net force and moment that is non-zero and thus an acceleration, over time a velocity and again over time a position offset. The position offset is used by the controller to determine the forces and moment that are required to regain position. The net forces and moment of the thrusters that are calculated by the thrust allocation afterwards are directed into the thruster dynamics. The result of the thruster dynamics is a net force that the thrusters exert, which is used in the EOM to calculate the motion again.

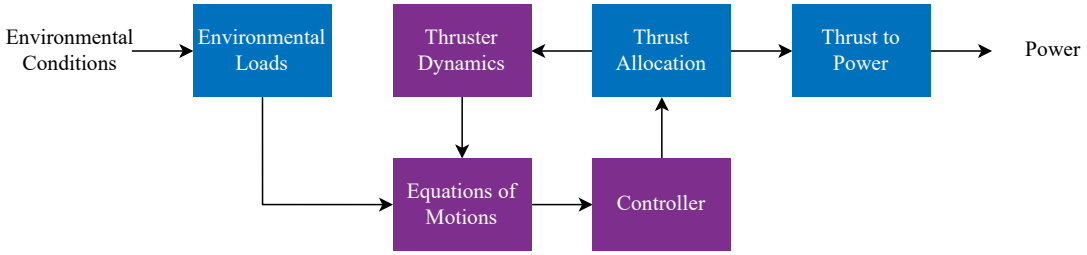

Figure 2.7: Dynamic model overview

Equations of Motions

The ship performing a DP operation is considered as a body moving in 3 DOF: surge, sway and yaw. This means that the heave, roll, and pitch motion of the ship, which contain restoring elements in the EOM, are not considered. The 3 DOF EOM for this research, which are deduced from the book of Fossen [39], are presented in equation 2.8.

$$(M_{RB} + A) \cdot \dot{\nu} + (C_{RB}(\nu) + C_A(\nu) + D_L + D_{NL}(\nu)) \cdot \nu = \tau_{env} + \tau_{thr} \tag{2.8}$$

in which:

M_{RB}	$[t]$	-	Rigid body mass matrix
A	$[t]$	-	Added mass matrix
C_{RB}	$[t/s]$	-	Rigid body centripetal and Coriolis matrix
C_A	$[t/s]$	-	Added mass centripetal and Coriolis matrix
D_L	$[t/s]$	-	Linear damping matrix
D_{NL}	$[t/s]$	-	Non-linear damping matrix
ν	$[m/s]$ / $[rad/s]$	-	Velocity in surge, sway, and yaw in body fixed frame
τ_{thr}	$[kN]$	-	Net combined thruster force in 3 DOF

For this research, the matrices from the EOM are determined based partially on the article of Berge and Fossen [43] and partially on a scaling of a similar vessel. The rigid body mass matrix M_{RB} can be calculated using basic specifications of the ship, using the displacement Δ, the rotational moment of inertia around the z-axis and the longitudinal location of the Centre of Gravity (COG) of the ship. A known added mass matrix A of a similar ship is used to determine the added mass matrix of the ship of this research. This is done by first determining the ratio between the displacements of the two ships. By taking the cubic root of this ratio, a scaling factor, α, can be determined. The added mass matrix of the ship for this research is then determined by scaling the components of translational inertia with α^3 and the components of rotational inertia with α^5 from the added mass matrix of the similar ship according to Froude scaling. The rigid body mass matrix and the added mass matrix as described by Berge and Fossen [43] are presented in equation 2.9.

$$M_{RB} = \begin{bmatrix} \Delta & 0 & 0 \\ 0 & \Delta & \Delta x_g \\ 0 & \Delta x_g & I_{zz} \end{bmatrix}, \quad A = \begin{bmatrix} -A_{11} & 0 & 0 \\ 0 & -A_{22} & -A_{26} \\ 0 & -A_{62} & -A_{66} \end{bmatrix} \tag{2.9}$$

in which:

Δ	$[t]$	-	Displacement of the ship
x_g	$[m]$	-	Longitudinal location of COG
I_{zz}	$[tm^2]$	-	Rotational moment of inertia around the z-axis
A_{ij}	$[t]$ / $[tm^2]$	-	Hydrodynamic coefficients for $i \in \{1,2,6\} \wedge j \in \{1,2,6\}$

The rigid body centripetal and Coriolis matrix, $C_{RB}(\nu)$, can also be determined using the basic specific of the ship. The scaled hydrodynamic coefficients from the added mass matrix can be used to determine the added mass centripetal and Coriolis matrix, $C_A(\nu)$. These two matrices are shown in equation 2.10 [43].

$$C_{RB} = \begin{bmatrix} 0 & 0 & -\Delta(x_g\nu_6 + \nu_2) \\ 0 & 0 & \Delta\nu_1 \\ \Delta(x_g\nu_6 + \nu_2) & -\Delta\nu_1 & 0 \end{bmatrix}$$
$$C_A = \begin{bmatrix} 0 & 0 & A_{22}\nu_2 + A_{26}\nu_6 \\ 0 & 0 & -A_{11}\nu_1 \\ -A_{22}\nu_2 - A_{26} & A_{11}\nu_1 & 0 \end{bmatrix} \tag{2.10}$$

The linear damping matrix, D_L, is deduced from the book of Fossen [39]. Linear damping consists of potential damping and frictional damping, both captured in one matrix. Only the diagonal terms are included, as those are expected to be more significant and only require limited knowledge about the ship. The linear damping matrix that is used for the model is shown in equation 2.11.

$$D_L = \begin{bmatrix} \frac{\Delta + A_{11}}{T_{surge}} & 0 & 0 \\ 0 & \frac{\Delta + A_{22}}{T_{sway}} & 0 \\ 0 & 0 & \frac{I_{zz} + A_{66}}{T_{yaw}} \end{bmatrix} \tag{2.11}$$

in which:

T_{surge}	$[s]$	-	Typical time constant for surge motion
T_{sway}	$[s]$	-	Typical time constant for sway motion
T_{yaw}	$[s]$	-	Typical time constant for yaw motion

The known value of the linear damping matrix can be used to determine the values for the non-linear damping matrix. At constant maximum forward speed, the thrusters exert maximum force to compensate for both the linear and the non-linear components of the damping. The non-linear damping component is assumed to be quadratically dependent on the velocity, as also stated by Berge and Fossen [43]. With the speed, thrust force, linear damping and the shape of the non-linear damping known, the only unknown part is the non-linear damping and this value can therefore be determined. The calculation of the non-linear damping matrix is shown in equation 2.12.

$$\begin{aligned} \tau_{thr,max} &= D_L \cdot \nu_{max} + D_{NL} \cdot \nu_{max}^2 \\ &\Downarrow \\ D_{NL} &= \frac{\tau_{thr,max} - D_L \cdot \nu_{max}}{\nu_{max}^2} \end{aligned} \tag{2.12}$$

in which:

$\tau_{thr,max}$	$[kN]$ / $[kNm]$	-	Maximum net combined thruster force in 3 DOF
ν_{max}	$[m/s]$ / $[rad/s]$	-	Maximum velocity in 3 DOF

Controller

The goal of the controller is to determine the required force to remain on position when on position and to regain position when off position. The input of the controller is the position of the ship, the velocity of the ship, the reference position and the reference velocity. By subtracting the position from the reference position, a position error is calculated. The reference velocity is calculated in advance to prevent high position derivatives, which would cause the controller to trip. Subtraction of the actual velocity from the reference velocity leads to the velocity error. The position error and the velocity error are input to a Proportional Integral Derivative (PID) controller. A schematic overview of the PID controller, which is based on the book of Fossen [39], is shown in Figure 2.8.

Equation 2.13 shows the mathematical formulation of the PID controller. The first term is the proportional term, which effectuates a force directly proportional to the position error. The second term is the integral term, resulting in a force proportional to the average error since the start of the control. The last term is the derivative

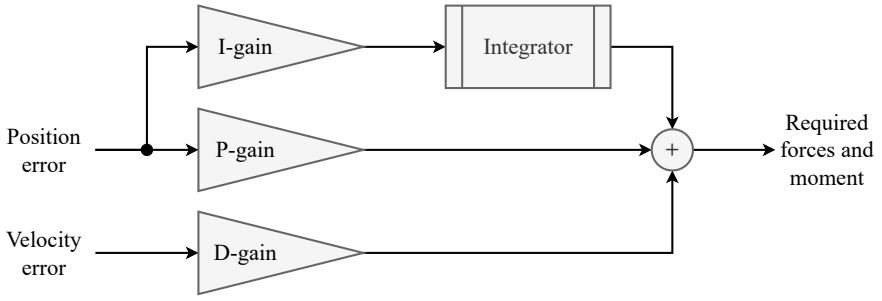

Figure 2.8: Schematic overview of PID controller

term, which is directly proportional to the velocity error. As long as the reference position does not change, this term will only result in minimizing the velocity, while a change in position will not result in significant derivative action. The contribution of each of the terms is determined by tuning the gain of each term, which is a tradeoff between the three to obtain the desired behaviour.

$$\tau_{req} = K_p e_{pos} + K_i \int_0^t e_{pos} dt + K_d e_{vel} \tag{2.13}$$

in which:

τ_{req}	$[kN]$ / $[kNm]$	-	Required net force and moment
e_{pos}	$[m]$ / $[rad]$	-	Position error
e_{vel}	$[m/s]$ / $[rad/s]$	-	Velocity error
K_p	[-]	-	Proportional gain
K_i	[-]	-	Integral gain
K_d	[-]	-	Derivative gain

The gains of the PID controller need to be tuned to obtain desired behaviour. Desired behaviour is a stable system with high station keeping performance, taking into account the fluctuations in power consumption. The PID controller of the heading is first tuned, such that the heading can be maintained during the tuning phase of the other directions. Tuning a PID controller consisted of first assigning a value for the proportional gain, K_p, in the order of magnitude in which the force was expected. Dependent on the response, this gain or one of the other gains was adjusted iteratively to eventually obtain a stable system with high station keeping performance.

Thruster Dynamics

The thruster dynamics require as input the result from the thrust allocation, which are the set points of the thrusters. The output for the thruster dynamics is a net force in surge and sway and a moment in yaw that the thrusters exert on the ship. This block accounts for the dynamics of the thrusters in a highly simplified way. In reality, the thruster dynamics are dependent on the water flow through the propeller and other specific phenomena affecting the thrust force.

For this model, however, only a few thruster limitations are implemented. Firstly, an azimuth is assumed to be able to rotate maximally 2 rotations per minute. Also, the rate at which a thruster can increase or decrease its speed is limited. The assumption is made that a thruster can change its power from 0 % to 100 % in 10 seconds. After taking these limitations into account, the net force and moment that the thrusters exert are calculated and this is forwarded to the EOM.

Simulation

All components in the PMs have to cooperate in order to estimate the power consumption correctly. As the model aims to capture an actual DP system to estimate power consumption, a large part of the correctness of the model can be verified by a station keeping simulation. Therefore, a simulation was performed, which is shown in Appendix C. The simulation shows that the ship is able to maintain position correctly. This means the model is operating correctly and indicates the power consumption, which is just one conversion step from the DP model, is correct.

2.3. Data-driven models

In this section, the methodology for the DDMs are elaborated. At this stage, the DDM is described in a way that it can predict the total power consumption without considering the PM. Furthermore, the DDM is first merely developed to predict the instantaneous power consumption and afterwards, the extension is explained which leads to the power forecast.

The methods that are selected to obtain the DDMs are based on a number of characteristics of the problem. The model needs to be tuned based on a set of samples to obtain a low error for that set. However, the model also needs to be able to estimate the power of a sample that has not been used for tuning. Both objectives can be achieved using the Regularized Least Squares (RLS) method. The linear model in the RLS method, however, will not be able to capture all effects, as a number of those are non-linear. The KRLS method is an extension of the RLS method. In this method, the relation between the independent variables and the dependent variable is captured regardless of the fact that the relation is linear or non-linear. This way, all effects can be captured, including the non-linear effects. Afterwards, a forecast over time is to be developed. The TS forecasting method uses past information to estimate a future value, which can be used in combination with the KRLS method to develop the forecast.

Each of the methods, RLS, KRLS and TS forecasting, contain a parameter that needs to be chosen based on the performance of the model. Such a parameter is called a *hyperparameter* and to determine its value, another method is required. K-fold cross validation is a method that enables evaluating the performance of the model with low bias. Three hyperparameters are introduced throughout this section, being the regularization parameter λ, the kernel shape factor σ and the amount of past samples Δ^-.

The DDMs consist of three phases. The hyperparameter selection is the first phase, in which the hyperparameters are determined. Afterwards, the tuning phase consists of tuning the model by determining the values of the weight vector c. Then, the model is made, so the results can be generated in the simulation phase.

The methods that are introduced above are elaborated in this section. The DDM projection, containing RLS and KRLS, is first explained in Section 2.3.1. Afterwards, the extension to the forecast using TS is elaborated in Section 2.3.2. Lastly, the selection of the hyperparameters using k-fold cross validation is explained in Section 2.3.3.

2.3.1. Data-driven projection

The instantaneous power consumption during DP operation needs to be estimated based on the environmental conditions using the historical data of the ship. This can be formulated into a mathematical description of the problem. The dataset contains a set of independent variables X, the environmental conditions, and a set of dependent variables Y, the consumed power. The set of independent variables consists of M independent variables sampled N times, such that $X \in \mathbb{R}^{N \times M}$. One data point is described as x_i^m, in which i is the sample indication and m the independent variable indication. Each sample in the set of independent variables x_i is related to a sample in the set of dependent variables y_i, leading the set of the dependent variable to be shaped as $Y \in \mathbb{R}^N$.

Regularized Least Squares (RLS)

A model needs to be tuned with data, which is called the *seen data*. The data that the model has not used before and thus has not affected the tuning of the model, is called *unseen data*. A model that results in low errors for the seen data, but in disproportional high errors for the unseen data, is a model that is overfit, which is also described by Bocchetti et al. [44]. Overfitting needs to be prevented, as this leads to poor predictive performance in new situations. The RLS method, which is described by Rifkin and Lippert [45], aims to find a model h with a low error while preventing overfitting. These objectives can be conflicting, so a tradeoff needs to be made between the two. Both objectives can be expressed mathematically, which is individually described below.

In the situation that a linear model is considered, each element of the input vector x is linearly scaled with a weight w. Therefore, the model can be described as $h(x, w)$ to estimate the value of the dependent variable $\hat{y}_i$ at moment i in time. The estimated value for any input needs to be as close as possible to the actual value that is related to that input. The parameter that represents the error of the estimation for this research is the Root Mean Squared Error (RMSE), which is shown in equation 2.14. This is the objective of minimizing the error.

$$RMSE = \sqrt{\frac{1}{n}\sum_{i=1}^{n}(\hat{y}_i - y_i)^2} \tag{2.14}$$

The second objective is to prevent overfitting. An aggressive tuning that is properly fit on the seen data will show large values of the weights w. When validating the model with unseen data, the error could be significantly higher. In that case, lower values of the weights w can result in lower error on the unseen data, which is regularizing the model. Therefore, the objective to prevent overfitting is the minimization of the weights w.

The relative importance of each of the two objectives needs to be determined before tuning the weights w. This ratio is mathematically expressed using a regularization parameter, λ. λ determines the relative weight between the RMSE squared and the weights w squared in the objective function. This leads to one objective, as expressed in equation 2.15.

$$\begin{aligned}\min_w \left(\frac{1}{n}\sum_{i=1}^{n}(\hat{y}_i - y_i)^2 + \lambda w^2\right) \\ = \min_w \left(\frac{1}{n}\sum_{i=1}^{n}(h(x_i, w) - y_i)^2 + \lambda w^2\right)\end{aligned} \tag{2.15}$$

The regularization parameter λ is a hyperparameter, which needs to be chosen before the calculation of the weights w. λ influences the way the model will be tuned based on the data and the eventual fit to unseen data. Therefore, the choice of λ should be dependent on the data. This choice of λ is made using the k-fold cross validation method, as explained in Section 2.3.3.

Kernel Regularized Least Squares (KRLS)
The KRLS method is an extension of the RLS method and is described by Hainmueller and Hazlett [36]. In the RLS method, the proposed model is written as $h(x, w)$. In the KRLS method, the proposed model will be $f(x)$. The model can be described as $f(x) = Kc$, in which K is a kernel matrix and c is the weight vector. The elements of the kernel matrix K are the result of the input of two data points into a kernel function, which is described by $k(x_i, x_j)$. The multiplication of the kernel matrix and the weight vector results in the estimated value of the dependent variable $\hat{y}_i$. For this, the weight vector c needs to be tuned.

A Gaussian Kernel is used, which is mathematically described in equation 2.16. In the equation, the two data points x_i and x_j are considered, which are both vectors with a length M of which the elements represent each independent variable m. Both vectors are subtracted from each other and the Euclidean norm is taken of the result. This is then squared and divided by σ squared. The exponent is always negative, leading to the fact that if the data points x_i and x_j are very dissimilar, the value of the kernel function $k(x_i, x_j)$ will run to 0. In the situation that the data points are very similar, the exponent will run to 0, leading the value of $k(x_i, x_j)$ to run to 1. The region in between these two situations is continuous, making this Gaussian Kernel to be a measure of similarity with output values in the range $0 < k(x_i, x_j) \leq 1$.

$$k(x_i, x_j) = e^{-\frac{||x_j - x_i||^2}{\sigma^2}} \tag{2.16}$$

A visualization of the shape of the Gaussian Kernel function for different values of σ is shown in Figure 2.9. At the x-axis, the adapted Euclidean distance[3] between the two data points x_i and x_j is shown. At the y-axis, the value of the output of the formula in equation 2.16 is shown. In the situation that σ has a low value, the data points x_i and x_j need to be very similar in order to provide an output value that is not close to 0. On the other hand, if σ is large, the output values tend to remain close to 1. The similarity measure is thus highly dependent on the value of σ. As this influences the performance of the model and thus the accuracy of the forecast, the choice of σ is of high importance. σ is also a hyperparameter that needs to be determined based on the data, so its value is again determined using k-fold cross validation, described in Section 2.3.3.

[3]The Euclidean distance is indicated as "adapted", as a Euclidean distance can never be smaller than 0 in $\mathbb{R}$. The negative values are included in the plot to enhance visualization and show that either x_i or x_j can be larger with respect to the other, or equal.

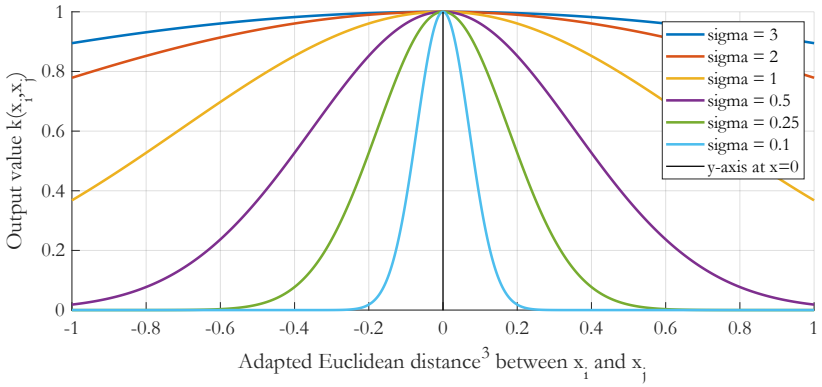

Figure 2.9: Shape of Gaussian Kernel for different values of σ

In the KRLS method, the matrix K needs to be set up, of which all elements are kernel outputs of two data points. During the phase of tuning the weights, the matrix K is a square matrix of $n \times n$. The rows are indexed with subscript i and the columns with subscript j. Both i and j vary in the range of $\{1..n\}$. At the diagonal of the matrix K, the subscripts i and j are equal, leading the output of the kernel function and thus the values at the diagonal of K to be equal to 1. The selected data points that are included in the matrix K are the data points that are to be compared to a new data point after the tuning phase. The amount of data points included, n, does affect the accuracy as a new data point can be compared to more historical data points. However, increasing n requires more computational power, which is the limitation during the hyperparameter selection phase of the model, both for calculation of weights c and due to the number of iterations during k-fold cross validation.

Tuning the weights c in the KRLS method is also described by Hainmueller and Hazlett [36]. The tuning first requires the definition of the objective function, which is slightly deviating from the objective function in the RLS method. The objective function is presented in equation 2.17.

$$\min_f \sum_i (f(x_i) - y_i)^2 + \lambda ||f||_K^2 \tag{2.17}$$

The function $f(x)$, as stated before, is defined as $f(x) = Kc$ and can be substituted in the objective function. Furthermore, $c^T Kc$ is used as regularizer $||f||_K^2$. By substituting these components in the objective function, a new objective function arises in a positive quadratic shape. By taking the derivative of this function, equalizing to zero and solving for c, the values for c that result in the minimum value for the objective function are found. This is shown in equation 2.18.

$$\begin{aligned}
(Kc - y)^2 + \lambda I c^T Kc \quad \Rightarrow \quad \frac{\partial}{\partial c} &= 2K(Kc - y) + 2\lambda IKc \\
&\Downarrow \\
0 &= 2K(Kc - y) + 2\lambda IKc \\
0 &= Kc - y + \lambda Ic \\
(K + \lambda I)c &= y \\
c &= (K + \lambda I)^{-1} y
\end{aligned} \tag{2.18}$$

At this point, the values for the weights c, corresponding to the kernel matrix K are known, which are used to determine the power of a new sample. When estimating a new sample, a new kernel matrix K needs to be set up. As stated before, the elements of the matrix K consist of the result of the kernel function $k(x_i, x_j)$. To determine the power of a new sample, the original n samples need to be used that are substituted in the kernel function as x_j. x_i is the new sample, such that size of matrix K is $[1 \times n]$ if one new sample is considered and $[s \times n]$ if s new samples are considered. Multiplication of the new kernel matrix K with the weight vector c of size $[n \times 1]$ results in the power consumption estimation.

2.3.2. Data-driven forecast

The DDM forecast is developed using the TS forecasting method. The difference between a projection and a forecast, as described in Section 2.1.1, is that the sequence in time is not relevant in a projection model, while this is relevant in a forecast model. Therefore, the forecast, as described in this section, uses the sequence of past information to forecast future values.

Time Series Forecasting

TS is a method of reshaping the input of a model to obtain a value of the dependent variable some distance ahead in the future. A schematic overview of TS is shown in Figure 2.10 as deduced from the paper of Walker et al. [37]. In the figure, the value of a number of independent variables $\{x_1, x_2, .., x_m\}$ and a dependent variable y are plotted over time. The values of the independent variables are known in the past, but are unknown for the future. For a number of independent variables, x_m in this case, a forecast of the values is available. This can be a weather forecast that forecasts the variable based on sophisticated meteorological models, which contributes to a higher accuracy of the forecast. Furthermore, two important parameters are shown, which are Δ^- and Δ^+. Δ^- is the period of past values that is included in the input. Δ^+ is the period ahead in the future that is being forecast. The blue shaded area is the input of the model, while the green shaded area is the output of the model.

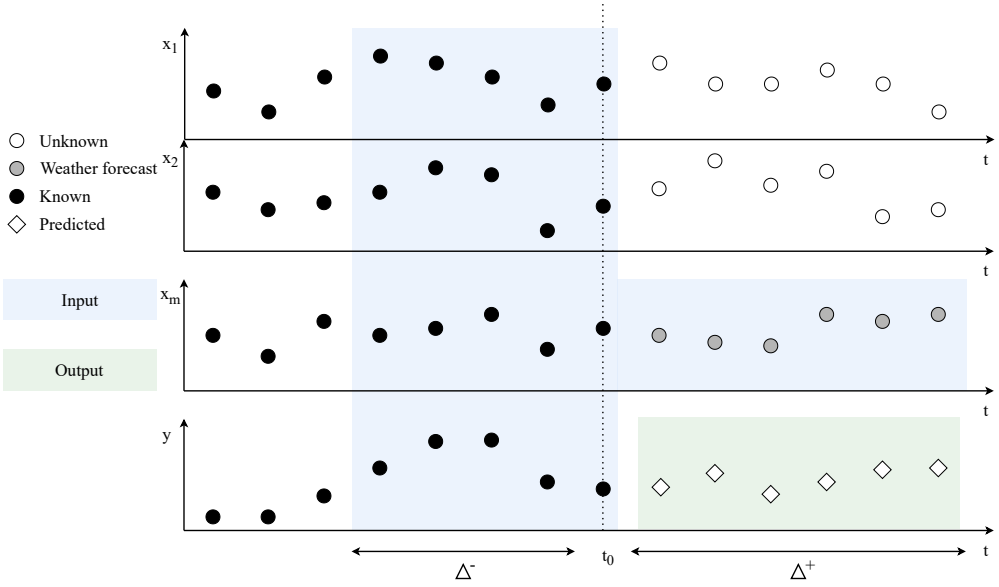

Figure 2.10: TS input and output overview

The input of the model can be categorized in three parts, which can then be formulated mathematically. The mathematical formulation of the adapted input, which is denoted at moment i in time as $x'_i(\Delta^-, \Delta^+)$, is shown in equation 2.19. The categories are:

- the values of all selected independent variables from Δ^- until the current moment.
- the values of the dependent variables from Δ^- until the current moment.
- the values of the forecast independent variables at Δ^+.

$$x'_i(\Delta^-, \Delta^+) = \begin{cases} x^m_{i-\Delta^-},\, x^m_{i-\Delta^-+1},\, ...,\, x^m_{i-1},\, x^m_i & \forall\ m \in M \\ y_{i-\Delta^-},\, y_{i-\Delta^-+1},\, ...,\, y_{i-1},\, y_i & \\ x^{m_w}_{i+\Delta^+} & \forall\ m_w \in M_w \end{cases} \tag{2.19}$$

The output of the TS method is the forecast of the dependent variable a certain period in the future. For each moment in the future from $(t+1)$ to $(t+\Delta^+)$, a new model needs to be tuned, resulting in an amount of

Δ^+ models. These models are denoted by $f_i(x)$ for $i = \{1, 2, .., \Delta^+\}$ and estimate the value of the dependent variable a certain moment i in the future, denoted by $\hat{y}_i$. The input for these models is x, which is defined by the TS method when considering a forecast, such that the models become $f_i(x'(\Delta^-, i))$. The output of the models together is the forecast of the dependent variable over time. The mathematical formulation of the models is shown in equation 2.20.

$$\begin{aligned} \hat{y}_1 &= f_1(x'(\Delta^-, 1)) \\ \hat{y}_2 &= f_2(x'(\Delta^-, 2)) \\ &\vdots \\ \hat{y}_{\Delta^+} &= f_{\Delta^+}(x'(\Delta^-, \Delta^+)) \end{aligned} \tag{2.20}$$

The period in the past that is considered, Δ^-, needs to be determined for each model, based on the performance of the model with that specific Δ^- value. Therefore, Δ^- is a hyperparameter that needs to be determined together with the other hyperparameters. The TS forecasting method with KRLS model thus requires the selection of three hyperparameters: the regularization parameter λ, the kernel shape factor σ and the amount of considered samples in the past Δ^-. This is again done using k-fold cross validation, as described in Section 2.3.3.

2.3.3. Hyperparameter selection

The models described above contain three hyperparameters that need to be chosen in the hyperparameter selection phase before tuning the actual model. The first one, λ, is the regularization parameter, which prevents the model to be overfit on the training data. The second one, σ, is the kernel shape factor, which determines the shape of the Gaussian Kernel in the KRLS method. The last one, Δ^-, is the amount of samples in the past that is considered, which is necessary for the development of a TS forecast. The values for these hyperparameters are dependent on the problem and need to be determined in a way with minimal bias. This is done using k-fold cross validation.

K-fold cross validation

The two level k-fold cross validation that is used for this research is schematically shown in figure Figure 2.11. The k-fold cross validation method as described by Kohavi [46] consists of only one level, which is in the figure shown as the high level k-fold. A low level k-fold is added for this research, as this structure has two tasks. The first one is the model selection, which is the selection of the combination of hyperparameters. The second one is the check whether the results are consistent.

At the left part of the figure, the total set of data, containing N samples, is shown in blue. This set is split up in a number of smaller sets of equal size, called *folds*. The amount of folds is k and the amount of samples per fold is N/k. Then, k iterations will be performed in which each time different samples are part of a *test set*, while the rest is part of the *learning set*. The figure shows the location of the green learning set and the yellow test set changing each iteration. The aim of implementing this structure is different for the high level and for the low level.

Each iteration at the high level, the set is split up in a learning set and a test set. The learning set is used to develop a model and the test set is used to test the performance of the model. The learning set contains again an inner loop of the low level k-fold, with an amount of $(k-1)$ folds, thus with an equal amount of samples per fold in the high level folds. The low level split is a split into a *training set*, shown in purple, and a *validation set*, shown in red. The training set is used to tune a model, which means calculating the values of the weights c in the KRLS method, for each combination of hyperparameters. Each combination of hyperparameters is then evaluated with the validation set, of which the results are recorded. This is iterated $(k-1)$ times such that $(k-1)$ results are recorded for each combination of hyperparameters. By averaging the results of each iteration, the hyperparameter combination with the lowest error can be selected. The result of the low level k-fold is thus a combination of hyperparameters that show the best results for the considered learning set.

The learning set now has a combination of hyperparameters that result in the lowest error for that set. The hyperparameter combination is tested using the test set and again, the results are recorded. This is iterated k

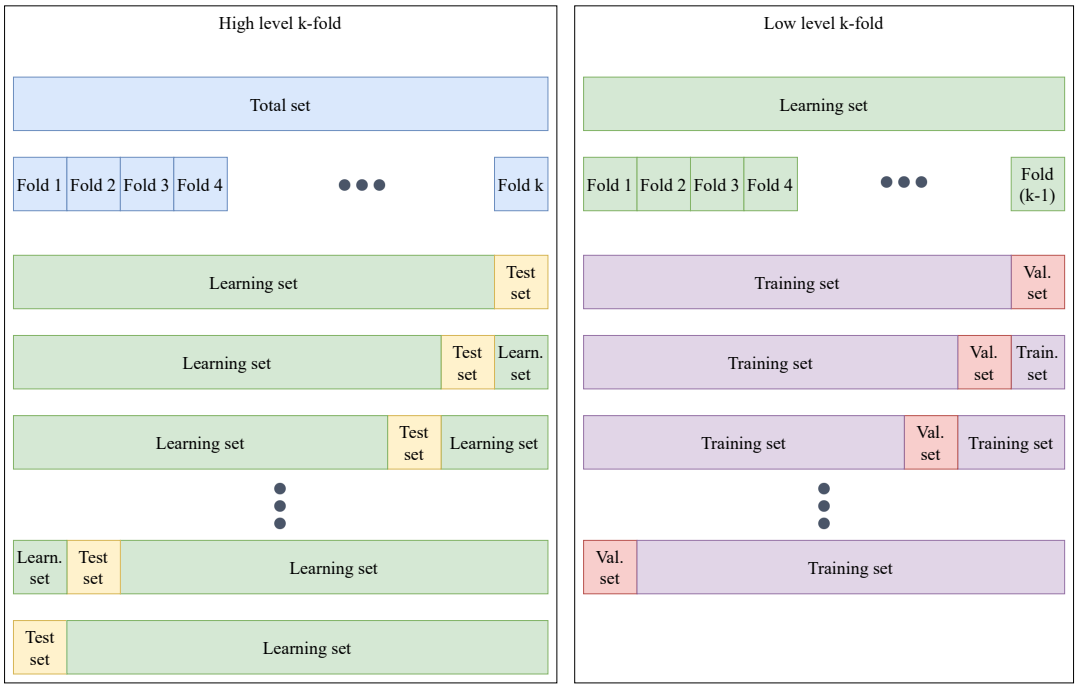

Figure 2.11: Two level k-fold cross validation diagram

times, such that k hyperparameter combinations with associated results are recorded. If the hyperparameter combinations are consistent over the iterations, then a model is found with low bias.

This process is computationally expensive, as a model needs to be tuned for each combination of hyperparameters $k \cdot (k-1)$ times. However, once the combination of hyperparameters for a model is found, the model can be tuned and the result is a model that can be implemented real-time. In the data-driven projection model, only two hyperparameters are included, and only one model needs to be developed. This does not require an excessive amount of computational effort. The computational effort, however, is more challenging when implementing a TS forecast. This is because in that situation, a third hyperparameter is included, and a new model needs to be developed for each distance in the future. For this situation, an efficient script is required, and appropriate choices need to be made in the range of the hyperparameters and the size of the kernel matrix.

2.4. Hybrid models

The hybrid models are a combination between a PM and a DDM, resulting in a GBM. A hybrid projection model is explained in Section 2.4.1. The more extensive hybrid forecast model is elaborated in Section 2.4.2.

2.4.1. Hybrid projection

The basis of the hybrid projection model is the DDM projection that is described in Section 2.3.1. KRLS is here the method that is used, which is also used for the hybrid projection. In the KRLS method, two data points are compared using a Gaussian Kernel, resulting in a measure of similarity. By including a large amount of data points, a Kernel matrix can be constructed by comparing each, which is used to determine the weight vector c. The power consumption of a new data point is then estimated by setting up a kernel vector and multiplying this with the weight vector c.

The hybrid method deviates from the DDM projection model at the input stage. The data points do not only contain values of the environmental conditions, but also the result of the PM. This way, the same method as the data-driven projection model is applied, but now including a physical element to the model, leading to a GBM. The PM that is used, is the dynamic model, as this model has a higher fidelity than the static model.

The focus in this research is on the performance of the model within the range of the data that is provided. The interpolation performance of a BBM is high with respect to a WBM. However, the extrapolation performance of a WBM is higher compared to a BBM. Integration of the BBM with the WBM to obtain a GBM can be done in multiple ways, dependent on the aim of the model. As this research is aimed at achieving the highest accuracy within the range of the data, the dynamic model is integrated by treating this only as extra input of the DDM and tuning the model again with the observed power from the data. All input, as well as the observed power, is normalized to ensure equal weights for each input and a minimization of bias in the selection of the hyperparameter selection.

2.4.2. Hybrid forecast

The hybrid forecast model shows high similarity with the hybrid projection model, apart from the fact that the dynamic model is not directly used as input for the KRLS, but considered as a feature in the TS of which a forecast exists. This way, the power consumption a certain period ahead in the near-future is estimated using the environmental conditions, the dynamic model estimation and the past power consumption. The adaptations of the input that are performed in the TS method for the DDM are described in equation 2.19. This is extended with the PM to obtain the input for the KRLS of the hybrid model, as shown in 2.21.

$$x'_i(\Delta^-, \Delta^+) = \begin{cases} x^m_{i-\Delta^-},\, x^m_{i-\Delta^-+1},\, ...,\, x^m_{i-1},\, x^m_i & \forall\, m \in M \\ y_{i-\Delta^-},\, y_{i-\Delta^-+1},\, ...,\, y_{i-1},\, y_i & \\ x^{m_w}_{i+\Delta^+} & \forall\, m_w \in M_w \\ y^{PM}_{i-\Delta^-},\, y^{PM}_{i-\Delta^-+1},\, ...,\, y^{PM}_{i-1},\, y^{PM}_i & \\ y^{PM}_{i+\Delta^+} & \end{cases} \tag{2.21}$$

2.5. Results set up

The methods described in the previous sections are integrated such that six different models exist. In order to assess the performance of the models, the results need to be generated and assessed. The models require a certain input in a specific format, which is explained in Section 2.5.1. Afterwards, the way the performance of each model is assessed is elaborated in Section 2.5.2.

2.5.1. Model set up

Each model requires a certain input to determine the value of the power consumption. As stated in Ho, Pepyne, and Simaan [34]: "the algorithms must use the same information", only equal chances for the models are given once provided with the same input information. The models can be compared equally on the performance of the method for this specific problem, future power consumption estimation during DP operation, when the same input is provided to all. Therefore, the choice is made to provide all models with the same input.

The environmental conditions would be a suited choice as input, because of their availability and their applicability. Firstly, the availability is high, as the environmental conditions can be measured and recorded on board of the ship, but also future estimations of these are available from the weather forecast. Secondly, the applicability is high, as the environmental conditions exert a force on the ship, and this force needs to be counteracted by the thrusters, which require power to do this.

The choice is therefore made to develop all models with the same input features, being the environmental conditions. This enables an equal comparison for each model, and all models are able to use these. The input features that are consistently used are shown in Table 2.1.

These features require some basic mathematical operations specific for each model. The PMs will directly use these features without any adaptation. The input for the DDMs are changed for wind and current such that the speed and angle is split into a velocity in x-direction and a velocity in y-direction. Afterwards, these vectors are normalized to ensure equal weight is given to each feature. The hybrid models require the same input as the DDMs, but only include the normalized result from the dynamic model as extra input. The forecast algorithms then require the adaptation of the input according to the TS method. The post-processing for the DDMs and the hybrid model is scaling of the normalized output to an actual power.

Number	Input feature	Symbol	Unit
1	Wind speed	V_{wind}	m/s
2	Relative wind angle	γ_{wind}	rad
3	Current speed	V_{curr}	m/s
4	Relative current angle	γ_{curr}	rad
5	Significant wave height	H_s	m
6	Mean wave period	T_{wave}	s
7	Mean relative wave angle	γ_{wave}	rad

Table 2.1: Input features

The DDMs and the hybrid models require the hyperparameters to be determined. This is an iterative process of testing the performance of each combination of hyperparameters, as described in Section 2.3.3. For this, the range of the hyperparameters from which the algorithm chooses need to be determined. The ranges are shown in Table 2.2.

	Projection models	Forecast models
λ	$\{10^{-6}, 10^{-5.8}, ..., 10^{4}\}$	$\{10^{-6}, 10^{-5.5}, ..., 10^{4}\}$
σ	$\{10^{-2}, 10^{-1.75}, ..., 10^{2}\}$	$\{10^{-3}, 10^{-2.5}, ..., 10^{3}\}$
Δ^-	-	$\{0, 2, 30, 60, 120, 240\}$

Table 2.2: Ranges for hyperparameters

The ranges for the projection models are based on the information found in literature. Regarding the projection model hyperparameter ranges, the range for λ is taken standard, as also defined by Coraddu et al. [47]. The range for σ is determined based on the article of Hainmueller and Hazlett [36]. In the article, the order of magnitude of σ^2 should be the amount of inputs of the KRLS. From this point on, multiple iterations showed a tendency to smaller values for σ and therefore the choice for the range as in Table 2.2 is chosen.

The hyperparameters for the forecast models are significantly less dense to reduce computational effort. The range for λ is equal to the projection model range, but contains only steps to the power of 0.5, instead of 0.2. Furthermore, the range for σ is slightly increased, with the same motivation of the order of magnitude as for the projection model. Its density is reduced from steps to the power of 0.25 to steps to the power of 0.5, again to reduce computational effort. The range for Δ^- is assumed equal to the range of Δ^+, with the addition of a 0 to allow no past information to be included. Due to the sampling frequency of 2 Hz, the values in this range are twice the range in seconds.

Lastly, to ensure an equal comparison can be made within all DDM and hybrid models, the kernel size is set equal for all models. The number of considered samples in the kernel n is 4000. This is determined based on multiple iterations, in which a tradeoff is made between the computational effort and the accuracy of the models.

2.5.2. Measures of accuracy

The accuracy of each model is assessed by calculation of a number of measures of accuracy. For this, each model is run with a dataset that contains at each sample both the values of the inputs from Table 2.1 and the values of the total power consumption. The estimated power consumption, based on the inputs, is compared to the power consumption, as observed onboard and included in the dataset. The performance of each model is assessed based on a number of measures of accuracy by comparing the estimated power consumption $\hat{y}$ with the observed power consumption y. These measures are enumerated below, and their mathematical expression is shown in equation 2.22.

PPMC - Pearson Product Moment Correlation
MAE - Mean Absolute Error
RMSE - Root Mean Squared Error
MAPE - Mean Absolute Error Percentage
REP - Relative Error Percentage

$$
\begin{aligned}
PPMC &= \frac{n\sum_{i=1}^{n}(\hat{y}_i \cdot y_i) - \sum_{i=1}^{n}(\hat{y}_i) \cdot \sum_{i=1}^{n}(y_i)}{(n\sum_{i=1}^{n}(\hat{y}_i)^2 - (\sum_{i=1}^{n}\hat{y}_i)^2)\,(n\sum_{i=1}^{n}(y_i)^2 - (\sum_{i=1}^{n}y_i)^2)} \\
MAE &= \frac{1}{n}\sum_{i=1}^{n}|\hat{y}_i - y_i| \\
RMSE &= \sqrt{\frac{1}{n}\sum_{i=1}^{n}(\hat{y}_i - y_i)^2} \\
MAPE &= \frac{100}{n}\sum_{i=1}^{n}\left|\frac{\hat{y}_i - y_i}{y_i}\right| \\
REP &= 100\sqrt{\frac{\sum_{i=1}^{n}(\hat{y}_i - y_i)^2}{\sum_{i=1}^{n}(y_i)^2}}
\end{aligned}
\tag{2.22}
$$

3

Data Description

This chapter provides an overview of the data that is used for this research and the actions that are taken to prepare the data for the model. At first, the main contents of the dataset and the adaptations to obtain a practicable set are presented in Section 3.1. Afterwards, in Section 3.2, the approach to obtain the power consumption data explained, as this was not directly included in the dataset. Section 3.3 provides an analysis of the main contents of the dataset. Lastly, some features are measured by multiple sensors, of which the way of integration into one signal is explained in Section 3.4. This section also contains the spread of the data that is eventually used as input for the models.

3.1. Dataset reduction

For this research, RH Marine has provided a dataset with the logging of the DP system of a DP ship. The DP ship of which the data is recorded has a length in the range of 75 - 100 m. The raw logs contain 108 h of data, in which 371 parameters were recorded at a frequency of 2 Hz. The size of the dataset was reduced such that only relevant information for the development of a power forecast is included. This resulted in a reduction both in the amount of samples and in the amount of parameters.

The dataset contained 108 h of data which was not all considering DP operation. One of the measured parameters was the indication whether the ship was in DP mode or not. Therefore, the data was removed for the periods in which the ship was not in DP operation, reducing the dataset to 39.8 h.

This reduction resulted in a discontinuous dataset. For the projection models, in which time is not relevant, this is not a problem. The dataset is therefore first reduced as described above, and the projection algorithms are run afterwards. For the forecast models, however, the time is relevant, and the reduction has to be performed at a different point in the model. The point where this is done is after the definition of the TS input and before putting this in the KRLS model. This ensures that the continuity of time is preserved, but does result in a slightly higher amount of samples that are to be removed, as outliers should be omitted if these are located anywhere between $t - \Delta^-$ and $t + \Delta^+$ for every t.

The 371 parameters that were recorded in the data were not all relevant for the power forecast. A selection was made, reducing the amount of parameters to 32. These parameters are shown in Table 3.1.

Environmental Loads and Time		Kinematics		Power Plant	
Feature	**Unit**	**Feature**	**Unit**	**Feature**	**Unit**
Time	[s]	Surge Error	[m]	Angle Azimuth 1	[rad]
Wind angle 1	[rad]	Sway Error	[m]	Speed Azimuth 1	[% rpm]
Wind angle 2	[rad]	Yaw Error	[rad]	Angle Azimuth 2	[rad]
Wind speed 1	[m/s]	Surge Velocity	[m/s]	Speed Azimuth 2	[% rpm]
Wind speed 2	[m/s]	Sway Velocity	[m/s]	Speed Bow thruster 1	[% rpm]
Wind speed 3	[m/s]	Heading	[rad]	Speed Bow thruster 2	[% rpm]
Current Angle	[rad]	Roll Angle 1	[rad]	Speed Bow thruster 3	[% rpm]
Current Speed	[m/s]	Roll Angle 2	[rad]	Power DG 1	[% kW]
		Roll Angle 3	[rad]	Power DG 2	[% kW]
		Pitch Angle 1	[rad]	Power DG 3	[% kW]
		Pitch Angle 2	[rad]	Power DG 4	[% kW]
		Pitch Angle 3	[rad]	Power DG 5	[% kW]

Table 3.1: Selected parameters from dataset

3.2. Total power

In the data, the power percentage set point of each of the five DGs is recorded. These set points are converted into the generated power that the DG provides, using the nominal power of that generator. The sum of the powers of each individual DG is the total DG power. The assumption is made that a load balance is pursued in the power grid, such that the total generated power is equal to the total consumed power on board. This assumption is made because the data does not contain more information about the power consumption in the grid. The observed power from the data, being the total generated power or total consumed power, is plotted over time in Figure 3.1.

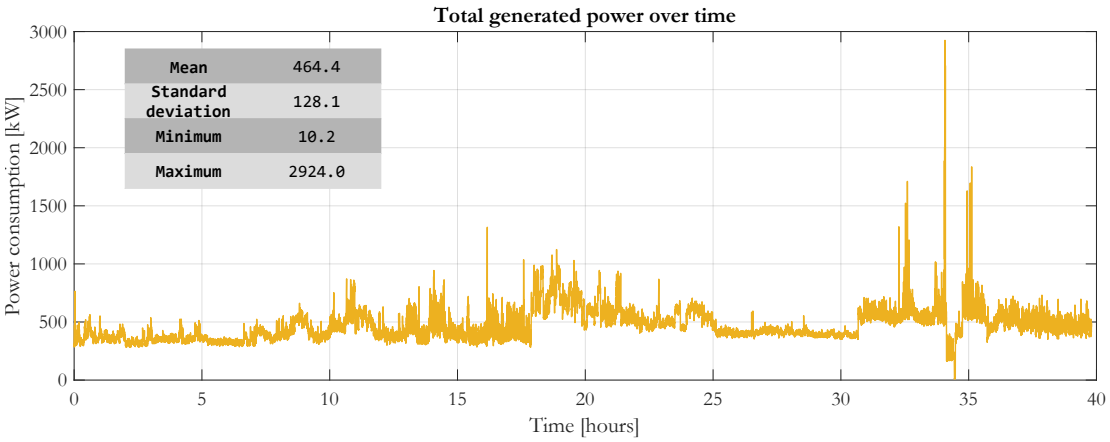

Figure 3.1: Total generated power over time

Moreover, a distinction between thruster power and auxiliary power is not included in the data, which needs to be taken into account when generating and interpreting the results. The observed power in this research is therefore the total consumed power, containing both thruster power and auxiliary power. As the auxiliary power is dependent on numerous amount of variables, such as the outside temperature, the operation that is executed and the time of the day, this is the largest uncertainty of the model.

The last factor that influences the power consumption, and is not included in the data, is the thruster bias. The thruster bias is a setting that changes the configuration of the azimuth thrusters to enable fast thruster response. A change in thrust of a thruster occurs rather slowly, which could be insufficient in some situations. The change of angle of the azimuth thrusters, on the other hand, can be effected more quickly. Therefore, thruster

bias can be added, which is setting the thrusters at a higher set point while partially directing their forces in opposite direction of each other. This results in high flexibility by only having to change the angle of the azimuths, but results in a significant waste of energy. The thruster bias mode is not included in the data, but since this mode has a significant effect on the power consumption, another uncertainty in the power forecast exists.

Each type of model is set to treat these uncertainties differently. For the PMs, a constant value of the power uncertainty of 250 kW is assumed. The DDMs and the hybrid models are developed to also account for unmodelled effects. The models are tuned using the total generated power based on the seven input features and capture the relation between those. Therefore, the expectation is that the DDMs and the hybrid models will have higher accuracy than the PMs. However, the contribution of the implementation of the PM in the hybrid model can possibly contribute to a model that outperforms the DDMs.

3.3. Dataset contents

In this section, the dataset is further explored. This is done by first presenting histograms of frequencies to show the spread of the data in Section 3.3.1. Afterwards, in Section 3.3.2, the correlation of each parameter to the observed power is analysed. Lastly, the correlation of each parameter to each other is described in Section 3.3.3.

3.3.1. Histograms of frequencies

Figure 3.2 contains a histogram of frequencies of each parameter, from which basic information about the dataset can be deduced. Firstly, the time figure shows that the data was not recorded continuously, but with a gap in between. Furthermore, considering the fact that both wind angle sensors measure the same quantity, the graphs are deviating considerably. A correspondence in the wind angle measurements is that most of the time, the wind is coming approximately from the front. The wind speed sensor 1 and 3 show rather good correspondence, while sensor 2 does not comply and contains notable outliers. The current is mainly going to port side, deducing from the current angle measurement, and is mainly of magnitude 0.1 to 0.4 m/s.

Then, considering histograms of frequencies of the kinematics, the surge error, sway error and yaw error are mainly very close to zero, with some exceptions considering the large scale of the x-axis. The exceptions are limited, as none are actually visible, and the cause is a change in the reference position and heading, automatically increasing the error suddenly. Considering the surge velocity and sway velocity, the data appears, apart from some outliers, normally distributed. The normal distribution is caused by the fact that the DP system aims to keep the ship on position, but in reality moves slightly around the reference position. The outliers are located again due to the change in set points, after which the ship will move with a constant velocity to the new position, leading to the smaller peaks further away from zero. Lastly, the roll and pitch motion, all measured by three sensors, show similar response for each feature. Apart from some outliers, these parameters are normally distributed, which is in line with the natural motion of a ship.

The third category that is included in the histograms of frequencies is the power plant. Both azimuths are mainly facing forward, which is particularly in line with the wind also mainly coming from the front. Also, the RPM set point of both azimuths are similar, which is logical considering their comparable location and the quadratic objective function of the thrust allocation algorithm. The comparable behaviour of two thrusters is also applicable to bow thruster 1 and 2 for the same reason as for the azimuths. Bow thruster 3, however, is turned off in the complete dataset. Lastly, the DG histograms show that mainly DG 1 and 4 are used and all run mostly on low power. The other DGs are mainly switched off.

3.3.2. Correlation to power consumption

The measured parameters from Table 3.1 are correlated to a certain extent to the generated power. To improve the understanding of the content of the dataset, the correlation between each feature and the generated power is calculated. The measure that is used for the expression of the correlation between two features is the PPMC, which is presented as a linear measure of accuracy between the observed and the estimated power in equation 2.22 and as correlation between two independent variables in equation 3.1. A value of the PPMC is denoted by ρ_{x_i,x_j} and varies from -1 to 0 to 1, which is the indication whether the two features are negatively correlated, not correlated, or positively correlated respectively. The result of the calculation of the PPMC of each feature with respect to the total generated power is shown in Table 3.2.

Environmental Loads and time		Kinematics		Power Plant	
Feature	**PPMC**	**Feature**	**PPMC**	**Feature**	**PPMC**
Time	-	Surge Error	-0.05	Angle Azimuth 1	-0.05
Wind angle 1	0.09	Sway Error	0.06	Speed Azimuth 1	0.41
Wind angle 2	-0.02	Yaw Error	-0.01	Angle Azimuth 2	-0.05
Wind speed 1	0.26	Surge Velocity	0.05	Speed Azimuth 2	0.41
Wind speed 2	0.30	Sway Velocity	-0.01	Speed Bow thruster 1	-0.17
Wind speed 3	0.29	Heading	-0.17	Speed Bow thruster 2	-0.16
Current Angle	-0.19	Roll Angle 1	0.03	Speed Bow thruster 3	-0.09
Current Speed	0.41	Roll Angle 2	0.03	Power DG 1	0.35
		Roll Angle 3	0.02	Power DG 2	0.02
		Pitch Angle 1	0.19	Power DG 3	0.54
		Pitch Angle 2	-0.20	Power DG 4	0.45
		Pitch Angle 3	0.20	Power DG 5	0.69

Table 3.2: Correlation of parameters and total generated power (PPMC)

$$\rho_{x_i,x_j} = \frac{n\sum_{i=1}^{n}(x_i \cdot x_j) - \sum_{i=1}^{n}(x_i) \cdot \sum_{i=1}^{n}(x_j)}{(n\sum_{i=1}^{n}(x_i)^2 - (\sum_{i=1}^{n} x_i)^2)\,(n\sum_{i=1}^{n}(x_j)^2 - (\sum_{i=1}^{n} x_j)^2)} \tag{3.1}$$

Table 3.2 shows a significant difference in correlation between the three categories of features. The environmental loads and time category shows a relatively high correlation to the power for the speed of the current and the wind. The angles, however, show low correlation, which is logical due to the fact that these are parameters between 0 and 2π that affect the power non-linearly. Then, considering the kinematics of the ship, the correlation is low again. Lastly, the power plant category shows for the azimuths a relatively high correlation, which is logical due to the fact that a higher thruster set point would require more power. The bow thrusters are less correlated due to the fact that these can operate in two directions, in which the power would both increase. The DGs show high correlation, due to the fact that the total generated power value is calculated using the set points of the individual DGs. The remarkably low value for DG 2 is due to the fact that this DG was turned off during the complete period of the dataset, which is also shown in Figure 3.2.

3.3.3. Feature correlation

The correlation of each parameter to another is shown in a table form in Figure 3.3. This table confirms the previous observations from the histograms of frequencies. Considering the wind speed sensors, sensor 1 and 3 are highly similar, while sensor 2 is deviating considerably. Furthermore, the rotational speeds of the azimuths correlate relatively high to the wind speed. Then, considering the sensors of the pitch and roll angles of the ship, the three show an unambiguous result.

Considering the power plant components, the azimuths show high correlation both in RPM and in their angle. Also, bow thruster 1 and 2 cooperate significantly, which is all the result of the thrust allocation algorithm. Another observation from the table is the fact that the azimuths mostly receive their power from DG 3. The correlation within the other DGs is very low, which is an indication that the load is not equally shared over all DGs.

To summarize, Figure 3.3 shows that the data is not linearly correlated. The methods that are elaborated in Chapter 2 are developed to treat non-linearities and are therefore able to capture the non-linearities that are observed in the correlation matrix.

3.4. Feature identification

The parameters that have been analysed in this chapter may not directly be suited as input for a model. A feature is deduced from one or multiple parameters, leading to an actual quantity that can be used in a model. Table 3.1 shows that some quantities appear more than once in the dataset. This means that multiple parameters express this quantity, which are generated by individual sensors. In order to obtain the correct value of the features such that it can be used in a model, these parameters need to be combined into one. This is then assumed to be the true value of that feature.

Three different approaches are used to determine the true value of the feature. Firstly, for the roll angle and the pitch angle, the signals are very similar, apart from a constant difference between each. The average of the three parameters is taken to determine the actual value. The second approach is applicable to the wind angle, of which only two signals exist. Both signals are decomposed in an x-component and a y-component, which are then averaged. The angle between these average values is then calculated to obtain the actual value for the wind angle. Lastly, for the wind speed, a voting algorithm is implemented as the values of the individual signals are not consistent, which is proposed in Sørensen [48]. This algorithm first determines whether one of the sensor has a faulty measurement, which is either a sudden extreme high change or a sudden value of zero. If a sensor provides a faulty measurement, the average between the other two sensors is taken. Most of the time, the sensors provide a non-faulty measurement. In that situation, the average of the two sensors that are closest to each other is taken, yet taking a transition period into account to prevent excessive switching.

The dataset does not contain any information about waves, so this needs to be deduced from the dataset. A table is used to scale the significant wave height and the mean wave period from the wind speed. This table is included in a DP capability analysis of the ship is performed by MARIN. The table is presented in Appendix E, as adopted from the capability analysis [49].

The result from the processing of the parameters to obtain feature data is shown in Figure 3.4. Firstly, Figure 3.4a at the top left considers the magnitude and the direction of which the wind is coming from. From the figure, it is clear that the ship is mostly positioned with the bow pointing towards the wind. Secondly, at the top right in Figure 3.4b, the speed and direction towards which the current is flowing is plotted. Lastly, the wave data is plotted in the figures below, Figure 3.4c and Figure 3.4d. As this data is scaled from the wind data, the similarity to the wind plot is high. The mean wave periods that the ship encountered ranged approximately between 3 and 9 s.

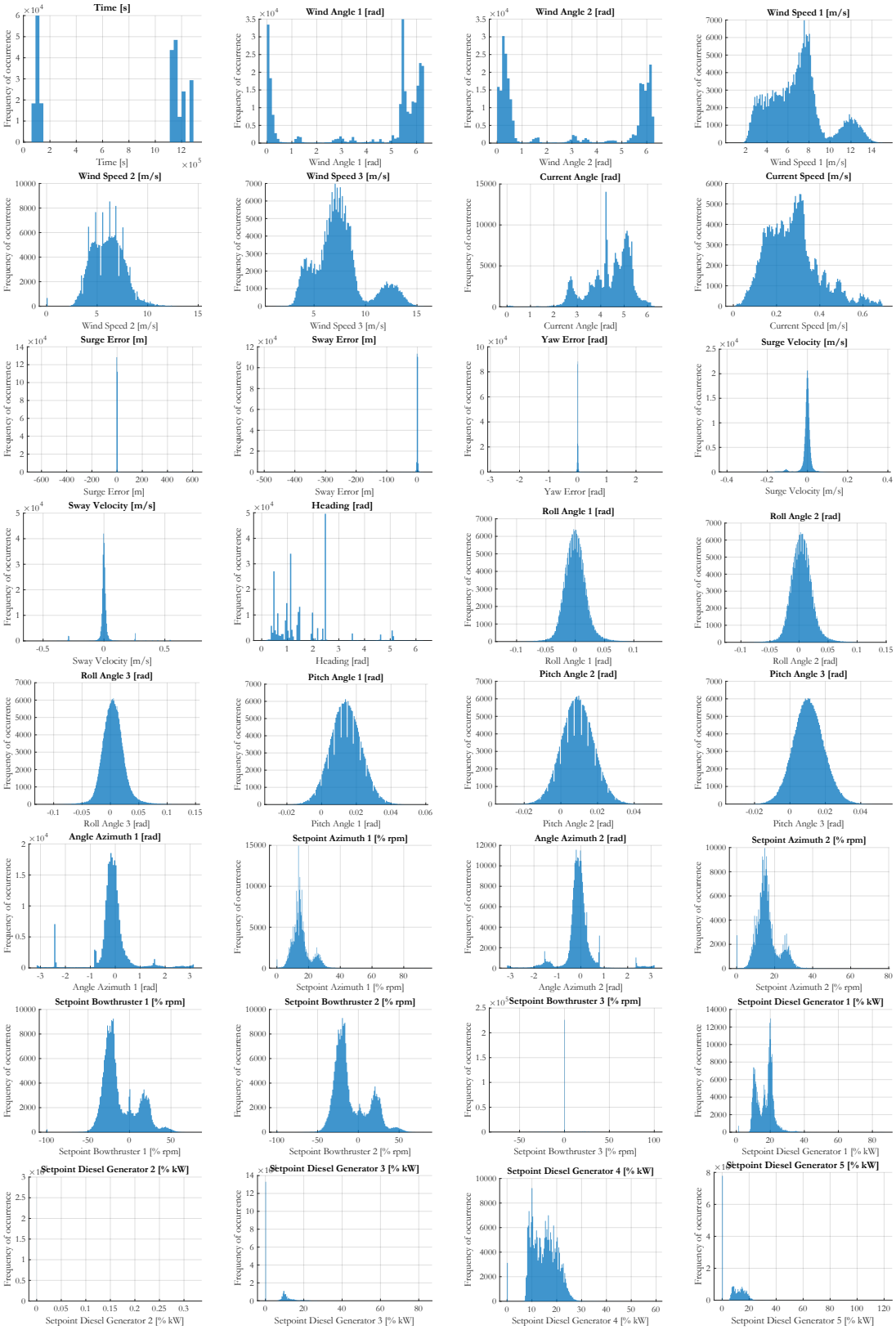

Figure 3.2: Histograms of frequencies of parameters

Figure 3.3: Correlation matrix

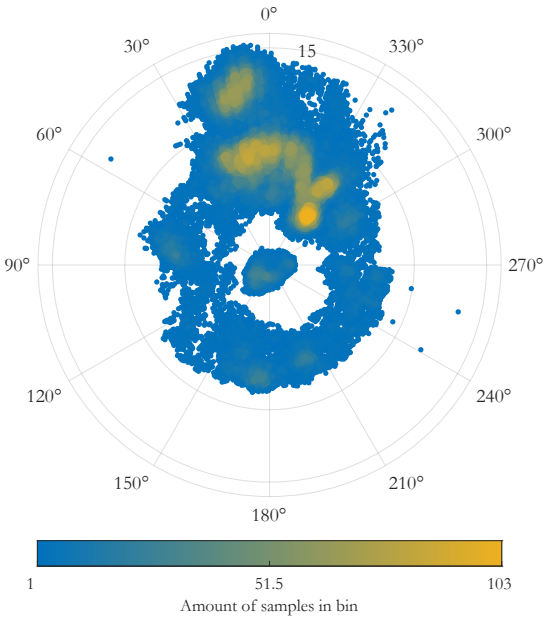

(a) Wind speed $[m/s]$ and direction distribution

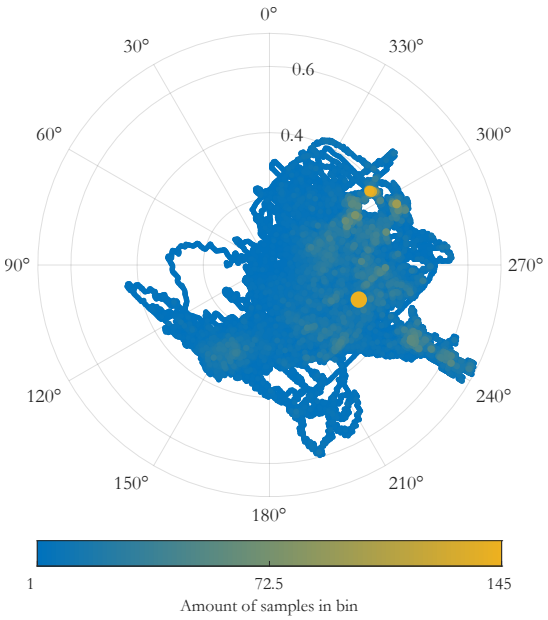

(b) Current speed $[m/s]$ and direction distribution

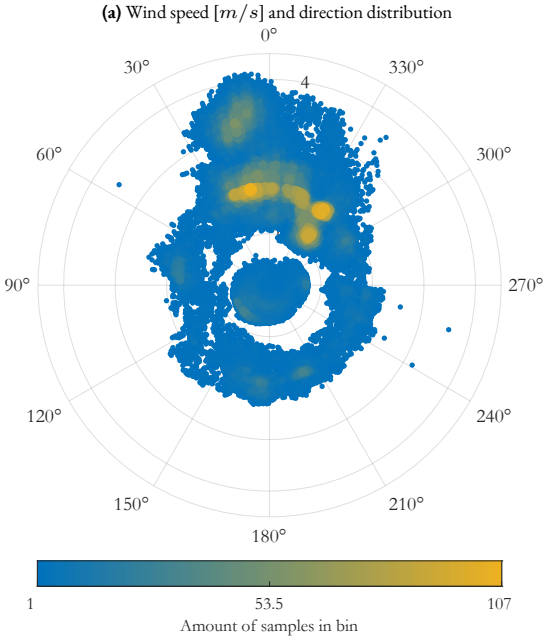

(c) Significant wave height $[m]$ and direction distribution

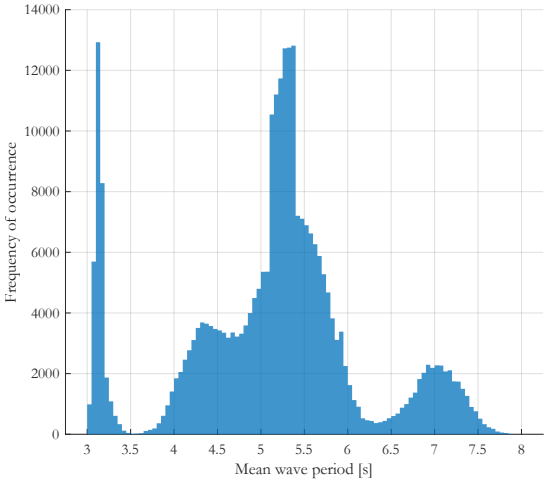

(d) Histogram of wave period

Figure 3.4: Input feature contents

4

Results

In this chapter, the results of the application of the methods described in Chapter 2 to the data as described in Chapter 3 are presented. The structure of this chapter is according to the model previously introduced structure, shown in Figure 4.1. In this figure, the models have been given a colour, which is used consistently throughout this chapter in the visualization of the results. This chapter starts with the presentation of the results of the four projection models in Section 4.1. Afterwards, in Section 4.2, the results of the two forecast models are shown.

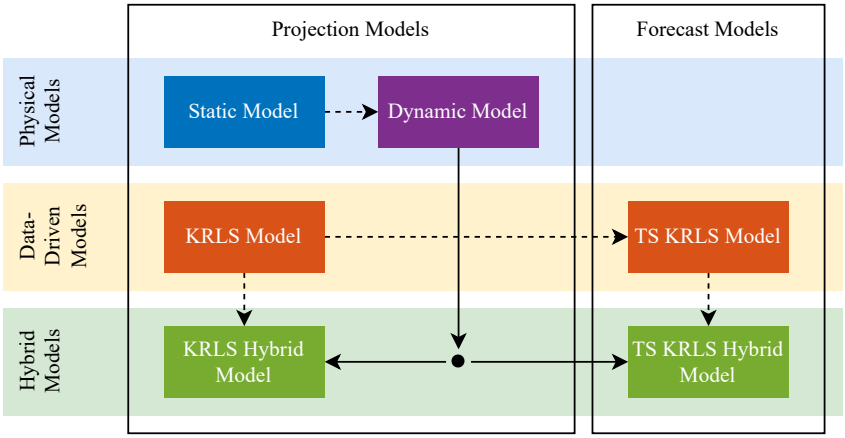

Figure 4.1: Structure of models with colour indication

4.1. Projection models

In this section, the results of the projection models are presented. This starts by elaborating on the measures of accuracy of each model, which is visualized using a bar chart. Afterwards, the distribution of the errors is further elaborated. Lastly, scatter density plots are presented to enhance understanding of the accuracy of each model.

In Table 4.1, the measures of accuracy for each model are shown. The first measure of accuracy, the PPMC, is a measure of linear correlation between the observed power and the estimated power, whereas the other measures only express the error. The PPMC values for the PMs are very similar, but the dynamic model correlates slightly higher to the observed power compared to the static model. The PPMC of the DDM shows a value that significantly outperforms the PMs. Furthermore, a slight improvement in correlation is found when including the dynamic model in the DDM, being the hybrid model. The other measures are expressions for the error specifically, rather than the more broad expressions of accuracy. These are discussed below, supported by Figure 4.2.

Model	PPMC [-]	MAE [kW]	RMSE [kW]	MAPE [%]	REP [%]
Static model	0.334	110.0	159.6	21.2	32.2
Dynamic model	0.341	112.6	163.7	21.7	33.1
DDM	0.743	53.7	85.9	11.2	17.3
Hybrid model	0.749	52.6	85.4	10.9	17.2

Table 4.1: Measures of accuracy of projection models

The last four measures of accuracy are visualized in a bar chart in Figure 4.2. These measures of error show the same behaviour regarding the performance of the models relative to the others. The PMs show similar performance, but with a slightly less accurate estimation of the dynamic model with respect to the static model, which is the opposite trend of the PPMC. The DDM estimates the power consumption with a significantly higher accuracy than the PMs. Lastly, the hybrid model, integrating the dynamic model in the DDM, results in a slightly higher performance than the regular DDM.

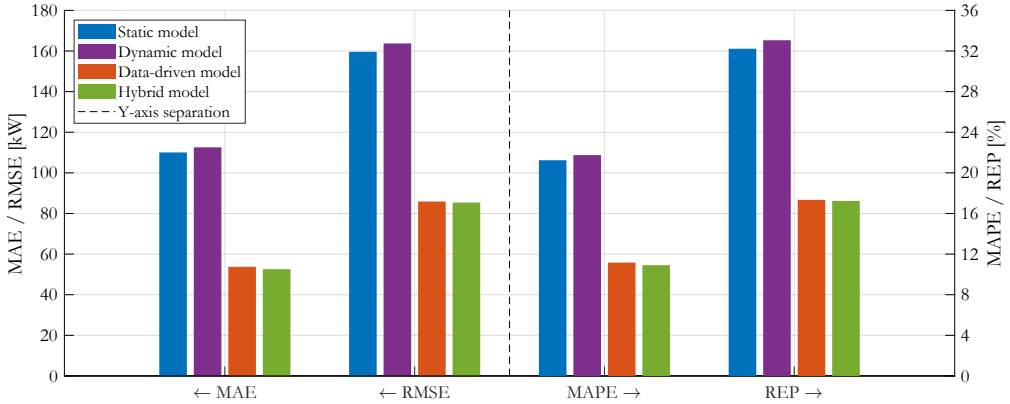

Figure 4.2: Measures of error comparison of projection models

The MAE and the MAPE are further investigated to highlight the differences in the accuracy of the models. Figure 4.3 shows the distributions of the absolute error at the left and the absolute percentage error at the right for all four models. These are divided into PMs at the top, Figure 4.3a and Figure 4.3b, and the DDM and hybrid model at the bottom, Figure 4.3c and Figure 4.3d. The horizontal axis of the bottom figures are aligned with the horizontal axis of the top figures, and equal bin sizes are taken to enable correct comparison. The vertical lines in the graphs are the mean values of the distributions of each model, being the MAE at the left and the MAPE at the right.

The results of the absolute error and the absolute percentage error distributions are complementary. The static model is again similar to the dynamic model. In the bottom figures, the shape of the distribution deviates significantly from the ones at the top. The DDM and the hybrid model have a concentration of the error closer to zero, which also results in their means to be located closer to zero. Furthermore, considering the difference between the hybrid model with respect to the DDM, the distribution is even more concentrated close to zero. The inclusion of the dynamic model has thus resulted in a slightly more accurate projection based on these figures.

The spread of the results is visualized in scatter density plots in Figure 4.4. The top figures, Figure 4.4a and Figure 4.4b, show again the PMs, while the bottom ones, Figure 4.4c and Figure 4.4d, show the DDM and the hybrid model. In each figure, the horizontal axis shows the observed power consumption, as recorded in the data, and the vertical axis shows the power that is estimated by each model. For improvement of the visualization, the figures are zoomed in to the range where the majority of the data points are located. Furthermore, the density of the points is marked as a gradient from the model specific colour towards yellow. A perfect model would result in the points being located at the diagonal line where the estimated values are equal to the observed values.

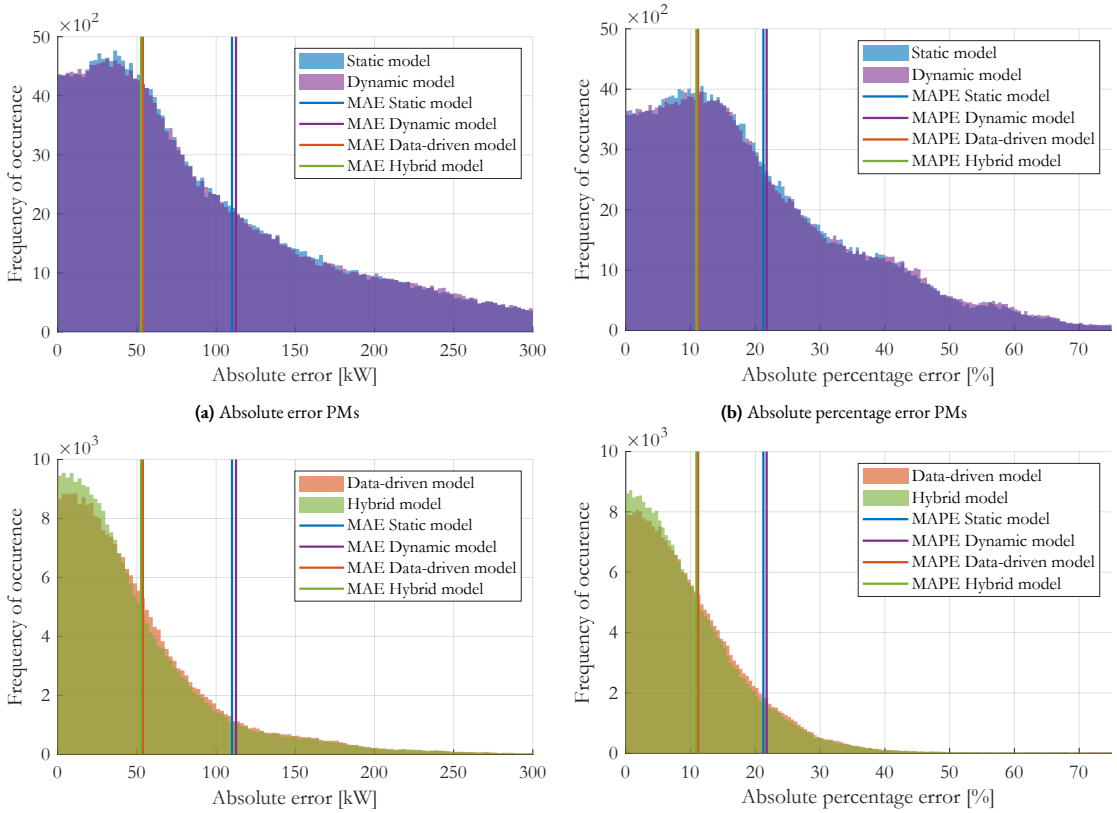

(a) Absolute error PMs

(b) Absolute percentage error PMs

(c) Absolute error DDM and hybrid model

(d) Absolute percentage error DDM and hybrid model

Figure 4.3: Distribution of errors of projection models

From the top figures, the relatively high error in the estimation of the PMs is visible, as the points are spread over the figures. The bottom figures show a more accurate estimation, as the points are more concentrated near the diagonal. Comparing the DDM with the hybrid model, the hybrid model is more spread over the figure. However, in the hybrid model, a more yellow area is located around the diagonal. This means that the hybrid model outperforms the DDM most of the time, but suffers from a decrease in accuracy caused by outliers.

The last visualization of the results of the projection models is a plot of estimated power consumption over time in comparison with the observed consumed power. Figure 4.5 shows the power over the complete dataset and an enlarged version of one hour for each model. The Figure 4.5a and Figure 4.5c consider the PMs, while Figure 4.5b and Figure 4.5d consider the DDM and hybrid model. Using the observed power, shown in yellow, for comparison, the performance of each model is clearly visible.

Firstly, the large time horizon, shown in Figure 4.5a and Figure 4.5b, is considered. Both the static model and the dynamic model, in Figure 4.5a, show large similarity, only the dynamic model is less sensitive to fluctuations. Both models, however, deviate considerably from the observed power. The DDM in Figure 4.5b, on the other hand, is able to approximate the observed power rather accurately, as well as the hybrid model.

Considering the enlarged graphs, the behaviour of the models is even more clear. Again, the dynamic model is consistently in the order of magnitude of the static model, but fluctuates less, as shown in Figure 4.5c. Their accuracy, however, is at the first half of the hour very low, as the power is highly overestimated. Afterwards, in the second half of the hour, the PMs are slightly underestimating the observed power. The DDM and the hybrid model, on the other hand, do capture the correct trend, also in the enlarged graph, which is shown in Figure 4.5d. The DDM in particular is also able to follow the observed power during transients, which is shown at $t = 8.55h$ and between $t = 8.9h$ and $t = 9.0h$. The hybrid model shows a larger deviation during transients and is fluctuating more in than the DDM.

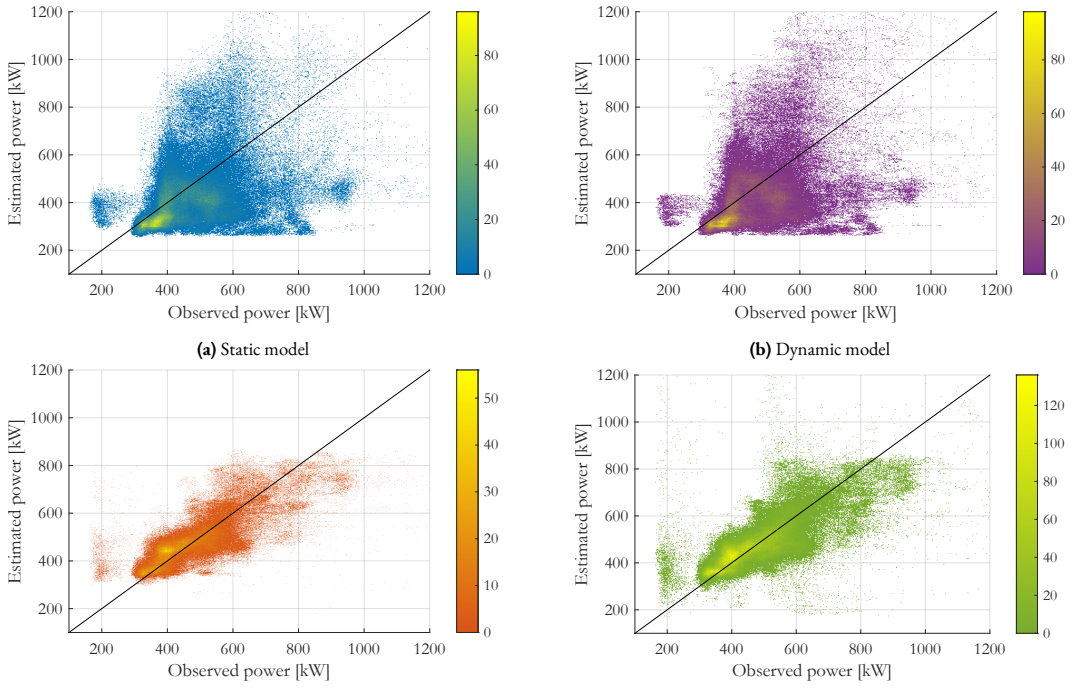

(a) Static model

(b) Dynamic model

(c) DDM

(d) Hybrid model

Figure 4.4: Scatter density plots of projection models

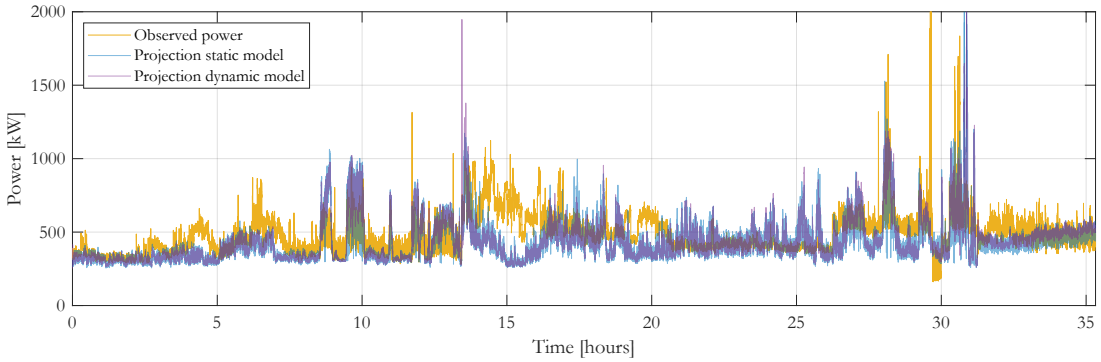

(a) Power over time PMs

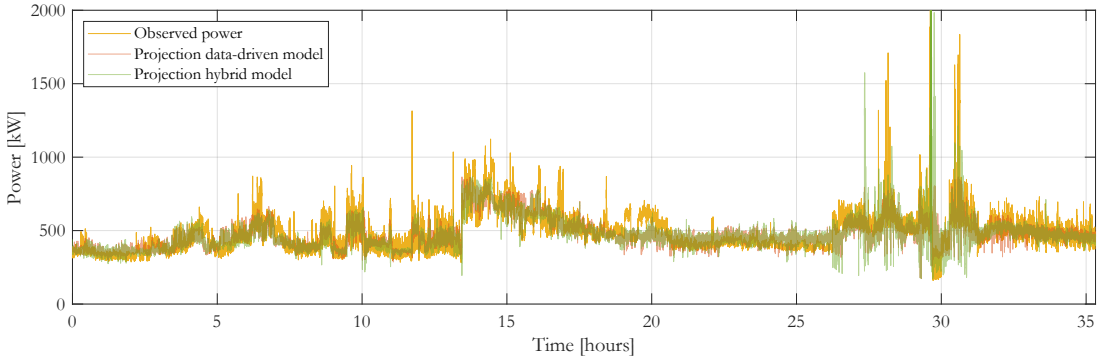

(b) Power over time DDM and hybrid model

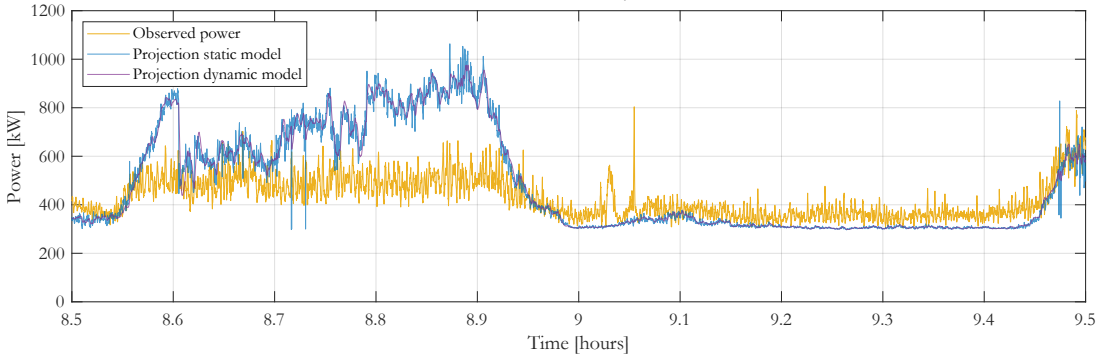

(c) Power over time PMs - enlarged

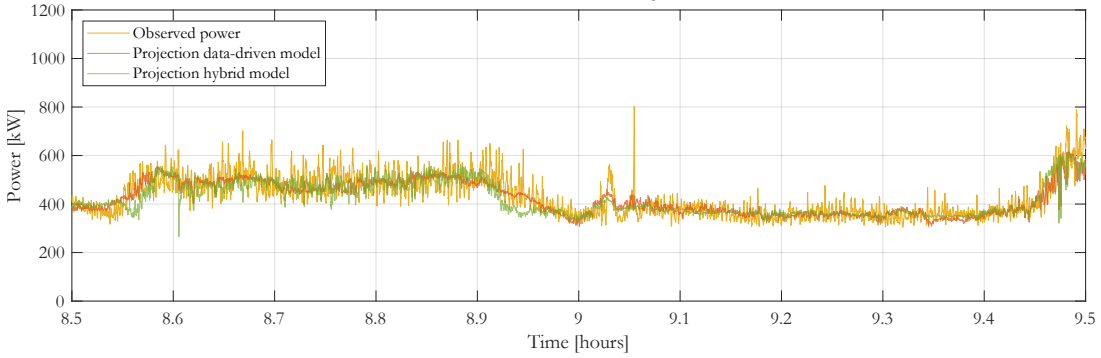

(d) Power over time DDM and hybrid model - enlarged

Figure 4.5: Power over time comparison of projection models to observed power

4.2. Forecast models

This section contains the results of the model selection, tuning, and simulation of the forecast models. Firstly, the measures of error for the DDM and the hybrid forecast model are presented. Afterwards, a visualization of the error over the forecast length is shown. Then, the evolvement of the accuracy is elaborated using scatter density plots for each model. Lastly, an example plot over time is presented.

Table 4.2 contains the values of the four measures of error for the DDM and the hybrid forecast model for each forecast horizon. The values of the measures of error are very similar for the DDM and the hybrid model. The general trend is an increase of the error as a point further in the future is estimated.

Forecast length [s]	MAE [kW]		RMSE [kW]		MAPE [%]		REP [%]	
	DDM	Hybrid	DDM	Hybrid	DDM	Hybrid	DDM	Hybrid
$\Delta^+ = 1$	12.2	12.1	19.8	19.5	2.8	2.9	4.1	4.0
$\Delta^+ = 15$	25.4	26.0	54.7	50.4	6.0	6.1	11.3	10.5
$\Delta^+ = 30$	27.2	30.1	56.7	56.9	6.4	7.4	11.8	11.8
$\Delta^+ = 60$	29.8	30.3	59.7	55.1	6.8	7.1	12.4	11.4
$\Delta^+ = 120$	31.1	30.6	59.0	55.5	6.9	6.8	12.2	11.5

Table 4.2: Measures of error of forecast models

The values of the measures of error can be plotted over forecast length to show the evolvement of the errors, which is done in Figure 4.6. This is shown for the MAE in Figure 4.6a, the RMSE in Figure 4.6b, the MAPE in Figure 4.6c and for the REP in Figure 4.6d. The orange lines consider the DDM and the green lines consider the hybrid model. The dashed lines are the associated values of the prediction models from Section 4.1. This is shown here to indicate the accuracy of the forecast models with respect to the prediction models.

The accuracies of the forecast models decrease generally when forecasting further in the future. The evolvement of the accuracy, however, is slightly different for each measure of error. Considering the estimates of 30 s, 60 s and 120 s in the future, the accuracy remains relatively constant. When comparing the lines of the DDM forecast and the hybrid forecast, the performance is very similar. Comparing the forecast models to the prediction models, the error is always significantly lower.

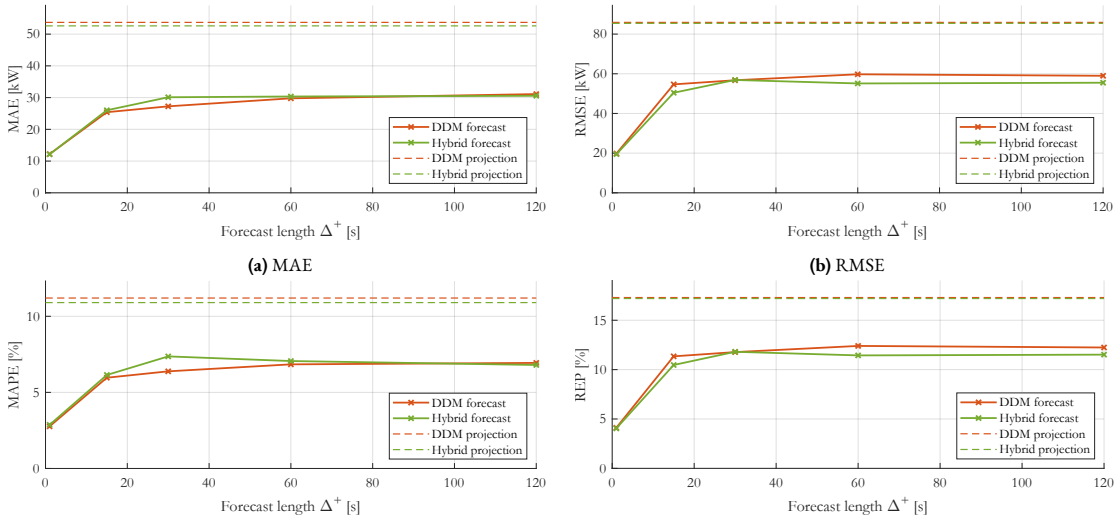

(a) MAE **(b)** RMSE **(c)** MAPE **(d)** REP

Figure 4.6: Measures of error over forecast length of forecast models

The scatter density plots for the DDM and the hybrid model forecasts are shown in Figure 4.7 and Figure 4.8 respectively. The orange scattered figures consider the DDM forecasts, and the green scattered figures consider the hybrid forecasts. Yellow areas represent the highest concentration of points in that figure, which changes gradually towards either orange or green as the density decreases. Each scatter plot is the result of a single model that forecasts a certain Δ^+ in the future.

The decrease in accuracy as the forecast length increases is also visible in the scatter density plots for both forecast models. For $\Delta^+ = 1$, the points are highly concentrated around the diagonal, implying the estimations to match the observations accurately. The points are more scattered as the forecast length increases, although still containing the highest concentration, marked with yellow, at the diagonal.

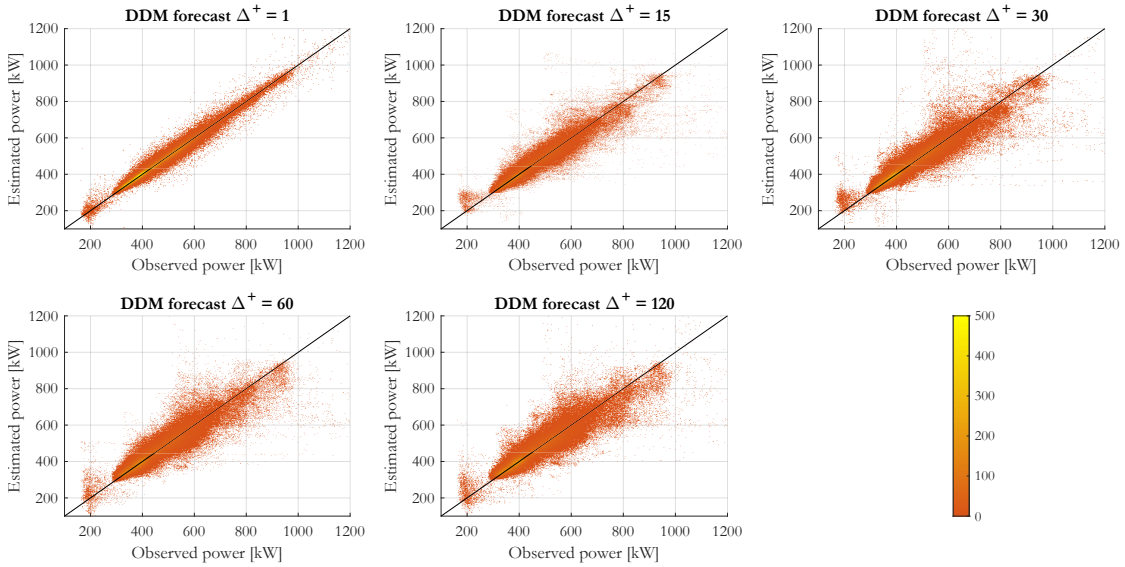

Figure 4.7: Scatter density plots of data-driven forecast

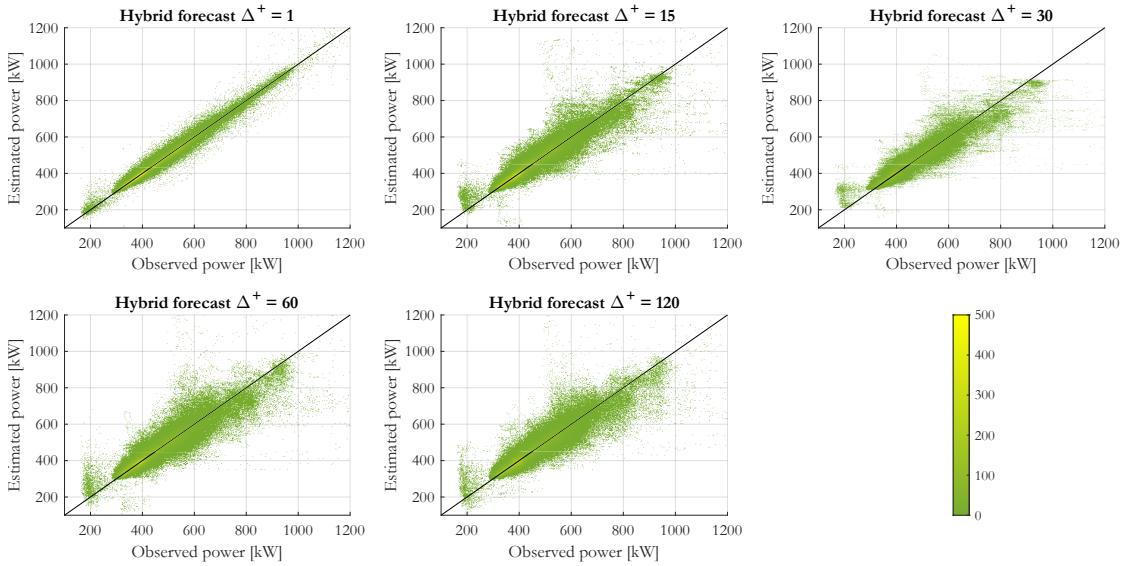

Figure 4.8: Scatter density plots of hybrid forecast

The last visualization of the performance is again the power over time, which is shown in Figure 4.9. The length of the time horizon is smaller than the one of the projection models, due to the nature of the model. The projection models are developed for the long term and are merely based on the weather forecast to estimate the power, while the forecast models are dependent on recent behaviour. In the figure, the yellow line is again the observed power, while the orange and the green line are distinct forecasts of the DDM and the hybrid model, respectively. Five points are considered, from which a forecast is made certain periods ahead in the future, Δ^+, which are $\{1, 15, 30, 60, 120\}s$.

The graph clearly shows the short-term behaviour of the models, which is the core of the forecast models. In the start of each forecast, 1 s and 15 s in particular, the models are able to capture the high frequency fluctuation. When forecasting further in the future, up until 120 s, the overall trend is correctly captured. A deviation is found, however, when comparing the DDM with the hybrid model. The DDM captures the behaviour of the observed power slightly more accurate than the hybrid model.

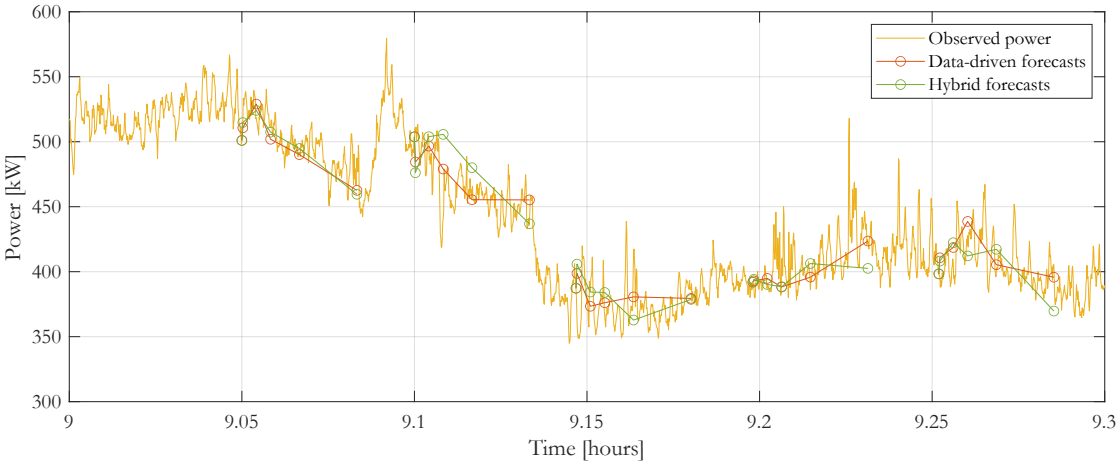

Figure 4.9: Examples of power over time of forecast models

5

Discussion and Recommendations

In Chapter 4, the results of each of the six models were presented and described. This chapter continues on the results by first further discussing and interpreting the results, which is done in Section 5.1. Afterwards, in Section 5.2, the connection to the implementation in an EMS is made, as this is the initial motivation of developing a power forecast. The last part of this chapter describes recommendations for further research in Section 5.3.

5.1. Discussion

This section starts with an elaboration on the results of the PMs. Afterwards, this is put in a larger perspective by including the DDM projection and the hybrid projection. Then, the forecast models are added to the comparison to obtain an overall view of the results and to determine the way the models are integrated for a long-term forecast.

The accuracy of the static model is slightly higher than the dynamic model for each measure of error. As the dynamic model captures more of the physics of the actual system, this is contradicting. A reason for this is that the dynamic model contains significantly more uncertainties than the static model. The EOM contain matrices with values that are scaled from a similar ship. This leads to reasonable behaviour, but also to a deviation from the actual behaviour. The PID controller needs to respond to the behaviour of the ship, so a deviating behaviour will lead to deviating controller response.

Furthermore, the implemented controller is a PID controller that is tuned with only one setting to capture the complete range of environmental conditions from the data. In the actual system, the controller is a significantly more advanced algorithm that pre-processes the signal. This was not available for this research, thus the response and the associated power consumption also deviate. As explained in Section 2.2, the PID controller was tuned iteratively. Each time that stable and reasonable behaviour was achieved, the error of the power consumption was calculated. The results from the iterations showed that the power consumption was not highly affected by the settings of the PID controllers. The error of the dynamic model power estimation with respect to the observed power was in the range of approximately 20 tot 25 % error (MAPE), in which the eventual model was 21.7 %.

As mentioned in Section 4.1, the scatter density plots of the DDM projection and the hybrid projection deviate. This deviation was particularly visible in the spread of the data points. The hybrid model had a larger spread and a stronger density at the diagonal with respect to the DDM of which the net results showed a slightly higher accuracy for the hybrid model. As the only difference between the two models is the inclusion of the dynamic model, this is also the cause for the deviation. The spread of the dynamic model is high and as equal weight is given to each of the input features, the inaccuracy of the dynamic model affects the hybrid model too. Within regular behaviour, the dynamic model was able to improve the hybrid model, but at deviating conditions, the dynamic model negatively affected the hybrid model performance.

Throughout the results, the DDMs perform very similar to the hybrid models. Thus, including the dynamic model in a DDM to obtain a hybrid model does not result in significantly higher accuracy. The environmental conditions, as input of the models, however, are dependent on a weather forecast, which has its own accuracy too. The combination between the accuracy of the weather forecast and the accuracy of the power consumption estimation decreases the relevance of the decimal digits of the errors. As the error values of the DDMs and the hybrid models are approximately equal, the choice should not merely be based on the accuracy of the models. Another relevant aspect of the performance of a model is the model complexity. The inclusion of the dynamic model does lead to additional computational complexity. Therefore, choice should be made to use the DDMs for the estimating future values of the power consumption.

The measures of error for the forecast models show that the accuracy at 120 s in the future is similar to the forecasts at 60 s and 30 s. This is counterintuitive, as an estimation of a point further in the future should be less accurate than an estimation of a point nearer in the future. The expectation is that this is caused by two limitations in the models. Firstly, the observed power throughout the complete research is total generated power, including auxiliary load. The auxiliary load is dependent on significantly more variables than merely the environmental conditions, such that the model was not able to estimate the power consumption correctly and the accuracy decreased already significantly at 30 s in the future. Secondly, the size of the kernel, which was set for these results at 4000, may not be sufficient to capture the behaviour accurately. A kernel size of 4000 was chosen as the result of a tradeoff between accuracy and computational complexity.

Apart from the forecast models for 30, 60 and 120 s distinctly, the forecast models generally decrease in accuracy when forecasting further in the future. This is a logical trend, as the states of the ship in the recent past become less relevant when forecasting a point further in the future. At a certain point of future estimation, the recent past will become less relevant in such a way that the projection model will outperform the forecast model. From that point on, the future values of the power consumption should be estimated by the projection model. The exact point to switch from forecast model to projection model should be when the projection model outperforms the forecast model. This point, however, is not known yet, as the forecast is made up to 120 s, for computational complexity reasons, at which the forecast is still more accurate than the projection model.

Considering a bigger picture, the choice for the forecast models in the near-future and the projection models for the far-future is also a logical choice. The reason for this is that the recent past behaviour of the local environmental conditions, as measured on board, and the power consumption are highly relevant in the near-future. This is because the exact situation the ship is experiencing at a certain moment can be retrieved from recent data and is likely to be also applicable to the near-future. For the far-future, the relevance of the recent past behaviour is lower, because the environmental conditions change due to the meteorological behaviour of a larger area. The environmental conditions in the far-future can therefore be predicted with a higher accuracy by advanced meteorological models, hence projecting the power consumption from the weather forecast is more relevant in the far-future.

5.2. Applicability

Chapter 1 contained an introduction to the topic of this research and indicated a clear research gap. The power plant on board of ships performing a DP operation are now often controlled with a relatively simple EMS. As previous research has shown, for ships performing a transit, a more advanced EMS can significantly improve performance. Therefore, more advanced strategies in the control of the power plant during DP operation will also increase performance during these operational modes. A more advanced strategy includes future load and optimizes for a horizon in the order of magnitude of the operation horizon. The main issue, however, is that future load is unknown.

This research aimed to investigate how the future power consumption during DP operations can be predicted. The results showed that a distinction can be made between a near-future forecast and a far-future projection, with the switch at 120 s. In the near-future, TS in combination with a KRLS approach can accurately forecast the power consumption. The length of the near-future forecast is sufficient to decide whether a DG needs to be started and to complete the actual starting and connection procedure. With an error of approximately 7 % at 120 s, the forecast is also sufficiently accurate to make this decision thoughtfully. Moreover, a

far-future projection using KRLS based on the weather forecast can be extended to a length in which the accuracy of the weather forecast is sufficiently reliable. With an error of 11 % approximately, the overall course of the power consumption can be predicted sufficiently accurate to enable the EMS to define a schedule of the set points of the components in the power plant. Additionally, the far-future projection algorithm is lower in computational complexity, enabling the far-future power consumption to be calculated real-time. The multi-horizon prediction strategy can thus enable the EMS to proactively control the power plant, maximizing its performance.

5.3. Recommendations for future research

The main objective for the development of an algorithm to predict future power consumption is the implementation in an EMS that can optimize over a larger horizon. Therefore, succeeding research should be the development of an EMS that takes this future power consumption into account. This has already been investigated for transits, but as a DP operation is deviating considerably from the operational profile of a transit, the EMS will deviate too. One of the most commonly used method for inclusion of future knowledge is MPC, which is also used often throughout the studies regarding the EMS of a transit.

An improvement of this research can be made if it is developed with a more complete dataset and a more realistic dynamic model. The used dataset contained raw signals of the wind sensors and this was processed to obtain wave information. Furthermore, only the total generated power was included in the data, rather than merely the thruster power consumption. Also, the thruster bias setting was not included in the data, nor the model. Considering the development of a more realistic model, a more advanced calculation should be made for the EOM, and the actual algorithm of the PID controller and thrust allocation, including pre-processing of the signals, should be implemented. Lastly, adding as input the changes in set position can further improve the accuracy of the models. However, this would, when considering the implementation of the power prediction in an EMS, require the operator to define the path of the position set point in advance, which is often complicated. These adaptations could significantly improve the performance of all models, but should be implemented or not dependent on the application of the power prediction.

Another recommendation for future research considers the fact that the focus of the models has been on the interpolation performance. An interesting extension would be to focus on the extrapolation performance of the models. This is particularly interesting when developing the hybrid models such that the extrapolation performance is high. The expectation is that this model will then outperform the DDM considerably.

The last suggestion for future research considers the influence of the accuracy of the weather forecast. As indicated in the demarcation of the research in Section 1.5, the accuracy of the weather forecast is not considered in this research. This is, however, an important point, as no weather forecast is perfect. This imperfection will lead to additional deviations from actual power, especially in the projection models. Research on the influence of the weather forecast accuracy on the future load estimation would be valuable, and from its conclusions, an assessment can be done whether measures need to be taken to increase accuracy in other ways.

6

Conclusion

In order to reduce the environmental footprint of the maritime sector, ships should reduce their energy consumption. Ships equipped with a DP system require significantly more energy with respect to conventional systems to keep the ship on position. The power plants on board of these ships that provide energy to the DP system have increased in complexity, requiring more advanced strategies of EMSs to benefit from this increase in complexity. State-of-the-art strategies for EMSs during DP only optimize for the current state, while considering the complete operation horizon would enable a significant improvement in total performance. One of the major difficulties for this, however, is the fact that research on power predictions is limited. This research aims to predict the power consumption of a ship performing a DP operation.

In Section 1.4, the research questions for this research are formulated. Below, the three SRQs are answered first distinctly. Afterwards, based on these answers, the answer on the MRQ is answered, being the final conclusion of this research.

SRQ1:	How can the instantaneous power consumption of a DP operation be predicted?

For the prediction of instantaneous power consumption during a DP operation, four models are compared: a static model, a dynamic model, a DDM, and an integration of the latter two, a hybrid model. The static and the dynamic model, being the PMs, perform similar, but often show significant deviations from the observed power, leading to a MAPE of respectively 21.2 % and 21.7 %. The dynamic model, although capturing more physics, performs slightly less accurate than the static model, which is due to the large uncertainties in the choices in the EOM and the PID controller. A model with a higher accuracy is the DDM, which is based on the KRLS method. This model results in an error of 11.2 %. Similar performance is found for the hybrid model, integrating the dynamic model in the DDM, as the error is 10.9 %.

SRQ2:	How can the near-future power consumption of a DP operation be predicted?

For the prediction of the near-future power consumption, two forecast models are developed. These models are based on the recent past behaviour of the environmental conditions and the power consumption, as well as the weather forecast at the moment that is to be forecast. The first model, the DDM, uses a TS approach as input for a KRLS model. The second model considers a hybrid model, integrating the dynamic model as extra input in the latter model. The results show that the inclusion of the dynamic model does not significantly improve the performance of the model. Both models are highly accurate when forecasting only a few seconds in the future, as the error is less than 3 %. As the forecast length increases, the accuracy first decreases slightly, but after 30 s, the error remains constant until 120 s, approximately 7 %. It is expected that this is caused by choice of the kernel matrix size and the fact that the observed power also contains auxiliary power.

SRQ3:	How can the far-future power consumption of a DP operation be predicted?

For the prediction of the far-future power consumption, the models of the instantaneous power prediction from the first SRQ are used. These models are labelled as the projection models, as the power consumption is calculated from the weather forecast. The projection models are able to project the power consumption from the weather forecast as long as the weather forecast is reasonably accurate. The accuracy of the weather forecast, however, is not considered in this research, thus successive research to investigate the influence of this would enhance the correctness of the power prediction in the far-future.

MRQ:	How can the power consumption of a dynamic positioning operation of a ship real-time be predicted most accurately?

The power consumption of a DP operation can most accurately be predicted real-time using a multi-horizon data-driven prediction. The multi-horizon is split up in a near-future and a far-future, for which the switch is located at 120 s. In the near-future, a combination between TS and KRLS, merely based on past data, results in a prediction that is sufficiently accurate to enable short-term decision-making of the EMS. For the far-future, a projection model, merely using past data as input for a KRLS model, is sufficiently accurate to enable the EMS to define a schedule for optimal settings of the power plant. Implementation of this multi-horizon power prediction in an EMS will therefore lead to a more sustainable DP operation, and thus to a lower environmental footprint of the maritime sector.

References

[1] Danfoss Engineering Tomorrow. *Offshore*. https://www.danfoss.com/en/markets/marine-and-offshore/shared/offshore/#tab-overview [Retreived:31-05-2022]. 2022.

[2] Intergovernmental Panel on Climate Change. *Climate Change 2021 The Physical Science Basis*. IPCC, 2021. URL: https://www.unep.org/emissions-gap-report-2022.

[3] United Nations. *ADOPTION OF THE PARIS AGREEMENT*. United Nations, Dec. 2015. URL: https://unfccc.int/sites/default/files/english_paris_agreement.pdf.

[4] European Commission. *The European Green Deal*. 2019.

[5] International Maritime Organization. *Third IMO Greenhouse Gas Study 2014*. International Maritime Organization, 2015. URL: https://www.imo.org/en/OurWork/Environment/Pages/Greenhouse-Gas-Studies-2014.aspx.

[6] International Energy Agency. *World Energy Balances: Overview*. Tech. rep. Licence: CC BY 4.0. IEA, 2021. URL: https://www.iea.org/reports/world-energy-balances-overview.

[7] Asgeir J. Sørensen. "A survey of dynamic positioning control systems". In: *Annual Reviews in Control* 35 (1 2011), pp. 123–136. ISSN: 13675788. DOI: 10.1016/j.arcontrol.2011.03.008.

[8] R. D. Geertsma et al. "Design and control of hybrid power and propulsion systems for smart ships: A review of developments". In: *Applied Energy* 194 (Mar. 2017), pp. 30–54. ISSN: 03062619. DOI: 10.1016/j.apenergy.2017.02.060.

[9] Kyaw Hein et al. "Rule-based operation task-aware energy management for ship power systems". In: *IET Generation, Transmission and Distribution* 14 (25 Dec. 2020), pp. 6348–6358. ISSN: 17518695. DOI: 10.1049/iet-gtd.2020.0668.

[10] Angelo Accetta and Marcello Pucci. "Energy management system in DC micro-grids of smart ships: Main gen-set fuel consumption minimization and fault compensation". In: *IEEE Transactions on Industry Applications* 55 (3 May 2019), pp. 3097–3113. ISSN: 19399367. DOI: 10.1109/TIA.2019.2896532.

[11] Jingang Han, Jean Frederic Charpentier, and Tianhao Tang. "An energy management system of a fuel cell/battery hybrid boat". In: *Energies* 7 (5 2014), pp. 2799–2820. ISSN: 19961073. DOI: 10.3390/en7052799.

[12] Truong Q. Dinh et al. "Optimal Energy Management for Hybrid Electric Dynamic Positioning Vessels". In: vol. 51. Elsevier B.V., Jan. 2018, pp. 98–103. DOI: 10.1016/j.ifacol.2018.09.476.

[13] Liza Chua Wan Yuan et al. "Equivalent Consumption Minimization Strategy for hybrid all-electric tugboats to optimize fuel savings". In: vol. 2016-July. Institute of Electrical and Electronics Engineers Inc., July 2016, pp. 6803–6808. ISBN: 9781467386821. DOI: 10.1109/ACC.2016.7526743.

[14] Zehui Zhang, Cong Guan, and Zhiyong Liu. "Real-Time Optimization Energy Management Strategy for Fuel Cell Hybrid Ships Considering Power Sources Degradation". In: *IEEE Access* 8 (2020), pp. 87046–87059. ISSN: 21693536. DOI: 10.1109/ACCESS.2020.2991519.

[15] Ameen M. Bassam et al. "Development of a multi-scheme energy management strategy for a hybrid fuel cell driven passenger ship". In: *International Journal of Hydrogen Energy* 42 (1 Jan. 2017), pp. 623–635. ISSN: 03603199. DOI: 10.1016/j.ijhydene.2016.08.209.

[16] Mohsen Banaei et al. "A Comparative Analysis of Optimal Operation Scenarios in Hybrid Emission-Free Ferry Ships". In: *IEEE Transactions on Transportation Electrification* 6 (1 Mar. 2020), pp. 318–333. ISSN: 23327782. DOI: 10.1109/TTE.2020.2970674.

[17] Janne Huotari et al. “Hybrid ship unit commitment with demand prediction and model predictive control”. In: *Energies* 13 (18 Sept. 2020). ISSN: 19961073. DOI: 10.3390/en13184748.

[18] Spyros Antonopoulos et al. “MPC framework for the energy management of hybrid ships with an energy storage system”. In: *Journal of Marine Science and Engineering* 9 (9 Sept. 2021). ISSN: 20771312. DOI: 10.3390/jmse9090993.

[19] Kyaw Hein et al. “Coordinated Optimal Voyage Planning and Energy Management of All-Electric Ship with Hybrid Energy Storage System”. In: *IEEE Transactions on Power Systems* 36 (3 May 2021), pp. 2355–2365. ISSN: 15580679. DOI: 10.1109/TPWRS.2020.3029331.

[20] Fotis D. Kanellos, George J. Tsekouras, and Nikos D. Hatziargyriou. “Optimal demand-side management and power generation scheduling in an all-electric ship”. In: *IEEE Transactions on Sustainable Energy* 5 (4 Oct. 2014), pp. 1166–1175. ISSN: 19493029. DOI: 10.1109/TSTE.2014.2336973.

[21] Yijie Zhang et al. “Two-level model predictive control energy management strategy for hybrid power ships with hybrid energy storage system”. In: *Journal of Energy Storage* 52 (Aug. 2022), p. 104763. ISSN: 2352152X. DOI: 10.1016/j.est.2022.104763. URL: https://linkinghub.elsevier.com/retrieve/pii/S2352152X22007733.

[22] Tuyen V. Vu et al. “Predictive Energy Management for MVDC All-Electric Ships”. In: 2017. ISBN: 9781509049448.

[23] Tuyen V. Vu et al. “Predictive Control for Energy Management in Ship Power Systems under High-Power Ramp Rate Loads”. In: *IEEE Transactions on Energy Conversion* 32 (2 June 2017), pp. 788–797. ISSN: 08858969. DOI: 10.1109/TEC.2017.2692058.

[24] Hyeongjun Park et al. “Real-Time Model Predictive Control for Shipboard Power Management Using the IPA-SQP Approach”. In: *IEEE Transactions on Control Systems Technology* 23 (6 Nov. 2015), pp. 2129–2143. ISSN: 10636536. DOI: 10.1109/TCST.2015.2402233.

[25] Thanh Long Vu et al. “Power Management for Electric Tugboats Through Operating Load Estimation”. In: *IEEE Transactions on Control Systems Technology* 23 (6 Nov. 2015).

[26] Jun Hou, Jing Sun, and Heath Hofmann. “Mitigating power fluctuations in electrical ship propulsion using model predictive control with hybrid energy storage system”. In: Institute of Electrical and Electronics Engineers Inc., 2014, pp. 4366–4371. ISBN: 9781479932726. DOI: 10.1109/ACC.2014.6858803.

[27] Jun Hou, Jing Sun, and Heath Hofmann. “Control development and performance evaluation for battery/flywheel hybrid energy storage solutions to mitigate load fluctuations in all-electric ship propulsion systems”. In: *Applied Energy* 212 (Feb. 2018), pp. 919–930. ISSN: 03062619. DOI: 10.1016/j.apenergy.2017.12.098.

[28] Jun Hou, Jing Sun, and Heath F. Hofmann. “Mitigating Power Fluctuations in Electric Ship Propulsion with Hybrid Energy Storage System: Design and Analysis”. In: *IEEE Journal of Oceanic Engineering* 43 (1 Jan. 2018), pp. 93–107. ISSN: 03649059. DOI: 10.1109/JOE.2017.2674878.

[29] Chengquan Ju et al. “A two-layer energy management system for microgrids with hybrid energy storage considering degradation costs”. In: *IEEE Transactions on Smart Grid* 9 (6 Nov. 2018), pp. 6047–6057. ISSN: 19493053. DOI: 10.1109/TSG.2017.2703126.

[30] Miltiadis Kalikatzarakis et al. “Optimizing Fuel Consumption in Thrust Allocation for Marine Dynamic Positioning Systems”. In: *IEEE Transactions on Automation Science and Engineering* 19 (1 Jan. 2022), pp. 122–142. ISSN: 15583783. DOI: 10.1109/TASE.2021.3069779.

[31] Truong M.N. Bui et al. “Development and real-time performance evaluation of energy management strategy for a dynamic positioning hybrid electric marine vessel”. In: *Electronics (Switzerland)* 10 (11 June 2021). ISSN: 20799292. DOI: 10.3390/electronics10111280.

[32] Thomas L. Saaty and Luis G. Vargas. *Prediction, Projection and Forecasting*. 1st ed. Springer Dordrecht, 1991. ISBN: 978-94-015-7954-4.

[33] Andrea Coraddu et al. "Vessels fuel consumption forecast and trim optimisation: A data analytics perspective". In: *Ocean Engineering* 130 (Jan. 2017), pp. 351–370. ISSN: 00298018. DOI: 10.1016/j.oceaneng.2016.11.058.

[34] Y C Ho, D L Pepyne, and M A Simaan. "Simple Explanation of the No-Free-Lunch Theorem and Its Implications 1". In: *JOURNAL OF OPTIMIZATION THEORY AND APPLICATIONS* 115 (3 2002), pp. 549–570.

[35] Spyros Makridakis. *A Survey of Time Series*. The European Institute of Business Administration, 1976, p. 29. URL: https://about.jstor.org/terms.

[36] Jens Hainmueller and Chad Hazlett. "Kernel regularized least squares: Reducing misspecification bias with a flexible and interpretable machine learning approach". In: *Political Analysis* 22 (2 2014), pp. 143–168. ISSN: 14764989. DOI: 10.1093/pan/mpt019.

[37] Jake Walker et al. "Digital twins of the mooring line tension for floating offshore wind turbines to improve monitoring, lifespan, and safety". In: *Journal of Ocean Engineering and Marine Energy* 8 (1 Feb. 2022). ISSN: 21986452. DOI: 10.1007/s40722-021-00213-y.

[38] Werner Blendermann. "Parameter identification of wind loads on ships". In: *Journal of Wind Engineering and Industrial Aerodynamics* 51 (1994), pp. 339–351.

[39] T.I. Fossen. *Handbook of Marine Craft Hydrodynamics and Motion Control*. 1st ed. John Wiley & Sons, 2011. ISBN: 9781119991496.

[40] O.M. Faltinsen. *Sea Loads on Ships and Offshore Structures*. Cambridge University Press, 1990.

[41] MathWorks. *quadprog - quadratic programming*. 2022. URL: https://nl.mathworks.com/help/optim/ug/quadprog.html.

[42] Yushi Wei et al. "Quadratic Programming Thrust Allocation and Management for Dynamic Positioning Ships". In: *TELKOMNIKA* 11 (3 2013), pp. 1632–1638. ISSN: 2302-4046.

[43] S. P. Berge and T. I. Fossen. "On the Properties of the Nonlinear Ship Equations of Motion". In: *Mathematical and Computer Modelling of Dynamical Systems* 6 (4 2000), pp. 365–381. ISSN: 13873954. DOI: 10.1076/mcmd.6.4.365.3660.

[44] Dario Bocchetti et al. "A statistical approach to ship fuel consumption monitoring". In: *Journal of Ship Research* 59 (3 Sept. 2015), pp. 162–171. ISSN: 15420604. DOI: 10.5957/JOSR.59.3.150012.

[45] Ryan M Rifkin and Ross A Lippert. *massachusetts institute of technology Notes on Regularized Least Squares*. 2007. URL: www.csail.mit.edu.

[46] Ron Kohavi. *A Study of Cross-Validation and Bootstrap for Accuracy Estimation and Model Selection*. Stanford University, 1995. URL: http://robotics.stanford.edu/~ronnyk.

[47] Andrea Coraddu et al. "Floating Spar-Type Offshore Wind Turbine Hydrodynamic Response Characterisation: A Computational Cost Aware Approach". In: Institute of Electrical and Electronics Engineers Inc., Oct. 2020. ISBN: 9781728154466. DOI: 10.1109/IEEECONF38699.2020.9389074.

[48] Asgeir J Sørensen. *Marine Cybernetics Towards Autonomous Marine Operations and Systems Lecture Notes*. NTNU, 2018. URL: http://folk.ntnu.no/assor/.

[49] R. van Basten Batenburg. *DP CAPABILITY ANALYSIS Final Report*. MARIN, 2013. URL: www.marin.nl.

[50] E. Ovrum and T. F. Bergh. "Modelling lithium-ion battery hybrid ship crane operation". In: *Applied Energy* 152 (Aug. 2015), pp. 162–172. ISSN: 03062619. DOI: 10.1016/j.apenergy.2015.01.066.

[51] Hans Klein Woud and Douwe Stapersma. *Design of Propulsion and Electric Power Generation Systems*. The Institute of Marine Engineering, Science and Technology, 2012. ISBN: 1-902536-47-9.

[52] Jan Fredrik Hansen and Frank Wendt. "History and State of the Art in Commercial Electric Ship Propulsion, Integrated Power Systems, and Future Trends". In: *Proceedings of the IEEE* 103 (12 Dec. 2015), pp. 2229–2242. ISSN: 15582256. DOI: 10.1109/JPROC.2015.2458990.

[53] Aleksander Veksler, Tor Arne Johansen, and Roger Skjetne. "Thrust allocation with power management functionality on dynamically positioned vessels". In: Institute of Electrical and Electronics Engineers Inc., 2012. ISBN: 9781457710957. DOI: 10.1109/acc.2012.6315084.

[54] Görkem Kökkülünk, Adnan Parlak, and Hasan Hüseyin Erdem. "Determination of performance degradation of a marine diesel engine by using curve based approach". In: *Applied Thermal Engineering* 108 (Sept. 2016), pp. 1136–1146. ISSN: 13594311. DOI: 10.1016/j.applthermaleng.2016.08.019.

[55] C. D. Rakopoulos and E. G. Giakoumis. *Diesel engine transient operation: Principles of operation and simulation analysis*. Springer London, 2009, pp. 141–180. ISBN: 9781848823747. DOI: 10.1007/978-1-84882-375-4.

[56] Bijan Zahedi, Lars E. Norum, and Kristine B. Ludvigsen. "Optimized efficiency of all-electric ships by dc hybrid power systems". In: *Journal of Power Sources* 255 (June 2014), pp. 341–354. ISSN: 03787753. DOI: 10.1016/j.jpowsour.2014.01.031.

[57] Vicente P. Guerrero-Bote and Félix Moya-Anegón. "A further step forward in measuring journals' scientific prestige: The SJR2 indicator". In: *Journal of Informetrics* 6 (4 Oct. 2012), pp. 674–688. ISSN: 17511577. DOI: 10.1016/j.joi.2012.07.001.

[58] Haakon Elizabeth Lindstad, Gunnar S. Eskeland, and Agathe Rialland. "Batteries in offshore support vessels – Pollution, climate impact and economics". In: *Transportation Research Part D: Transport and Environment* 50 (Jan. 2017), pp. 409–417. ISSN: 13619209. DOI: 10.1016/j.trd.2016.11.023.

[59] Tomas Tronstad et al. *Study on the use of fuel cells in shipping*. DNV GL, 2017.

[60] Omer Berkehan Inal, Jean Frédéric Charpentier, and Cengiz Deniz. "Hybrid power and propulsion systems for ships: Current status and future challenges". In: *Renewable and Sustainable Energy Reviews* 156 (Mar. 2022). ISSN: 18790690. DOI: 10.1016/j.rser.2021.111965.

[61] Alireza Tashakori Abkenar et al. "Fuel Cell Power Management Using Genetic Expression Programming in All-Electric Ships". In: *IEEE Transactions on Energy Conversion* 32 (2 June 2017), pp. 779–787. ISSN: 08858969. DOI: 10.1109/TEC.2017.2693275.

[62] Ruoli Tang, Xin Li, and Jingang Lai. "A novel optimal energy-management strategy for a maritime hybrid energy system based on large-scale global optimization". In: *Applied Energy* 228 (Oct. 2018), pp. 254–264. ISSN: 03062619. DOI: 10.1016/j.apenergy.2018.06.092.

[63] Jun Hou et al. "Adaptive model predictive control for hybrid energy storage energy management in all-electric ship microgrids". In: *Energy Conversion and Management* 198 (Oct. 2019). ISSN: 01968904. DOI: 10.1016/j.enconman.2019.111929.

[64] Francesco Mauro and Radoslav Nabergoj. "Advantages and disadvantages of thruster allocation procedures in preliminary dynamic positioning predictions". In: *Ocean Engineering* 123 (Sept. 2016), pp. 96–102. ISSN: 00298018. DOI: 10.1016/j.oceaneng.2016.06.045.

[65] Håkon S. Halvorsen et al. "Wave motion compensation in dynamic positioning of small autonomous vessels". In: *Journal of Marine Science and Technology (Japan)* 26 (3 Sept. 2021), pp. 693–712. ISSN: 09484280. DOI: 10.1007/s00773-020-00765-y.

[66] Svenn A. Værnø, Astrid H. Brodtkorb, and Roger Skjetne. "Compensation of bias loads in dynamic positioning of marine surface vessels". In: *Ocean Engineering* 178 (Apr. 2019), pp. 484–492. ISSN: 00298018. DOI: 10.1016/j.oceaneng.2019.03.010.

[67] Damir Radan et al. "Reducing Power Load Fluctuations on Ships Using Power Redistribution Control". In: *Marine Technology* 45 (3 July 2008), pp. 162–174. URL: http://onepetro.org/MTSN/article-pdf/45/03/162/2200775/sname-mtsn-2008-45-3-162.pdf?casa_token=iCffNiTrYpUAAAAA:N23WgSyf1iHb7ZLdQW8MzKLmF-cnDVhs9XUcUImv89wH41PS-l7Vjv5RRSAp6nr0w1xJrf9N.

[68] Aleksander Veksler et al. "Reducing power transients in diesel-electric dynamically positioned ships using re-positioning". In: Institute of Electrical and Electronics Engineers Inc., Feb. 2014, pp. 268–273. ISBN: 9781479940325. DOI: 10.1109/IECON.2014.7048510.

[69] Aleksander Veksler et al. "Thrust Allocation with Dynamic Power Consumption Modulation for Diesel-Electric Ships". In: *IEEE Transactions on Control Systems Technology* 24 (2 Mar. 2016), pp. 578–593. ISSN: 10636536. DOI: 10.1109/TCST.2015.2446940.

[70] Tor A. Johansen et al. "Dynamic positioning system as dynamic energy storage on diesel-electric ships". In: *IEEE Transactions on Power Systems* 29 (6 Nov. 2014), pp. 3086–3091. ISSN: 08858950. DOI: 10.1109/TPWRS.2014.2317704.

[71] Aleksander Veksler et al. "Dynamic Positioning with Model Predictive Control". In: *IEEE Transactions on Control Systems Technology* 24 (4 July 2016), pp. 1340–1353. ISSN: 10636536. DOI: 10.1109/TCST.2015.2497280.

[72] Eirik Mathiesen, Bjørnar Realfsen, and Morten Breivik. "Methods for Reducing Frequency and Voltage Variations on DP Vessels". In: Oct. 2012.

[73] R.M. Ischerwood. "Wind resistance of Merchant Ships". In: *The Royal Institution of Naval Architects* (1972).

[74] OCIMF. *Prediction of wind and current loads on VLCCs*. Oil Companies International Marine Forum, 1977.

[75] Fumitoshi Kitamura et al. "Estimation of above water structural parameters and wind loads on ships". In: *Ships and Offshore Structures* 12 (8 Nov. 2017), pp. 1100–1108. ISSN: 17445302. DOI: 10.1080/17445302.2017.1316556.

[76] M R Haddara and Guedes Soares. "Wind loads on marine structures". In: *Marine Structures* (Apr. 1999), pp. 199–209.

[77] Marko Valčić, Jasna Prpić-Oršić, and Dean Vučinić. "Application of Pattern Recognition Method for Estimating Wind Loads on Ships and Marine Objects". In: Springer, 2020, pp. 123–158. ISBN: 978-9811398056. DOI: 10.1007/978-981-13-9806-3_5.

[78] J. Gerritsma and W. Beukelman. "Analysis of the resistance increase in waves of a fast cargo ship". In: *International Shipbuilding Progress* 19 (217 Sept. 1972), pp. 285–293. DOI: 10.3233/ISP-1972-1921701.

[79] G.R.M. Remery and G. van Oortmerssen. "The mean wave, wind and current forces on offshore structures and their role in the design of mooring systems". In: 1973.

[80] J A Pinkster. "Mean and Low Frequency Wave Drifting Forces on Floating Structures". In: *Ocean Engineering* 6 (1979), pp. 593–615.

[81] João Pessoa and Nuno Fonseca. "Second-order low-frequency drift motions of a floating body calculated by different approximation methods". In: *Journal of Marine Science and Technology (Japan)* 20 (2 June 2015), pp. 357–372. ISSN: 09484280. DOI: 10.1007/s00773-014-0288-8.

[82] J.O. de Kat and J.E.W. Wichers. "Marine Technology Behavior of a Moored Ship in Unsteady Current, Wind, and Waves". In: *Marine Technology* (Sept. 1991). URL: http://onepetro.org/MTSN/article-pdf/28/05/251/2199441/sname-mtsn-1991-28-5-251.pdf?casa_token=AKE6sDbmEOUAAAAA:KnqaTcIVMT2QW8T8Ot2wbe0KJNpA08NkALsimEs87CIzewWAohBWSJn9GsA46ntdzbXkHsGI.

[83] R S Mercier and F A Huijs. "Steady current forces on tanker-based FPSOs". In: WIT Press, 2005, pp. 259–268. URL: www.witpress.com,.

[84] Monika Bortnowska. "Prediction of power demand for ship motion control system of sea mining ship fitted with tubular winning system". In: *Polish Maritime Research* 14 (4 2007), pp. 24–30. ISSN: 1233-2585. DOI: 10.2478/v10012-007-0036-7.

[85] Chae og Lim et al. "Electric power consumption predictive modeling of an electric propulsion ship considering the marine environment". In: *International Journal of Naval Architecture and Ocean Engineering* 11 (2 July 2019), pp. 765–781. ISSN: 20926790. DOI: 10.1016/j.ijnaoe.2019.02.011.

[86] Øyvind N. Smogeli, Eivind Ruth, and Asgeir J. Sørensen. "Experimental validation of power and torque thruster control". In: vol. 2005. 2005, pp. 1506–1511. ISBN: 0780389360. DOI: 10.1109/.2005.1469805.

[87] E. F. G. Van Daalen et al. "A generic optimization algorithm for the allocation of DP actuators". In: 2011. URL: http://asmedigitalcollection.asme.org/OMAE/proceedings-pdf/OMAE2011/44335/87/4559327/87_1.pdf.

[88] ABS. *Guide for Dynamic Positioning Systems*. 2013. URL: www.eagle.org.

[89] Hamid Amini, Lucia Sileo, and Sverre Steen. "Numerical calculations of propeller shaft loads on azimuth propulsors in oblique inflow". In: *Journal of Marine Science and Technology (Japan)* 17 (4 Dec. 2012), pp. 403–421. ISSN: 09484280. DOI: 10.1007/s00773-012-0176-z.

[90] F. Arditti et al. "Thrust allocation algorithm with efficiency function dependent on the azimuth angle of the actuators". In: *Ocean Engineering* 105 (July 2015), pp. 206–216. ISSN: 00298018. DOI: 10.1016/j.oceaneng.2015.06.021.

[91] Jóan Petur Petersen, Daniel J. Jacobsen, and Ole Winther. "Statistical modelling for ship propulsion efficiency". In: *Journal of Marine Science and Technology* 17 (1 Mar. 2012), pp. 30–39. ISSN: 09484280. DOI: 10.1007/s00773-011-0151-0.

[92] Pasquale Erto et al. "A Procedure for Predicting and Controlling the Ship Fuel Consumption: Its Implementation and Test". In: *Quality and Reliability Engineering International* 31 (7 Nov. 2015), pp. 1177–1184. ISSN: 10991638. DOI: 10.1002/qre.1864.

[93] Andreas Brandsæter and Erik Vanem. "Ship speed prediction based on full scale sensor measurements of shaft thrust and environmental conditions". In: *Ocean Engineering* 162 (Aug. 2018), pp. 316–330. ISSN: 00298018. DOI: 10.1016/j.oceaneng.2018.05.029.

[94] Wengang Mao et al. "Statistical models for the speed prediction of a container ship". In: *Ocean Engineering* 126 (Nov. 2016), pp. 152–162. ISSN: 00298018. DOI: 10.1016/j.oceaneng.2016.08.033.

[95] Anna Swider, Helge Langseth, and Eilif Pedersen. "Application of data-driven models in the analysis of marine power systems". In: *Applied Ocean Research* 92 (Nov. 2019). ISSN: 01411187. DOI: 10.1016/j.apor.2019.101934.

[96] Ran Yan, Shuaian Wang, and Yuquan Du. "Development of a two-stage ship fuel consumption prediction and reduction model for a dry bulk ship". In: *Transportation Research Part E: Logistics and Transportation Review* 138 (June 2020). ISSN: 13665545. DOI: 10.1016/j.tre.2020.101930.

[97] Mojtaba Mehrzadi et al. "A deep learning method for short-term dynamic positioning load forecasting in maritime microgrids". In: *Applied Sciences (Switzerland)* 10 (14 July 2020). ISSN: 20763417. DOI: 10.3390/app10144889.

[98] Fred Gonsalves et al. "New Insights into the Propulsion Power Prediction of Cruise Ships". In: vol. 2021-November. IEEE Computer Society, 2021, pp. 846–850. ISBN: 9781665408981. DOI: 10.1109/ICTAI52525.2021.00135.

[99] Liqian Yang et al. "A genetic algorithm-based grey-box model for ship fuel consumption prediction towards sustainable shipping". In: *Annals of Operations Research* (2019). ISSN: 15729338. DOI: 10.1007/s10479-019-03183-5.

[100] Anna Swider and Eilif Pedersen. "Data-driven methodology for the analysis of operational profile and the quantification of electrical power variability on marine vessels". In: *IEEE Transactions on Power Systems* 34 (2 Mar. 2019), pp. 1598–1609. ISSN: 08858950. DOI: 10.1109/TPWRS.2018.2876252.

A

Literature review

A.1. Introduction

The large environmental footprint of the maritime industry needs to be reduced to contribute to the goal of limiting global warming. As the temperature of the earth has been rising over the past decades, countries all over the world have joined their efforts to limit the increase to $2°C$ [3]. The maritime industry has a significant share in the emission of greenhouse gasses that are the cause for this increase [5]. Therefore, measures need to be taken to reduce the environmental footprint of the maritime industry.

To reduce the environmental footprint, the use of fossil fuels and raw materials need to be reduced. Fossil fuels are nowadays used abundantly to power ships and are often required as energy source to manufacture ship parts from raw materials. Research on the reduction of both the consumption of fossil fuels as well as the use of ship parts is therefore highly relevant. The consumption of fossil fuels and the condition of ship parts are dependent on the way the power plant is being operated.

The operating strategy has an influence on both the energy consumption and the condition of the power plant components. The efficiency of diesel generators is dependent on their operating point [8]. Furthermore, charging and discharging an Energy Storage System (ESS) brings associated energy losses [50]. Moreover, a power plant contains multiple stages from fuel to thrust that also induce conversion losses [51, 52]. Additionally, a diesel engine can degrade having multiple causes, which are, among others, fluctuations in the load [53], running at part load [8] and frequent start/stop procedures [17]. As these phenomena lead in the long term to increased fuel consumption [54] and thus to harmful emissions [55], these must be prevented. An ESS can also decrease in efficiency due to ageing or inaccurate use [50]. As this is all mainly dependent on the way the power plant is operated, an EMS, which controls the settings of the power plant, is important [8, 28, 56].

During DP operations, a ship *"[...] maintains its position and heading (fixed location or pre-determined track) exclusively by means of active thrusters."* [7]. These thrusters require power, which is provided by the power plant. The amount of required power is dependent on the environmental loads acting on the ship, which can be fluctuating. This also induces fluctuations in the power plant, which leads to high energy consumption and an increased stress on the power plant. Low frequency fluctuations can lead to frequent start/stops procedures of diesel generators. These consequences of fluctuations could be reduced by adaptively adjusting the setpoints of the components in the power plant. This requires, however, a power forecast, which has not yet been developed for DP operations.

The research that is to be performed comprises two phases. The first phase is the development of an algorithm that forecasts the power demand during DP operations in the long term for real-time application. The second phase consists of the implementation of this power forecast in an EMS to minimize energy consumption while considering the impact on the condition of the power plant. This report is the literature review for the research and will investigate previously performed studies on several pillars to construct a basis for the actual research.

Several elements will not be included in this literature review, as those will be assumed to be known. Firstly, advanced weather models are widely available and used in DP systems, so this literature review will not treat this. Secondly, the power forecast should be applicable to the DP system of RH Marine. The thrust allocation algorithm has a large influence on the power consumption and thus, the algorithm of RH Marine will directly be used.

This report starts with the literature review in Section A.2 in which five pillars will be elaborated: Energy Management, Dynamic Positioning, Environmental Loads, Thruster Power Consumption and Data Processing for Forecast. Then, in Section A.3, a reflection will indicate the gaps in the literature, resulting to the unique contribution of this research. In Section A.4, the aims and objectives of the research are defined. Lastly, this report is concluded in Section A.5.

A.2. Literature Review

The research that is to be performed is based on a number of pillars of which the previous literature will be elaborated in this chapter. The first pillar is energy management (Section A.2.1), as the incentive of the development of a power forecast is its implementation in the EMS to improve performance. The second pillar is dynamic positioning (Section A.2.2) as the power forecast will be developed for DP operations. The third is the environmental loads (Section A.2.4), because the wind, waves and current all need to be compensated to maintain position and therefore affect the power consumption significantly. The fourth pillar is the power consumption calculation of a thruster (Section A.2.5), as this is the translation from electrical to mechanical energy. The last pillar is data processing for forecast (Section A.2.6), as the forecast will be based on historical data of the ship and this needs to be processed before use.

The structure of each section in this chapter will be consistent for each pillar. First, an overview of the literature for that specific pillar is provided. This is then summarized in a table in the second paragraph. The last paragraph concludes the pillar to establish a basis for the conclusion of the complete literature report in Section A.5. All literature is also included in an overview that indicates which specific elements are part of an article. This enables the literature review to be done in a systematic way. The overview is shown in appendix A.6.

Requirements of the literature

To ensure a proper scientific level of this research, the literature review needs to be based on literature of sufficient scientific level too. Therefore, the selection of literature needs to comply with certain self-defined requirements in order to be included in the review. However, as the maritime industry is quite a niche, the availability of a sufficient amount of literature is rather low. Therefore, a tradeoff is made to ensure both high scientific level and sufficient coverage of performed research.

Figure A.1 shows the flowchart to assess the scientific level of an article. The requirements are based on the credibility of the journal and the author, as well as the year of publishing. Scientific journals are categorized each year in four quartiles that rank their scientific journal prestige indicator (SRJ2), as described by Guerrero-Bote and Moya-Anegón [57]. If an article is included in a journal of quartile one, the article is directly considered to have sufficient scientific level. In the situation that the journal is in quartile two, the author's h-index is assessed. The minimal h-index of the author with the highest h-index needs to be 10 in order to consider the article to be of sufficient scientific level. In the situation that an article is part of a conference proceeding, the highest author also needs to comply with the previously mentioned criterion. Journals with a rating lower than quartile two are considered as insufficient. Furthermore, literature that is provided by authorities or class bureaus is also accepted to be included in the literature review, as well as books written by a credible author. In the situation that an article is too old such that an SRJ2 rank is not available, the article is assessed individually whether it complies with a comparable scientific level. Lastly, for each article, publishing year in combination with its content is assessed to ensure the article is not outdated.

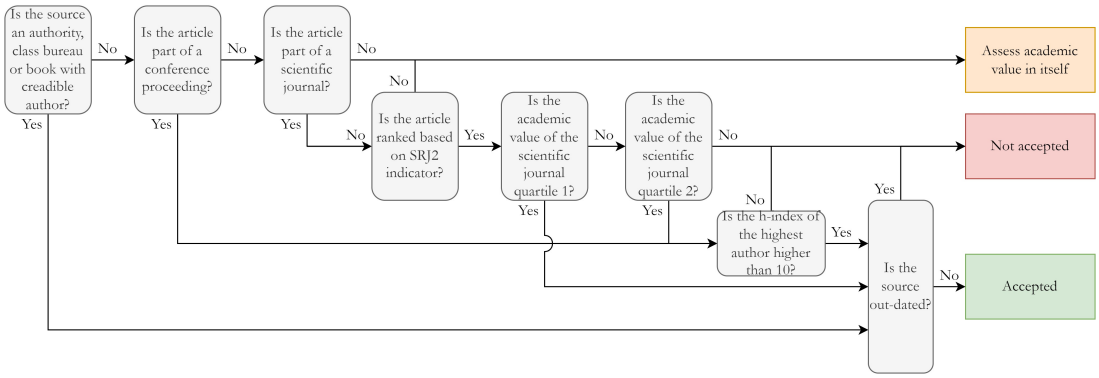

Figure A.1: Flowchart of requirement compliance for scientific value

A.2.1. Energy Management

An EMS is in fact a Power Management System (PMS) with extended functionality [48]. A PMS is responsible for the balance between power demand and supply for the instantaneous operating condition. An EMS considers a larger scope by controlling and monitoring the energy flow in the complete power plant. This way, the EMS not only ensures balance between power demand and supply, but can also be optimized for a predefined objective. The strategy of the EMS can also vary significantly dependent on the objective. This variety becomes clear when investigating previous research, as will be shown in this section.

The power plant of a ship is designed considering a specific operational profile and taking into account objectives defined by the shipowner. Each technology that is added to a power plant, results in more degrees of freedom that needs to be controlled by the EMS, but can also offer possibilities to reduce energy consumption, emissions and costs. An ESS, such as a battery, ultra-capacitor (UC) or a flywheel, can significantly reduce emissions by storing an excess amount of energy and releasing this when required [58]. Furthermore, a fuel cell is emission free, but requires a low ramp rate of the power [59]. Therefore, an EMS is crucial for the optimal use of the power plant.

Literature

A recent study about the current status and future challenges regarding hybrid power and propulsion systems is performed by Berkehan Inal, Charpentier, and Deniz [60]. Two significant challenges arise in this article, which is the improvement of energy storage and optimization of EMS. Moreover, Geertsma et al. [8] provide a review of developments in this research area. The authors state that the control strategy is one of the most import factors to exploit full potential of the power system. In this paragraph, literature about the various energy management strategies will be elaborated.

Rule based strategies Hein et al. [9] addressed the issue of the high computational burden of searching the global optimum in optimization methods for energy management. As constraints in different operational modes differ, a rule based EMS can significantly reduce computational efforts as only local optima would need to be found. The developed strategy showed proper performance in terms of reliability, redundancy and fuel consumption, but did not take the impact on the condition of the ESS into account. Accetta and Pucci [10] have performed a research with a similar aim. A yacht consisting of diesel generators, battery, PV solar panels and a wind turbine was considered. An EMS was implemented combining the advantages of both a rule based strategy and an optimization based strategy. This way, a global optimum can be found by only having to search for a local optimum, which was also done by Hein et al. The result showed a reduction in fuel consumption, a reliable operation and, in contrast to Hein et al., the strategy did not force high stresses on the battery when operating in normal conditions.

Han, Charpentier, and Tang [11] performed a more extensive study regarding EMS for a power plant with a fuel cell. In the study, a state based EMS dependent on the State of Charge (SoC) of the battery in a fuel cell/battery hybrid ship was developed. The constraints coming from the fuel cell were taken into account, but the results still showed considerable fluctuations in the fuel cell power.

Equivalent fuel consumption minimization Dinh et al. [12] proposed an Equivalent Fuel Consumption Minimization (EFCM) strategy which is simple but efficient and compared this with a rule based EMS. The power generation plant of the case study that is performed consisted of two diesel generators and an ESS. Although reducing fuel consumption, the EMS commanded often switching on and off of diesel generators in a short period while not using the full potential of the ESS. This switching on and off of diesel generators also occurred frequently in a short time period in the research of Yuan et al. [13]. Here, an EFCM strategy was used as well in a ship with a diesel generator and battery power plant. The results showed a depletion of the battery during the case study simulation without a tendency to recharge the battery again. In the real-time optimization EMS presented by Zhang, Guan, and Liu [14], load fluctuations were significantly reduced. The ship considered in this study was a fuel cell and battery/UC storage combination also managed by an EFCM EMS, translating power sources degradation into equivalent fuel consumption. This strategy is able to reduce both fuel consumption and power sources degradation with respect to rule based EMS. However, the simulation results showed minor use of the battery as long term energy storage, using again not the full potential of the ESS. These studies show that a power plant with ESS can be managed instantaneously optimally using an EFCM strategy, but that this does not necessarily result in meeting the objectives in the long term.

A state based strategy and an EFCM strategy of Han, Charpentier, and Tang and Zhang, Guan, and Liu respectively were part of a comparison of five strategies performed by Bassam et al. [15]. The last one of the five, the multi-scheme strategy, considered a different strategy for each operational. The result showed that this strategy performed best, reducing both energy and hydrogen consumption with respect to the basic strategy.

Population optimization Tashakori Abkenar et al. [61] considered a relatively simple power plant, where a fuel cell and a battery were directly linked to the DC bus without DC/DC converters. The only control variables in this configuration that were to be controlled by the PMS, were therefore the air flow and the hydrogen flow. The voltage of the bus was kept within a certain range by a genetic programming algorithm. This lead to the goal of maintaining efficient fuel cell performance.

Another population optimization based EMS was proposed by Tang, Li, and Lai [62]. A particle swarm optimization was used to find the large-scale global optimum in a ship with a power plant consisting of diesel generators, battery and PV panels. To ensure the feasible space was large enough, certain constraints were included in the objective function as penalty. By performing six simulations, the authors show that all constraints are satisfied while minimizing electricity costs significantly with respect to conventional algorithms. An import remark must be made, however; as the authors do not mention the computational effort, this strategy may not be feasible to apply real-time.

Model predictive control A method that is often used in research on EMS, is Model Predictive Control (MPC). Banaei et al. [16] applied this for a zero-emission ferry with a power plant that contained a fuel cells and batteries. Multiple scenarios were investigated to be compared with a rule based EMS in order to highlight the advantages of the proposed method. In the end, using the proposed method, the fuel cells used less hydrogen and the batteries less energy, which lead to a reduction of 4.1% in operational costs over the complete time horizon.

Huotari et al. [17] presented a method to balance the power usage and power production, in the paper called *"unit commitment"*, for the voyage of a cruise ship. An MPC model was formulated that predicted the future power demand profile of the ship, which was an input of the unit commitment optimization model. The objective function only contained minimization of fuel consumption and the method showed, using the simulation of a complete trip, near-optimal results. Yet, these results contained frequent diesel generator start/stops, the optimization was not adapted during the voyage and the advantages of a long-term battery planning were not harvested.

In contrast to the research performed by Huotari et al., Antonopoulos et al. [18] did take future disturbance into account by generating a reference trajectory for the battery SoC each time a new future update of the disturbance was available. A short time prediction of this reference trajectory was used for an MPC module to solve a new control optimization problem. This lead to a fuel consumption reduction of 3.5%. However, the impact of the control strategy on the condition of the power plant was not taken into account.

Another study that split the problem into two stages was performed by Hein et al. [19], considering a power plant with diesel generator, ESS and fuel cell. The first stage considered the generation of a reference trajectory. The second stage ensured compliance with the reference trajectory by real-time optimization. The result showed that fuel consumption and associated emissions can be reduced while considering the constraints on the power plant.

MPC was also applied by Vu et al. [23] to deal with the high power ramp rates of a rail gun on a naval vessel. The goal was to ensure a stable power grid consisting of diesel generators and an ESS, which was achieved by sustaining a certain SoC of the ESS. This research was extended by Vu et al. [22] to assess the contribution of the ESS in the power grid. The authors concluded that the application of an ESS is beneficial for the stability of the power grid. Fuel consumption and impact on the condition of the power plant components are not part of these studies. The focus was more to the stable power grid and therefore the time horizon of the MPC was also relatively short. High ramp rates were also part of the research performed by Park et al. [24]. In this research, a PMS using MPC was proposed to ensure the bus voltage, power demand and ramp rate limitation were satisfied. The authors aimed to apply this real-time and simulations have been performed to prove this is feasible.

Kanellos, Tsekouras, and Hatziargyriou [20] did take fuel consumption and degradation of the diesel engine into account in an optimal power management strategy using dynamic programming for an electrically propelled ferry without ESS. The authors assumed the ship load forecasting is available and aimed to optimize power generation and ship speed over a specific time horizon. A comparable study was performed by Vu et al. [25], but this considered a ship with battery. Therefore, the change of SoC of the battery is included in the objective function such that optimal use of the battery over its complete lifetime is ensured. A disadvantage of the control strategy, applying nonlinear optimization, in this article was the fact that the battery was depleted directly in the beginning of the simulation. Therefore, the full potential of the battery as energy storage was not utilized. This could be the cause of frequent diesel generator start/stops that occur in the simulation.

The authors of the article Hou, Sun, and Hofmann [26] have performed multiple studies to reduce load fluctuations. In this article, the combination of a battery and an UC as Hybrid Energy Storage System (HESS) was investigated to increase system efficiency and reliability and to protect the batteries. This was done by capturing the physical dynamic behaviour of the propeller and ship and use this in two different MPC strategies. Successive research of these authors, Hou, Sun, and Hofmann [27], compared two different configurations of HESS, one battery-flywheel combination and one battery-UC combination. Using an MPC energy management, the combination of battery/flywheel resulted in the highest efficiency of the system and the lowest load fluctuations for the diesel generators at higher sea states.

The focus was then shifted towards analysing the fluctuations and using that knowledge by Hou, Sun, and Hofmann [28]. The load fluctuations were decomposed into frequency ranges and each range was captured by either the battery or the UC, referred as *"control with prefiltering"*. This is compared with *"coordinated control"*, in which the system is considered as one single entity and the load fluctuations are counteracted by an optimization algorithm, which turned out best. Afterwards, Hou et al. [63] investigated uncertainties of parameters in the HESS. This showed that the impact of uncertainties on the performance can be significant. This was compensated by implementing real-time values for the parameters in the control strategy, leading to an adaptive MPC.

Multi-layer model predictive control Ju et al. [29] developed an extensive strategy, taking ESS degradation into account by bridging the long-term capital costs for a battery and UC by including this in the short-term operational costs. A two-layer EMS was introduced that minimized operational costs using non-linear receding MPC in the upper layer and minimizes uncertainties and fluctuations in the power in the lower layer by using quadratic MPC. After comparing various prediction horizons, 24 hour prediction showed to achieve highest performance. A two level MPC was also applied by Zhang et al. [21], although the focus was not economical as in the study of Ju et al., but technical by focusing on minimizing fuel consumption, peak shaving of power fluctuations and sustaining a certain SoC of the ESS. The high level MPC ensured fuel minimization based on a relatively large timescale, while the low level MPC handled the high-frequency power fluctuations by defining

the setpoint of the UC on short timescale. With respect to a conventional MPC-based strategy, the proposed strategy achieved best performance.

Overview

In Table A.1, an overview is provided for the literature regarding EMS in the previous paragraph. For each article, the subject is indicated. Furthermore, the method that is applied in each article is included, among with the objectives of the method. Lastly, the timescale is provided for the articles applying MPC or containing relevance for the timescale to show the current status of research about the application of predictions.

Table A.1: Overview of energy management literature

Article	Subject	Method	Objective	Timescale
[60]	Hybrid power systems	Current status and future challenges	Provide overview	
[8]	Hybrid power systems	Review of developments	Provide overview	
[9]	Rule-based task-aware EMS	Rule-based	Limit computational effort	
[10]	EMS for real-time application	Rule-based	Minimize fuel consumption	
[11]	State-based EMS for power plant with fuel cell	State-based	Maximize fuel cell efficiency	
[12]	Energy management optimization for DP	Equivalent Fuel Consumption Minimization	Minimize fuel consumption	
[13]	Energy management for hybrid tug	Equivalent Fuel Consumption Minimization	Minimize fuel consumption & satisfy load demand	
[14]	Real-time optimization EMS for power plant with fuel cell	Equivalent Fuel Consumption Minimization	Minimize fuel consumption & power sources degradation	
[15]	Multi-scheme EMS for power plant with fuel cell	State-based, Equivalent Fuel Consumption Minimization, charge-depleting charge-sustaining, PI, multi-scheme	Minimize energy and hydrogen consumption	
[61]	PMS for DC plant with fuel cell	Genetic algorithm	Maximize fuel cell efficiency	
[62]	Global optimization EMS in hybrid power plant	Particle Swarm Optimization	Minimize fuel consumption, energy consumption & battery stress	
[16]	Operation scenarios comparison for hybrid ship	Model Predictive Control	Minimize total operation costs	Total trip
[17]	Unit Commitment with Demand Prediction	Model Predictive Control	Minimize fuel consumption & location dependent emissions	Total trip
[18]	Mission-scale MPC with reference trajectory generation	Model Predictive Control	Minimize fuel consumption	Mission-scale
[19]	Route and powerplant trajectory optimization	Lexicographic and augmented constraint optimization	Minimize fuel consumption, emissions & power plant degradation	Total trip
[23]	Predictive control for high power ramp rate loads	Model Predictive Control	Ensure energy storage state of charge & satisfy load demand	$\pm$ 1 min
[22]	Energy storage contribution for high power ramp rate loads	Model Predictive Control	Satisfy load demand	$\pm$ 1 min
[24]	Power management with real-time MPC	Model Predictive Control	Satisfy load demand & minimize ramp rate	$\pm$ 10 sec
[20]	Optimal demand management and power generation scheduling	Optimization using dynamic programming	Minimize fuel consumption & generator start/stops	Total trip
[25]	Power management with load estimation for tug	Nonlinear optimization	Minimize fuel consumption and battery stress & satisfy load demand	$\pm$ 2 hours
[26]	MPC for ESD to minimize power fluctuations	Model Predictive Control	Satisfy load demand, maximize energy efficiency & protect power plant	$\pm$ 1 min
[27]	ESD configuration comparison to minimize power fluctuations	Model Predictive Control	Satisfy load demand & minimize ESD losses	$\pm$ 1 min
[28]	Minimize load fluctuations by frequency range decomposition	Model Predictive Control	Satisfy load demand & minimize ESD losses	$\pm$ 1 min
[63]	Adaptive MPC to cope with uncertainty in power management	Model Predictive Control	Satisfy load demand, optimize ESD efficiency & ensure ESD state of charge	$\pm$ 1 min
[29]	Two-layer MPC considering ESS degradation	Two-layer MPC	Minimize total operation costs	6 - 96 h
[21]	Two-layer MPC EMS with ESS	Two-layer MPC	Minimize fuel consumption & protect power plant	$\pm$ 1 h

Conclusion
The EMS is responsible for the energy flow among the power plant of ships and has a significant influence on the performance of the ship. The definition of performance is specific for each ship, resulting in a variation of objectives in which the most common are the minimization of fuel consumption, the minimization of negative impact on the condition of the power plant components and the ensuring a stable energy grid.

Methods to achieve highest performance can generally be split up in two categories, namely rule based and optimization based. Rule based methods are predefined settings dependent on the state of the system, generally yielding the optimal solution. Optimization based methods variate in extent and optimize for their objective, but are limited by the required computational effort for real-time application. One of the optimization based methods that achieves high performance over a larger time horizon is MPC, taking knowledge about the future into account.

Research showed that taking future into account improves performance. Studies that did not take future into account, often found instantaneously optimal results, but showed sub-optimal results in the long term. Methods that take future into account, however, require knowing the future. As research on power forecasts is scarce, methods to develop a power forecast can enable the EMS of ships to significantly increase performance.

A.2.2. Dynamic Positioning

DP ensures a ship is kept on position only by means of using the actuators with minimal interference of an operator. A DP system consists of multiple elements, which all affect its stationkeeping performance and, each to its own extent, the power consumption and the power fluctuation. This section will focus on the elements of a DP system that influence the power consumption and the power fluctuation most significantly.

Literature
One of the main components of a DP system is the thrust allocation. The thrust allocation determines the set-points of the actuators based on the required net forces and moment defined by the DP controller [7]. If a ship has a thruster system with more than three degrees of freedom, the ship is over-actuated and an infinite amount of solutions is possible to meet the required forces and moment. This way, the thrust allocation becomes an optimization problem. Mauro and Nabergoj [64] compared four thrust allocation methods, namely deterministic, pseudo-inverse, non-linear constraint optimization and genetic algorithm. The performance of the methods was assessed based on the capability of each. However, in situations were the environmental conditions were not the most severe, objectives regarding minimization of fuel consumption or load fluctuations are more relevant.

The frequency of encountering waves acting on a ship is considerably high. These wave-frequencies are usually not compensated by the DP system. Halvorsen et al. [65] did investigate methods to compensate for the wave-frequencies for smaller autonomous vessels by comparing six algorithms. Some algorithms clearly showed increased performance regarding wave-frequency compensation but resulted in very high load fluctuations. As these load fluctuations are not desirable, methods to filter out the high frequency variations have been investigated. Værnø, Brodtkorb, and Skjetne [66] compared four methods to enable the DP system to only compensate for mean and slowly varying environmental loads and unmodeled dynamics of the ship, thus filtering out the wave-frequency. The authors concluded the best method is by using the bias estimate of a separate bias observer. Filtering out the wave-frequency is justified due to the significantly larger natural period of the ship itself due to its high inertia, leading to a minimal influence on its stationkeeping performance.

Filtering out the high frequency variations of the environmental load can significantly reduce fuel consumption and load fluctuations while losing minimally on station keeping performance. This can be taken further by compensating for fluctuations in the auxiliary load using the thrusters, as done by Radan et al. [67]. Thrusters, and even more the ship itself, have a high inertia which was used to reduce fluctuations on the diesel generators. This was used by compensating auxiliary loads with thruster power and still having minimal effect on station keeping performance. Veksler, Johansen, and Skjetne [53] aimed to reduce load fluctuations too, but also aim to stabilize the network frequency. This was also, as the authors stated, at the cost of increased variation of the thrusters and deviations from thrust command. Succeeding research was performed by Veksler et al. [68] by continuously observing the direction of the environmental loads. Deviation in that direction was allowed by implementing this in the control algorithm to reduce power fluctuations. As the authors stated themselves, the

improvement was not large, but the method can be significant in certain operations. One of the reasons for the fact that the improvement was small was the fact that the angle of the thrusters were locked. Veksler et al. [69] afterwards performed a research that was more extensive and the thruster angles were not locked. This way, the load fluctuations imposed by other consumers on the ship could be compensated more. Tuning, however, turned out to be rather complicated as the duration of a load change is not known to the algorithm.

The allowance for deviation from the set position was even larger in the article of Johansen et al. [70]. The proposed approach used the ship itself as dynamic energy storage. The movement of the ship is kinetic energy and by moving, the set point deviation in combination with a certain angle of environmental load results in potential energy. The results of this type of dynamic energy storage showed reductions in fuel consumption and reduced negative impact on generator condition. These studies, however, all assume that the operation allows for a deviation in setpoint, which is not always allowed. Moreover, knowledge about the type of the change in the environmental load was not included, complicating the decision making in terms of deviating from setpoint in case of a temporal change or changing the power plant setpoints in case of a long term change.

Veksler et al. [71] introduced a new method for DP by combining the conventional controller and the thrust allocation. Both were captured in one MPC algorithm to improve constraint handling, to plan ahead and to simplify design and tuning. After the analysis of the length of the time horizon, the conclusion was that a large time horizon is best, but that the length is limited by the uncertainties in the prediction of environmental conditions. Within the time horizon boundaries, this control strategy increases the overall efficiency of the DP system.

Another study aiming to combine individual elements of a DP system was performed by Kalikatzarakis et al. [30]. Here, the thrust allocation and the power plant management were controlled in a more holistic way such that power demand and supply were balanced. Diesel generator limitations were taken into account in combination with the objective of minimizing fuel consumption, power consumption and thrust.

Mathiesen, Realfsen, and Breivik [72] took diesel generator limitations into account by predicting the load to reduce variations in voltage and frequency of the power grid. This is achieved by accepting small changes in the station-keeping control and indeed results in a more stable grid frequency. The authors indicated the possibility of reducing the amount of generators running as redundant engines by using their control strategy. This would result in reduced fuel consumption and reduced maintenance.

A.2.3. Overview

Table A.2 shows an overview of the literature presented in the previous paragraph. Of each article, the subject is indicated. Moreover, the objective is provided and the method to achieve the objective is given.

Table A.2: Overview of dynamic positioning literature

Article	Subject	Method	Objective
[64]	Comparison thrust allocation methods	Deterministic, pseudo-inverse, non-linear constraint optimization and genetic algorithm	Achieve highest capability
[65]	Compensate wave frequency loads for small autonomous vessel	Comparison of six thrust allocation algorithms	Achieve highest wave-frequency compensation performance
[66]	Filter out wave frequency loads	Comparison of four filtering methods	Minimal influence by wave frequency loads
[67]	Reduction of power load fluctuations	Compensation of auxiliary load fluctuations by compensation in thruster power	Minimize load fluctuations
[53]	Reduction of power fluctuations by set-point deviation	Allow deviations in position	Minimize load fluctuations & stabilize network frequency
[68]	Reduction of power fluctuations by set-point deviation in environmental load direction	Allow deviations in position in the environmental load direction	Minimize load fluctuations & stabilize network frequency
[69]	Reduction of power fluctuations by set-point deviation with overactuated thruster configuration	Allow deviations in position in the environmental load direction	Minimize load fluctuations & stabilize network frequency
[70]	Dynamic energy storage for DP	Use potential energy of ship encountering environmental loads	Minimize load fluctuations & fuel consumption
[71]	Thrust allocation and DP controller combination	Model Predictive Control	Feasibility investigation and time horizon determination
[30]	Fuel consumption optimization by holistic implementation of thrust allocation and PMS	Comparison of multiple population-based optimization methods	Minimize fuel consumption
[72]	Reduction of load fluctuations by power prediction	Allow small changes in the station keeping control	Minimize load fluctuations & fuel consumption

Conclusion

The thrust allocation algorithm is an element of a DP system that has a large influence on the fuel consumption.The reduction of load fluctuations in the power plant during DP is mainly achieved by deviations from the setpoints that the thrust allocation defined. The extent of the deviation varies throughout the studies. On the one hand, fluctuations in auxiliary power are compensated by deviations in thruster setpoint. On the other hand, the complete ship is used as dynamic energy storage by deviations from the position setpoint in the direction of the environmental forces. In the end, the decision making is complicated due to the unknown nature of the changes in loads and appropriate method should be found to overcome this complication.

A.2.4. Environmental Loads

A DP system needs to compensate for the forces exerted by the environment on the ship. A large variety can be found in the literature about environmental loads on a ship regarding complexity, accuracy and applicability of the methods. In this section, previous research on the environmental loads acting on the ship will be investigated, partly to indicate the variety, but mostly do show the general relation between environmental conditions and exerted force.

Literature

Environmental loads on ships and offshore structures have been investigated in the past by many researchers. Faltinsen [40], for example, described the theory for the calculation of environmental loads on ships and offshore structures. This theory is widely applicable and nowadays still used as a basis for sea load calculations. In this section, firstly the wind loads, then the wave loads and lastly the current loads will be elaborated.

Wind One of the most accessible methods for prediction of wind load is a regression based method. This method is based on historical data to predict the future wind load given a certain wind condition. Within the regression based methods, a distinction can be made between grey box models and black box models, which is further explained in Section A.2.6.

Ischerwood [73] combined multiple model test experiments to apply a multiple regression analysis. The result was a formulation using eight basic ship characteristics to predict the longitudinal force, transverse force and yawing moment on the ship due to the wind. The different angles between the wind direction and the ship are captured by defining specific parameters for each 10 degrees. Also OCIMF [74] performed model tests, but with the purpose of calculating the loads on Very Large Crude Carriers (VLCCs). The coefficients that were obtained were also made dimensionless. The coefficients were applicable for multiple draughts and two different types of bows.

Blendermann [38] developed a parametric continuous function to determine the wind load on a ship. Here, linear regression was applied using the results of multiple model tests of various ship types. Coefficients in the model were specific per ship type instead of adding, and thus requiring, more basic ship characteristics as input.

The required inputs to calculate the wind loads are significantly reduced by Kitamura et al. [75], as only the ship type and the length of the ship is required, with an optional inclusion of the beam. With this basic information, wind coefficients are determined based on wind tunnel tests. Least-squares regression is used to convert the data from the tests into the generalized equation.

Instead of using a grey box method as used by the studies above, Haddara and Soares [76] used a black box method to determine the wind coefficients. The experimental data of Blendermann [38] is used to train a neural network. These results are compared to the previously described methods for a tanker that was not used for training the model, both loaded and in ballast.

A more recent study to determine the wind coefficients is performed by Valčić, Prpić-Oršić, and Vučinić [77]. Here, the focus is more to obtain a representative formulation of the vessel contour. This is first done based on Freeman chain encoding and afterwards on an elliptic Fourier features method. This is then included in a generalized regression neural network, which is again a black box model.

Waves Fossen [39] proposed to simulate the wave-induced forces by making a distinction between first-order forces and second-order forces. The first-order forces are typically high frequency corresponding to the wave frequency. This first-order high frequency has zero-mean and the effect on large objects is low due to the fact that the period of the waves is much smaller than the natural period of the large object. The high frequency components of the signals are usually filtered out as responding to these would result in high amplitude and high frequencies of thrust fluctuations [48]. These thrust fluctuations lead again to excessive wear and tear of the power plant and are therefore not compensated.

The second-order forces are the drift forces due to the waves and have a mean and a slowly varying component. This second-order has a lower frequency and needs to be compensated by during DP operations [39]. Therefore, this second-order mean wave drift force is more relevant for this research than the first-order forces.

Gerritsma and Beukelman [78] developed a method to calculate the added resistance of a ship due to waves and compared this to an experimental model test. It was concluded that the added resistance of a ship due to waves can be approximated with a linear relationship to the squared wave height. Remery and Oortmerssen [79] also stated this linear relationship based on model tests results. A key element of the approximation of the wind force was a drift force coefficient for a flat plate, which was dependent on the wave frequency. The research of Pinkster [80] also presented a method to calculate the mean wave drift force, which are low frequency that is applicable in six degrees of freedom. The method concerned direct integration over the instantaneous wetted area of the ship.

More recent studies, such as Pessoa and Fonseca [81], to determine the second-order low-frequency wave loads on ships use a boundary element method. These methods, however, demand a considerable amount of computational power and require a definition of the hull shape.

Current In the paper of Remery and Oortmerssen [79] model tests were performed to determine the force acting on a ship due to current from different angles. At low current speeds, the sway force and the yaw moment could be measured properly, while the surge force was hard to measure due to the low values of the force. As pressure resistance is higher than frictional resistance at lower speeds, the authors state that frictional resistance was the main component of the current force in surge direction. Model tests suffer from a scaling problem when considering the frictional resistance and the authors proposed to estimate the longitudinal current force of the actual ship by calculating the flat plate frictional resistance. This was, however, not included in their formulation of the current loads.

In the study of OCIMF [74], the fact that frictional resistance dominates the surge force due to current is taken into account. Therefore, the length between perpendiculars was multiplied with the draught for the longitudinal component of the force. Based on this, the article defines the non-dimensional coefficients for the current forces and moment for VLCCs.

Kat and Wichers [82] assumed the same formulation and determined the coefficients for the current forces and moment for a case study tanker. First, numerical calculations were performed to determine the coefficients and these were compared to the results of a model tests with the ship. The calculations showed proper correspondence with the calculated values. Also Mercier and Huijs [83] assumed the longitudinal current force to be dependent on the length between perpendiculars and the draught. Model tests on a floating production, storage and offloading system were performed, which also showed reasonable agreement with the results of OCIMF [74]. The authors did make a remark, however, about the influence of bilge keels on the current force on the ship. The authors indicated that this was not properly taken into account in previous studies and therefore investigated its influence, highlighting the importance.

Overview

Table A.3 shows the literature about the environmental loads on ships that is presented in the previous paragraphs. For each article, the year is indicated as the most prominent studies regarding environmental loads have been performed a long time ago and recent studies show different methods. Furthermore, the subject, the ship type that is mainly considered and the required information to execute the calculation of the method is indicated for each article.

Table A.3: Overview of environmental load literature

Article	Year	Subject	Considered ship type	Required information
		Wind loads		
[73]	1972	Multiple regression on model tests	Merchant ships	8 ship specific parameters
[74]	1977	Multiple regression on model tests	VLCCs	Lateral and transverse wind area and length between perpendiculars
[38]	1994	Linear regression on model tests	15 ship types	Ship type and 7 ship specific parameters
[75]	2017	Least-square regression on model tests	9 ship types	Ship type, length and optionally beam
[76]	1999	Neural network for parametric identification	Merchant ships	6 ship specific parameters
[77]	2020	Neural network regression with elleptic Fourier descriptors of contour	Any ship type once it is tuned	Ship contour image and scale
		Wave loads		
[39]	2011	Generalized theory	All ships	Response amplitude operators
[78]	1972	Prove linear relation between wave force and significant wave height squared	Fast cargo ship	Significant wave height and historical ship data
[79]	1973	Mean wave drift force in irregular waves	All ships	Significant wave height, ship length and drift force coefficient
[80]	1979	Computation mean and low frequency wave forces	Rectangluar barge and semi-submersible	Hull shape and wave-spectrum
[81]	2015	Boundary element method to determine second-order low-frequency drift force	Floating body	Hull shape and wave-spectrum
		Current loads		
[79]	1973	Approximation based on flat plate frictional resistance	All ships	Wetted surface
[74]	1977	Multiple regression on model tests	VLCCs	Draught and length between perpendiculars
[82]	1991	Numerical calculations to determine current coefficients	Tanker	Draught and length
[83]	2005	Current coefficient calculation using model tests	FPSO	Draught and length

Conclusion

The calculation of the instantaneous environmental load acting on a ship is split up in wind, waves and current. The most commonly used methods to calculate environmental loads are based on regression on data from model test experiments. Throughout the studies, the relation for wind, waves and current force is linear with the wind speed squared, significant wave height squared and current speed squared respectively. A coefficient that is dependent on both the ship and the environmental condition needs to be determined to connect the two for each of the three environmental load components.

A.2.5. Thruster Power Consumption

The forces that are exerted by the environment on the vessel need to be compensated by the DP system. The DP system uses its actuators to maintain position. As the actuators require a certain amount of power based on the requested force, a translation needs to be made. Previous research shows a large variety in the calculation of this, as will come forward in this section.

Literature

The calculation of power consumption of a thruster can be subdivided into a few methods. Firstly, an approximation of the physics shows proper accuracy and is simple to perform. Also computational fluid dynamics can offer a good resemblance with reality, but requires a lot of computational effort. Thirdly, model tests can be performed but are time-intensive, not widely applicable and will suffer inaccuracies due to scaling effects. Lastly, regression based methods can be applied using historical data of ships in case this data is available. In this paragraph, previously performed research to determine the thruster power consumption will be elaborated.

The thruster power consumption is included in various studies that include the simulation of a ship or a voyage of a ship. Bortnowska [84] for example applied a *"usage factor"* of propeller power and assumed the power is equal to the thrust generated by a propeller divided by this usage factor. This relation was also used by Lim et al. [85] in the prediction of electric power consumption. However, the use of the usage factor as a constant means that the power would be linearly related to the thrust, which is physically not true.

A relation that is physically true is included in the article of Smogeli, Ruth, and Sørensen [86]. The study aimed to validate three local thruster control strategies using model tests. The strategies considered were shaft speed control, torque control and power control. The theory of the latter contained an expression for the power relation with rotational speed to the power of three, dependent on the propeller characteristics.

Daalen et al. [87] used a formulation directly relating thrust to power instead of rotational speed to power. This relation is used to determine the thruster configuration that requires the least engine power during DP operations. The relation is a linear relation between power and thrust to the power of 3/2. ABS [88] stated this as well and provided a value for the coefficient relating the two. The coefficient is applicable for DP operations, in which the flow velocities are generally close to zero, indicated as *"bollard pull"*. The given coefficients are applicable to either a regular and a ducted propeller. This formulation requires less knowledge about the propeller and is an approximation of the actual physics.

Ships with multiple azimuth thrusters can experience significant losses due to thruster-thruster interactions. In the situation that a certain azimuth thruster is providing a thrust in which the water directly flows towards another thruster, the downstream thruster can experience significant thrust loss. This is investigated by Amini, Sileo, and Steen [89] using computational fluid dynamics calculations that were compared with model tests. The results confirmed the significant loss in thrust. Modelling this using the shown method, however, requires a large computational force. As this is not desirable for real-time applications, a simplification is favorable.

The importance of considering the losses due to thruster-thruster interactions, but also due to thruster-hull interactions was indicated by Arditti et al. [90]. The authors developed a thrust allocation algorithm for DP that included the reduced efficiency of the thrusters dependent on their angle. In comparison with conventional algorithms, the algorithm met the total thrust requirement while the consumed power was lower. Thruster-thruster interactions were also considered in ABS [88]. Here, an equation was provided to calculate the thrust loss of the downstream thruster due to these interactions.

Overview

The articles relevant for the power consumption of a thruster in DP are summarized in Table A.4. For each article, the subject and the method to determine the power consumption is indicated.

Table A.4: Overview of thruster power consumption literature

Article	Subject	Method
[84]	Power consumption prediction for sea mining ship	Assumption linear relation power to thrust
[85]	Electric power consumption predictive modelling	Assumption linear relation power to thrust
[86]	Experimental validation of thruster control methods	Assumption linear relation power to rotational speed to the power of three
[87]	Power consumption minimization during DP	Assumption linear relation power to thrust to the power of 3/2
[88]	ABS guide for DP systems	Assumption linear relation power to thrust to the power of 3/2
[89]	Thruster-thruster interaction losses	Computational fluid dynamics compared to model tests
[90]	Thrust allocation for DP including thruster-thruster interaction losses	Azimuth angle dependent thruster efficiency

Conclusion
Thrusters convert electrical energy into mechanical energy to exert a certain thrust on a ship. During DP operations, this thrusts is generally used to compensate for the environmental loads. The thrusters require power to do this and therefore, if a power demand forecast is to be made, the power consumption of a thruster is highly relevant. The most used relation between power and thrust is the one supported by the actual physics. This is a linear relation between the power and the thrust to the power of 3/2. As DP ships often contain multiple thrusters near each other, thruster-thruster interactions can occur, which need to be accounted for in the power consumption calculation.

A.2.6. Data Processing for Forecast

One of the goals of this research is the development of a power forecast algorithm. A suitable method needs to be found to estimate the value for the power demand given a set of conditions. In the maritime industry, there are multiple methods to estimate a certain value. Petersen, Jacobsen, and Winther [91] suggested to divide these methods into four groups:

- Traditional and standard series methods
- Regression based methods
- Direct model tests
- Computational fluid dynamics

Traditional standard series methods are based on several parameters describing the hull of the ship and are mainly developed for sailing at constant speed. This research regards DP operations and the knowledge about the hull parameters are limited. Direct model tests require a model and results are specifically applicable to one ship. Computational fluid dynamics is a method to estimate parameters quite accurate, but are computationally expensive and require a specific description of the hull shape. Regression based methods estimate specific parameters based on previously recorded data. As data of multiple ships is available for this research, this option is the preferred one. This paragraph will focus on the regression based methods to estimate the power demand.

Literature
From the data analytics perspective, Coraddu et al. [33] described a distinction between white box models, black box models and grey box models. White box models rely on modelling using equations that represent the actual

physics. Black box models use historical data to determine the interdependencies of the parameters without physical motivation. Grey box models combine both models to benefit from the advantages of both, by requiring less historical data due to the addition of physical knowledge to the model.

Grey box models In 2015, Erto et al. [92] performed a study on the fuel consumption of a cruise ferry by using regression. Using historical data of one year to avoid seasonal effects, a multiple linear regression method was used with seven variables and eight regression coefficients. The result of the regression was an accurate fit specifically applicable to the considered cruise ferry.

Brandsæter and Vanem [93] aimed to predict the speed of a ship based on measurements that included environmental conditions. Three regression methods were applied and compared: linear regression models, generalized additive models and projection pursuit regression models. The authors found that the latter two showed sufficient accuracy in capturing the environmental loads on the ship whereas the linear regression model was only accurate in calm weather. Mao et al. [94] used the linear regression model as a basis for further investigation of two statistical approaches. Again, only linear regression showed poor results beyond calm weather conditions. However, by using autoregressive analysis or the mixed effect model, the accuracy of the prediction improved significantly.

Linear regression and generalized additive models were also compared by Swider, Langseth, and Pedersen [95] to find which method was best for estimating the power consumption of a ship in DP operation. The model was aimed to be used in selecting an appropriate dimension of the vessel power system. A power demand forecast that is to be used in the EMS was not in the scope of the article.

Bocchetti et al. [44] applied multiple linear regression to estimate the fuel consumption of a cruise ship. The phenomenon of overfitting was mentioned, which is finding a fit that represents the data properly, but will have poor predictive power. Also Coraddu et al. [33] discussed overfitting briefly. A tradeoff needs to be made between accuracy on matching the calibration data and the complexity of the model, which is a tradeoff between an overfitting tendency and an underfitting tendency.

Black box models A machine learning model, which is a black box model, was used by Yan, Wang, and Du [96]. The authors proposed a two-stage fuel consumption prediction and reduction model for a dry bulk ship. The prediction was based on random forest regressor and a reduction in fuel consumption was achieved using this prediction model to optimize ship speed with an arrival time constraint.

Another black box model was presented by Mehrzadi et al. [97] by using a nonlinear automatic regression method in combination with neural networks. This was used to predict the power consumption during DP. After splitting the data in a training, validation and testing set, the prediction results showed proper performance. However, these results are only applicable to the situation of the training data set. An extrapolation to more extreme conditions or a different ship for example brings more uncertainty due to the lack of knowledge of the actual physics. Thus, the applicability of the model is limited.

Data preparation Gonsalves et al. [98] compared two methods to develop a model in which the individual steps were the same and only the sequence in which the steps were performed deviated. Data was split in training, validating and testing data. The shuffle-split validated at random moments over time during training and the temporal-split used the data to train first and to validate afterwards. Both methods used the last part of the data for testing and the authors concluded that the temporal-split always showed better performance as the shuffle-split suffered a cross-talk problem. A cross-talk problem occurs when the training data is too similar to the testing data. Yang et al. [99] applied a genetic algorithm based model to predict fuel consumption and suggested to improve the model by separating the data in four sets based on the relative environmental load angle, distinguishing head sea, bow sea, beam sea and following sea. The reason for this was that the influence of the environmental load on the ship was significantly different at the four different angles. The result was a balanced accuracy for all weather conditions.

A method to extract useful information on power variability on board of a ship from a large dataset was described by Swider and Pedersen [100]. The main elements of the method were a frequency domain analysis of the data and the choice of a desirable cut-off frequency for filtering. Based on the result, a suggestion was done for the power plant configuration.

Overview
In Table A.5, the studies that have been elaborated in the previous paragraph have been summarized. Each article can be categorized in a certain type, namely statistical, grey box, black box and data preparation. Also the subject and the method to determine the prediction or forecast is indicated for each.

Table A.5: Overview of data processing for forecast literature

Article	Type	Subject	Method
[91]	Statistical	Statistical modelling of fuel efficiency	Artificial neural networks and Gaussian processes
[33]	Grey box	Fuel consumption forecast using grey box model	Combination white and black box model
[92]	Grey box	Fuel consumption prediction for cruise ferry	Multiple linear regression
[93]	Grey box	Ship speed prediction considering environmental conditions	Linear regression, generalized additive models and projection pursuit regression
[94]	Grey box	Speed prediction of container ship	Linear regression with autoregressive analysis and mixed effect model
[95]	Grey box	Power consumption during DP for dimensioning power system	Linear regression and generalized additive models
[44]	Grey box	Fuel consumption of cruise ship	Multiple linear regression
[96]	Black box	Fuel consumption of a dry bulk ship	Random forest regressor
[97]	Black box	Power consumption during DP	Nonlinear automatic regression in combination with neural networks
[98]	Data preparation	Comparison data split methods	Shuffle-split and temporal-split
[99]	Data preparation	Fuel consumption prediction	Data split into different relatice environmental load angles
[100]	Data preparation	Power plant configuration determination based on data	Frequency domain analysis to choose desirable cut-off frequency for filtering

Conclusion
Since historical data is available of a DP ship while not having a detailed definition of the hull and the exact power plant characteristics, a regression based method is to be used for the development of a power forecast algorithm. Various studies have shown that both grey box models and black box models offer the possibility to calculate the power consumption. In the execution of the regression, a tradeoff needs to be made to prevent both overfitting and underfitting. Furthermore, the data should be prepared in such a way that training, validating and testing can be performed properly and that the variance in environmental condition does not affect the accuracy of the prediction negatively.

A.3. Reflection

In this chapter, the most important aspects from the literature review in Section A.2 will be highlighted. The literature review showed various research gaps, of which the most important will be addressed in this chapter. This leads to the unique contribution of this study to the research field of energy management of DP in the marine industry.

In previously performed research regarding EMS, a few general topics recurred frequently. The minimiza-

tion of fuel consumption or the maximization of power plant efficiency is the most important one. Reductions of the load fluctuations experienced by the power grid has been a significant topic too. Lastly, the minimization of computational effort has been a requirement that influenced the developed systems as well.

These recurring topics have been investigated often and the limitation of not knowing the future has been raised frequently. Several energy management strategies have shown to optimize the performance of the power plant at each instant in time individually. Regarding the complete time horizon, however, the power plant is managed in a sub-optimal way. This is due to the fact that these strategies do not account for the future. Other studies indicate themselves that future is not known, yielding optimal results, or even assume that a power forecast is already known. However, actual research on a power forecast is scarce while the potential of its application is large.

Literature that did include future knowledge concerned MPC EMS. MPC has been used to improve performance, but most studies only considered relatively short term forecast horizons ($\pm 1\ min$). Huotari et al. [17] and Vu et al. [25] did regard larger time horizons of approximately 30 and 2 hours respectively. However, both studies calculated the prediction before starting the trip and did not adjust the initial prediction during the trip. This reduced the accuracy and thus deprived the full potential of the benefits of a prediction.

Lastly, most of the studies considered a ship performing a trip instead of DP operation. The load during DP operations is typically more fluctuating than during a transit voyage due to the fact that variations in the environmental conditions need to be compensated. The most conventional way of limiting high frequency fluctuations in the load is constraining the power ramp rate. This way, the load can still be fluctuating, only less severe. The way of handling low frequency fluctuations is starting or stopping diesel generators. However, the EMS does not know whether a change in load will be temporal, being high frequency fluctuation, or a more permanent change, being low frequency fluctuation. Knowing the future load would include the knowledge whether a change in power consumption is a temporal one or a steady one. The EMS can then define a more appropriate setpoint of the components in the power plant based on a long term planning.

To summarize, fuel consumption minimization and load fluctuation reductions have been aimed before and including a forecast shows promising results. However, most studies that included future knowledge did not apply a long term adaptive forecast and considered a trip instead of a DP operation. The unique contribution of this research will be the development of a relatively long term power forecast during DP operations with sufficient accuracy to be used in the EMS to reduce energy consumption while considering the impact on the condition of the power plant components.

A.4. Aims and Objectives

The research that is to be performed is split up in two phases. Each phase has its own aim and associated objectives. After capturing the aim of the phase, the objectives are defined that represent the red line of the research. A brief explanation of the objectives is afterwards provided. The aim of the first phase of this research is presented below.

Phase one of this research aims to develop a real-time adaptive forecasting algorithm of thruster power demand during dynamic positioning operations over a long time horizon and with sufficient accuracy.

The objectives associated with phase one are:

- Determine general expressions for the environmental load on a ship and the power consumption of a thruster.
- Determine instantaneous power consumption by applying an appropriate regression method on historical data of a DP ship.
- Determine the optimal length of the forecast horizon and the required accuracy.
- Develop the long-term power forecast based on the instantaneous weather forecast which computational complexity is at a level suited to be implemented real-time.
- Determine and implement additional elements for the algorithm to increase forecast accuracy.

- Validate the forecast.

The power forecast algorithm will be based on environmental loads and the required power for the thrusters to compensate for these loads. Firstly, the instantaneous power consumption needs to be determined, which will be based on a regression method that is suited for this model. After establishing the instantaneous power consumption, a trajectory over the complete time horizon can be calculated by including the weather forecast. The stochastic nature of the weather models decrease the reliability of the power forecast when considering a larger time horizon. Therefore, a tradeoff needs to be made between the accuracy of the forecast and the length of the forecast. After this has been achieved, additional elements for real-time application can increase the accuracy of the prediction. The specific interpretation of these additional elements will be determined later in the research based on the findings at that moment. In the end, the forecast will be validated.

The aim of the second phase of this research is presented below.

Phase two of this research aims to develop an energy management system that uses the power forecast of phase one to maximize energy efficiency of the power plant while considering the impact on its condition.

The objectives associated with phase two are:

- Determine the objectives of the EMS.
- Determine the constraints of the power plant.
- Establish optimization problem for the complete forecast horizon.
- Assess performance of the developed EMS by comparison with conventional EMS.

The EMS that is to be developed will be based on an optimization problem. The optimization problem needs to optimize for a certain objective, so the objectives need to be determined. Furthermore, the power plant contains certain limitations and these need to be captured by defining constraints. Capturing the objectives and the constraints, an optimization problem needs to be established that considers the power demand forecast. This way, energy efficiency will not only be maximized momentarily, but over the complete time horizon. A comparison with a conventional EMS will quantify the performance of the developed EMS.

A.5. Conclusion

In this report, the literature review is elaborated to develop a basis for the development of a power demand forecast algorithm during DP operations that is to be used in the EMS for reducing energy consumption while considering the negative impact on the power plant components.

The literature review is based on five pillars: EMS, DP, environmental loads, thruster power consumption and data processing for forecast. Fluctuations in power demand induce a high energy consumption and a negative impact on the condition of components in the power plant. During DP operations, the power plant can suffer from significant power fluctuations and conventional energy management strategies do not always suffice to mitigate these. The EMS is responsible for the optimal allocation of power among the power plant and is therefore able to minimize the harm on specific components. As often seen in literature, however, decision making in the EMS is hard due to the lack of knowledge about the future. A power demand forecast would enable the EMS to adaptively adjust the settings of the power plant such that energy consumption is minimized and the impact on its condition is minimal.

The research will be split up in two phases. The first phase considers the development of the forecast algorithm for the power demand during DP operations. The forecast should consider a sufficiently long time horizon while being sufficiently accurate for the use in the EMS. Furthermore, aiming to implement the forecast real-time, the computational effort of the algorithm should be limited. The second phase considers the development of an EMS that utilizes the power demand forecast of phase one. The developed EMS will be an optimization problem of which the objectives, the constraints and the optimization method need to be determined. The performance assessment will be done by comparison with a conventional EMS algorithm.

An improved EMS that takes future power demand into account will optimize for a minimization of load fluctuations in the components in the power plant, a minimization of diesel generator start/stops and a minimization of total energy consumption. Load fluctuations and generator start/stops have a negative impact on the condition of the components in the power plant which results in the long term to degradation of the components. Degradation induces increased maintenance and leads to additional energy consumption, increasing the negative environmental impact of the ship.Therefore, accurate application of a power forecast in the EMS of a DP ship will lead to a reduction of environmental footprint of the ship and therefore to a reduced environmental footprint of the maritime industry.

A.6. Matrix overview of all literature

The article that have been used throughout this report all contain specific elements that are relevant for the research. Table A.6 and Table A.7 show which relevant elements are included in each article. This has been used to provide the analysis in literature review, Section A.2.

Table A.6: Matrix overview of literature part 1

			Objective						Background					Individual elements									Power system						Regression		
Ref.	Year	Author	Start/stop	ESD usage fluctuations	Power prediction required	Power calculation	Engine degradation	Fuel cell	Emission footprint	Redundant engines	Power fluctuations	EMS control important	Tradeoff ESD	Wind	Waves	Current	Thruster performance	Thruster interactions	Optimization EMS	Thrust allocation	Ship motion	MPC	Diesel engine	Generator	Battery	ESD	DC network	ESD general	White box	Grey box	Black box
[3]	2015	United Nations							X																						
[5]	2015	IMO							X																						
[8]	2017	Geertsma et al.			X		X		X	X		X											X				X	X			
[50]	2015	Ovrum and Bergh		X																					X			X			
[51]	2012	Klein Woud and Stapersma															X														
[52]	2015	Hansen and Wendt		X																											
[53]	2012	Veksler, Johansen, and Skjetne					X				X									X											
[17]	2020	Huotari et al.	X		X		X	X	X				X									X								X	
[54]	2016	Kökkülünk, Parlak, and Erdem					X																								
[55]	2009	Rakopoulos and Giakoumis					X		X		X												X								
[28]	2018	Hou, Sun, and Hofmann		X			X				X	X	X						X		X	X			X	X		X			
[56]	2014	Zahedi, Norum, and Ludvigsen								X		X	X										X	X			X	X			
[7]	2011	Sørensen																		X	X										
[57]	2012	Guerrero-Bote and Moya-Anegón																													
[48]	2018	Sørensen					X							X	X	X	X	X		X	X		X	X							
[58]	2017	Lindstad, Eskeland, and Rialland		X																								X			
[59]	2017	Tronstad et al.						X																							
[60]	2022	Berkehan Inal, Charpentier, and Deniz						X	X										X				X		X	X					
[9]	2020	Hein et al.		X																						X					
[10]	2019	Accetta and Pucci		X							X																	X			
[11]	2014	Han, Charpentier, and Tang						X	X			X													X		X				
[12]	2018	Dinh et al.	X	X								X													X						
[13]	2016	Yuan et al.	X																X						X		X				
[14]	2020	Zhang, Guan, and Liu						X	X		X	X	X						X						X	X		X			
[15]	2017	Bassam et al.		X				X				X							X						X			X			
[61]	2017	Tashakori Abkenar et al.						X																	X		X				
[62]	2018	Tang, Li, and Lai																	X						X						
[16]	2020	Banaei et al.						X											X			X									
[18]	2021	Antonopoulos et al.		X	X							X	X									X			X						
[19]	2021	Hein et al.		X	X			X				X							X									X			
[23]	2017	Vu et al.		X	X						X								X			X									
[22]	2017	Vu et al.		X									X						X												
[24]	2015	Park et al.									X	X										X									
[20]	2014	Kanellos, Tsekouras, and Hatziargyriou			X														X												
[25]	2015	Vu et al.	X		X														X							X					
[26]	2014	Hou, Sun, and Hofmann		X			X				X	X	X		X				X		X										
[27]	2018	Hou, Sun, and Hofmann		X			X												X									X			
[63]	2019	Hou et al.		X							X	X	X									X				X		X			
[29]	2018	Ju et al.		X															X			X						X			
[21]	2022	Zhang et al.			X																	X			X		X	X			
[64]	2016	Mauro and Nabergoj																		X											
[65]	2021	Halvorsen et al.					X							X							X										

Table A.7: Matrix overview of literature part 2

			Objective						Background					Individual elements									Power system						Regression		
Ref.	Year	Author	Start/stop	ESD usage fluctuations	Power prediction required	Power calculation	Engine degradation	Fuel cell	Emission footprint	Redundant engines	Power fluctuations	EMS control important	Tradeoff ESD	Wind	Waves	Current	Thruster performance	Thruster interactions	Optimization EMS	Thrust allocation	Ship motion	MPC	Diesel engine	Generator	Battery	ESD	DC network	ESD general	White box	Grey box	Black box
[66]	2019	Værnø, Brodtkorb, and Skjetne									X										X										
[67]	2008	Radan et al.					X			X	X													X							
[68]	2014	Veksler et al.	X				X		X		X									X											
[69]	2016	Veksler et al.	X			X	X				X									X											
[70]	2014	Johansen et al.					X														X										
[71]	2016	Veksler et al.																		X	X										
[30]	2022	Kalikatzarakis et al.												X	X	X				X	X			X							
[72]	2012	Mathiesen, Realfsen, and Breivik			X		X			X	X																				
[40]	1990	Faltinsen													X																
[73]	1972	Ischerwood												X																X	
[74]	1977	OCIMF												X		X															
[38]	1994	Blendermann												X																X	
[75]	2017	Kitamura et al.												X																	
[76]	1999	Haddara and Soares												X																X	X
[77]	2020	Valčić, Prpić-Oršić, and Vučinić												X																	X
[39]	2011	Fossen												X	X	X					X										
[78]	1972	Gerritsma and Beukelman													X																
[79]	1973	Remery and Oortmerssen												X	X	X															
[80]	1979	Pinkster													X																
[81]	2015	Pessoa and Fonseca													X																
[82]	1991	Kat and Wichers														X															
[83]	2005	Mercier and Huijs														X															
[84]	2007	Bortnowska												X	X	X	X														
[85]	2019	Lim et al.												X	X	X	X				X										
[86]	2005	Smogeli, Ruth, and Sørensen				X	X				X						X														
[87]	2011	Daalen et al.				X														X											
[88]	2013	ABS															X	X													
[89]	2012	Amini, Sileo, and Steen															X	X													
[90]	2015	Arditti et al.				X											X	X		X											
[91]	2012	Petersen, Jacobsen, and Winther																													X
[33]	2017	Coraddu et al.																											X	X	X
[92]	2015	Erto et al.							X																					X	
[93]	2018	Brandsæter and Vanem												X	X														X	X	
[94]	2016	Mao et al.																												X	
[95]	2019	Swider, Langseth, and Pedersen				X																								X	X
[44]	2015	Bocchetti et al.																												X	
[96]	2020	Yan, Wang, and Du							X																					X	
[97]	2020	Mehrzadi et al.			X																										X
[98]	2021	Gonsalves et al.							X																					X	X
[99]	2019	Yang et al.																											X	X	X
[100]	2019	Swider and Pedersen				X	X			X	X																			X	

B

Environmental coefficients

In this appendix, the coefficients that are used in the calculation of the environmental load are presented. The wind coefficients are firstly presented in Section B.1. Afterwards, in Section B.2, the wave coefficients are shown. In the end, the current coefficients are presented in Section B.3.

B.1. Wind coefficients

The wind coefficients are adopted from the book of Blendermann [38]. The information from the graphs is translated into data points and included in a MATLAB workspace. This is then used in a 1-D lookup table in Simulink to obtain the value of the coefficient dependent on the angle. The 1-D lookup table is set to be linearly interpolating between two points, which is sufficiently accurate as the sizing between points is chosen to be smaller as the curvature of the line increases. The original graphs from Blendermann are shown in Figure B.1 and the values plotted in a MATLAB plot are shown in Figure B.2.

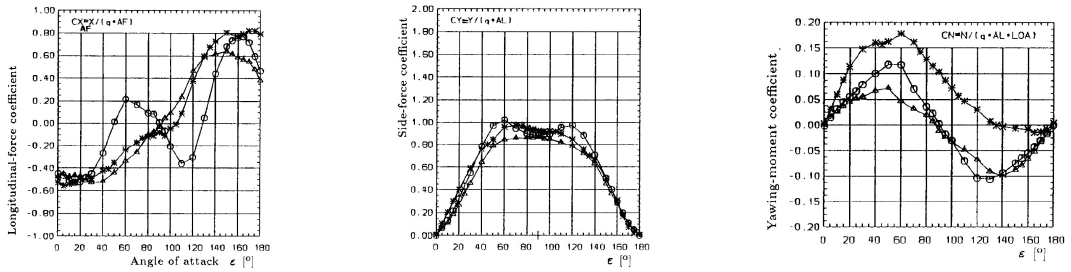

(a) Surge coefficients **(b)** Sway coefficients **(c)** Surge coefficients

Figure B.1: Wind coefficients from Blendermann [38]

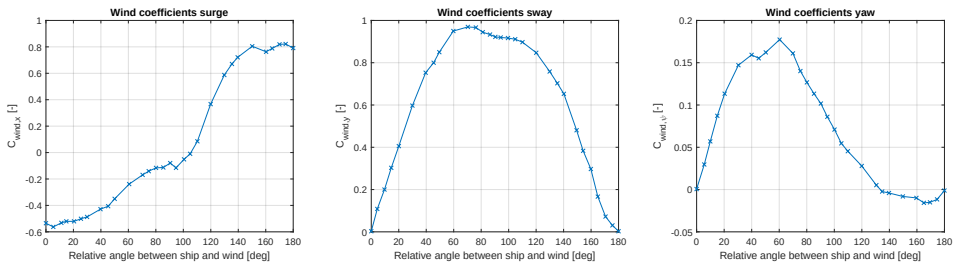

Figure B.2: Wind coefficients of Blendermann [38] in MATLAB

B.2. Wave coefficients

For the calculation of the wave loads on the ship during dynamic positioning, wave coefficients are used. These wave coefficients are scaled from similar ships. The values in each DOF are plotted both in 2D and in 3D in Figure B.3.

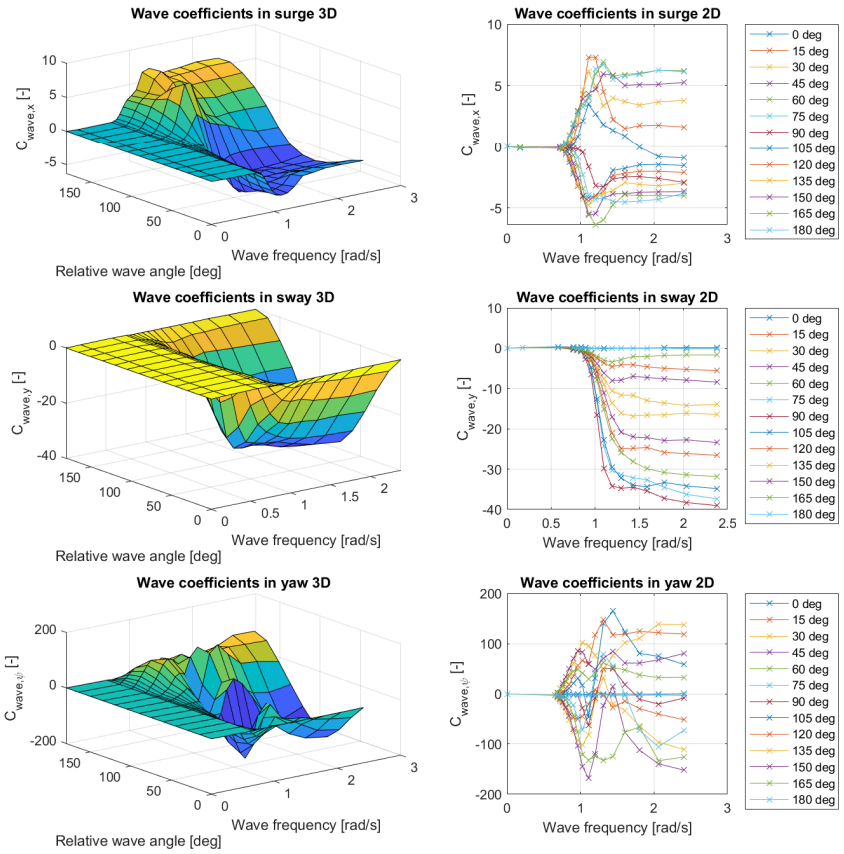

Figure B.3: Wave coefficients

B.3. Current coefficients

The current coefficients that are used for the calculation of the environmental loads are shown in Figure B.4 as determined by Faltinsen [40]. The coefficients shown apply only for the sway and yaw motion. The surge force of the current is calculated using the frictional component of the resistance, as this is the dominant force in the surge current force due to the slenderness of a ship in longitudinal direction. The wind coefficients graphs are copied into MATLAB, providing the plotted values shown in Figure B.5.

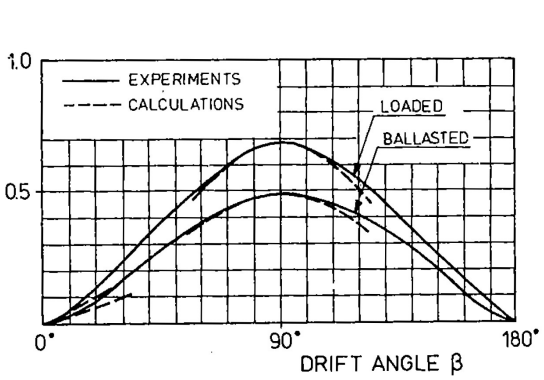

(a) Sway coefficients

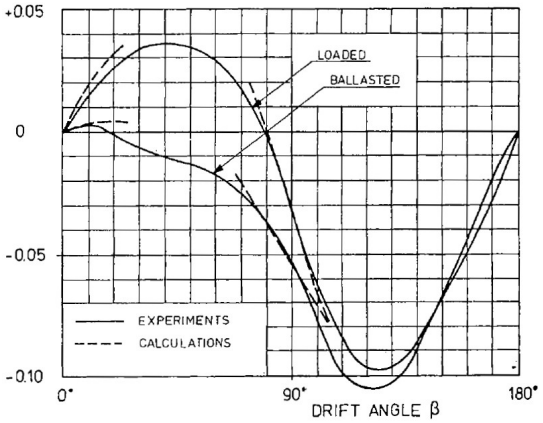

(b) Yaw coefficients

Figure B.4: Current coefficients from Faltinsen [40]

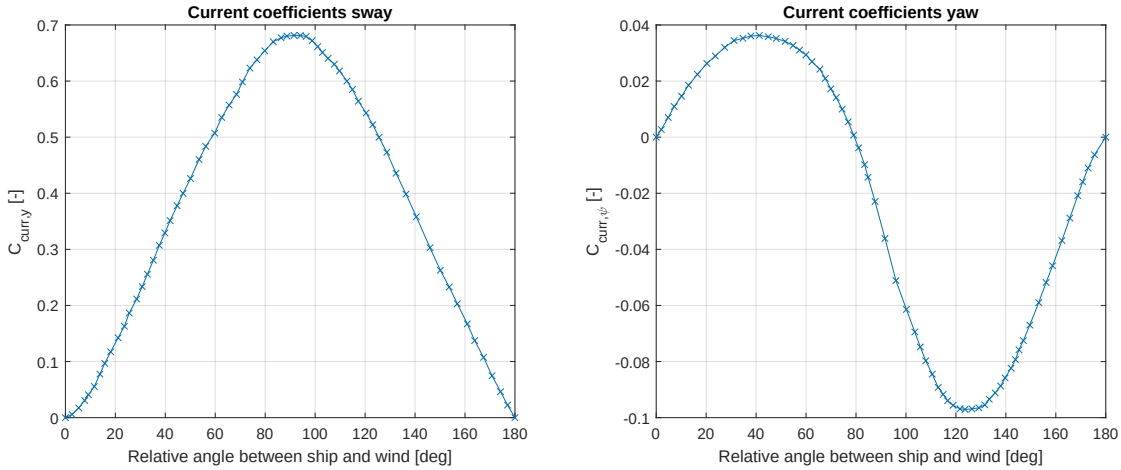

Figure B.5: Current coefficients of Faltinsen [40] in MATLAB

C

DP Simulation

The DP system that is designed for the PMs is an approximation of the actual system of RH Marine. This appendix chapter aims to show the fact that the DP system is operating correctly. For this, a simulation is performed, in which three edges of a square of 50 by 50 m needs to be sailed, after which the ship needs to go to the centre of the square. The changes in the set points are made every 1000 s. During the simulation, the heading is kept constantly at 0 rad. The environmental conditions during the simulation considered a part of the actual data, from 50,000 until 55,000 s. The wind is approximately 7 m/s from the right, the current is going approximately 0.4 m/s to the left, and the significant wave height is 2 m from the right.

Figure C.1 is a visualization of the position of the ship during the simulation in an X-Y plot. In the figure, the fact that the environmental loads are coming from the right is clearly visible, as the deviations are mainly to the left. Furthermore, the plot over time shows a small overshoot occurs when changing set points, particularly in the longitudinal direction. The system regains position, however, within a reasonable amount of time, meaning that the system is able to handle changes in set points. The simulation also indicates the estimations of the thruster forces are also included correctly. The only step towards total thruster power is the conversion from thruster force to thruster power, which is described in Section 2.2.2.

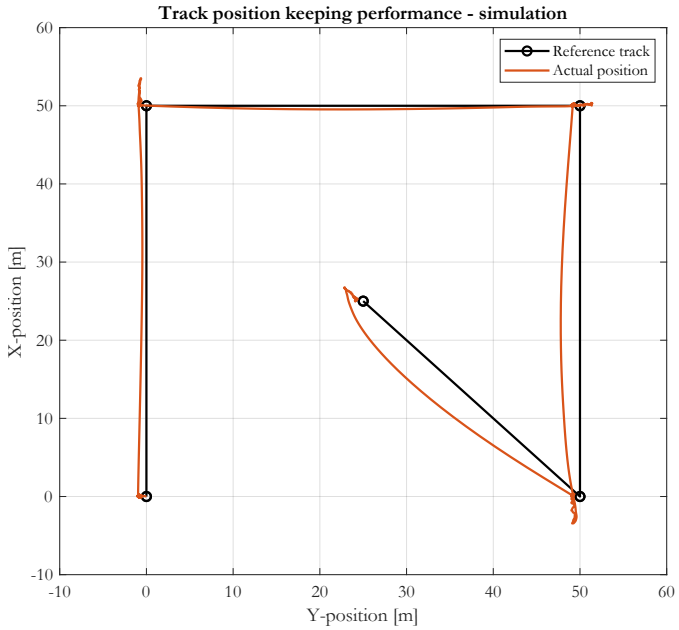

Figure C.1: DP Simulation of set point changes X-Y plot

D

Feature exploration

Feature	Unit	Mean	Standard Deviation	Minimum	Maximum
Wind Angle 1	rad	3.92	2.42	0.00	6.27
Wind Angle 2	rad	2.93	2.57	0.00	6.23
Wind Speed 1	m/s	6.25	3.13	0.01	15.20
Wind Speed 2	m/s	5.48	2.17	0.00	14.56
Wind Speed 3	m/s	6.73	3.09	0.00	15.68
Current Angle	rad	4.36	0.87	0.00	6.28
Current Speed	m/s	0.28	0.12	0.00	0.70
Current Velocity x	m/s	−0.18	0.18	−1.45	1.90
Current Velocity y	m/s	0.05	0.18	−0.55	0.70
Surge Error	m	2.18	74.38	−645.3	608.86
Sway Error	m	−3.94	29.15	−495.22	20.38
Yaw Error	rad	0.01	0.19	−2.82	2.63
Surge Velocity	m/s	0.00	0.03	−0.40	0.37
Sway Velocity	m/s	0.00	0.07	−0.59	0.73
Heading	rad	1.53	1.04	.000	6.28
Roll Angle 1	rad	0.00	0.02	−0.12	0.13
Roll Angle 2	rad	0.00	0.02	−0.11	0.14
Roll Angle 3	rad	0.00	0.02	−0.12	0.14
Pitch Angle 1	rad	0.01	0.01	−0.03	0.06
Pitch Angle 2	rad	0.01	0.01	−0.03	0.05
Pitch Angle 3	rad	0.01	0.01	−0.03	0.05
Angle Azimuth 1	rad	−0.08	0.78	−3.14	3.14
Setpoint Azimuth 1	% rpm	14.65	6.17	0.00	92.99
Angle Azimuth 2	rad	−0.08	0.71	−3.14	3.14
Setpoint Azimuth 2	% rpm	15.30	6.13	0.00	76.48
Setpoint Bowthruster 1	% rpm	−9.53	21.26	−100	77.14
Setpoint Bowthruster 2	% rpm	−6.91	21.54	−100	80.51
Setpoint Bowthruster 3	% rpm	0.38	7.70	−74.51	100
Setpoint DG 1	% kW	16.10	5.36	0.67	87.03
Setpoint DG 2	% kW	0.00	0.00	0.00	0.32
Setpoint DG 3	% kW	6.00	6.29	0.00	82.52
Setpoint DG 4	% kW	14.26	5.22	0.00	59.25
Setpoint DG 5	% kW	8.94	7.07	0.00	120.00

Table D.1: Feature information

E

Wave scaling

The wave information is not included in the data. Therefore, the wave information is deduced from the wind using a scaling table. This table contains the conversion from wind speed to significant wave height and mean wave period and is shown in Table E.1. The values are calculated and presented in a DP capability analysis of the ship by Basten Batenburg [49].

Wind speed $[m/s]$	**Significant Wave Height** $[m]$	**Mean Wave Period** $[s]$
0	0	3.0
1.4	0.7	3.2
2.2	0.8	3.5
3.3	1.0	3.9
5.0	1.4	4.6
6.2	1.7	5.1
7.5	1.9	5.4
8.7	2.3	5.9
10.0	2.6	6.3
11.4	3.0	6.8
13.1	3.5	7.3
15.5	4.2	8.0
17.6	4.9	8.7
19.3	5.3	9.0
19.9	5.6	9.3
20.6	5.8	9.4

Table E.1: Scaling table from wind to wave [49]